NAVAL POSTGRADUATE SCHOOL
Monterey, California

THESIS

CONTROL SYSTEM DESIGN OF THE THIRD
FLEXIBLE JOINT
OF PUMA 560 ROBOT

by

Robby Lee Knight

June 1989

Thesis Advisor Liang-Wey Chang

Approved for public release; distribution is unlimited.

nclassified

urity classification of this page

REPORT DOCUMENTATION PAGE

a Report Security Classification Unclassified		1b Restrictive Markings
a Security Classification Authority		3 Distribution/Availability of Report Approved for public release; distribution is unlimited.
b Declassification Downgrading Schedule		
Performing Organization Report Number(s)		5 Monitoring Organization Report Number(s)
a Name of Performing Organization Naval Postgraduate School	6b Office Symbol *(if applicable)* 69	7a Name of Monitoring Organization Naval Postgraduate School
c Address *(city, state, and ZIP code)* Monterey, CA 93943-5000		7b Address *(city, state, and ZIP code)* Monterey, CA 93943-5000
a Name of Funding Sponsoring Organization	8b Office Symbol *(if applicable)*	9 Procurement Instrument Identification Number
c Address *(city, state, and ZIP code)*		10 Source of Funding Numbers Program Element No | Project No | Task No | Work Unit Accession No

Title *(include security classification)* CONTROL SYSTEM DESIGN OF THE THIRD FLEXIBLE JOINT OF PUMA 560 OBOT

Personal Author(s) Robby Lee Knight

3a Type of Report Master's Thesis	13b Time Covered From To	14 Date of Report *(year, month, day)* June 1989	15 Page Count 141

Supplementary Notation The views expressed in this thesis are those of the author and do not reflect the official policy or position of the Department of Defense or the U.S. Government.

Cosati Codes			18 Subject Terms *(continue on reverse if necessary and identify by block number)*
eld	Group	Subgroup	MATRIXx, Control Syetem Design, Robot Manipulators.

Abstract *(continue on reverse if neccssary and identify by block number)*

With the increased demands for higher productivity in industry and the military, control of Robot Manipulators with exible joints is needed. The difficulties associated with the control of flexible joint robots include the following: (1) Nonnearity of the arm motion (2) Coupled large motion (motion of the motor) and small motion (mechanical vibration) and 3) measurements of feedback signals. This theis presents an controller designed to handle the difficulties related to flexible oint robots. The third joint of the PUMA 560 Robot was selected as an example. A control algorithm for flexible-body ontrol was devised and an observer was designed with the use of $\mathbf{MATRIX}_x$ to control tip motion of the single-link single-oint system. Computer simulation results are discussed, and a comparison between rigid-body controllers and the flexible-ody control is conducted.

Distribution Availability of Abstract ☒ unclassified unlimited ☐ same as report ☐ DTIC users	21 Abstract Security Classification Unclassified	
2a Name of Responsible Individual iang-Wey Chang	22b Telephone *(include Area code)* (408) 646-2632	22c Office Symbol 69Ck

D FORM 1473,84 MAR 83 APR edition may be used until exhausted
All other editions are obsolete

security classification of this page

Unclassified

Approved for public release; distribution is unlimited.

Control System Design of the Third Flexible Joint
of Puma 560 Robot

by

Robby Lee Knight
Lieutenant Commander, United States Navy
B.S., United States Naval Academy, 1978

Submitted in partial fulfillment of the
requirements for the degree of

MASTER OF SCIENCE IN MECHANICAL ENGINEERING

from the

NAVAL POSTGRADUATE SCHOOL
June 1989

ABSTRACT

With the increased demands for higher productivity in industry and the military, control of Robot Manipulators with flexible joints is needed. The difficulties associated with the control of flexible joint robots include the following: (1) Nonlinearity of the arm motion (2) Coupled large motion (motion of the motor) and small motion (mechanical vibration) and (3) measurements of feedback signals. This theis presents an controller designed to handle the difficulties related to flexible joint robots. The third joint of the PUMA 560 Robot was selected as an example. A control algorithm for flexible-body control was devised and an observer was designed with the use of **MATRIX**$_x$ to control tip motion of the single-link single-joint system. Computer simulation results are discussed, and a comparison between rigid-body controllers and the flexible-body control is conducted.

TABLE OF CONTENTS

LIST OF TABLES

LIST OF FIGURES

ACKNOWLEDGEMENTS

I would like to thank Professor Liang-Wey Chang for his unfailing guidance and full support during this research. I also wish to express my appreciation to David Marco and Edward Ward of the Mechanical Engineering Department for their assistance and help in the CAD/CAE Laboratory. Last but most important, I wish to thank my dear wife, Lecia, for her patience, moral support and help during my research and academic studies.

I. INTRODUCTION

A. ROBOT MANIPULATOR USES

There is an increasing trend within the United States Navy towards applications that utilizes robots to perform tasks which are considered routine or dangerous for humans to perform. These tasks include:

1. Under-water research and exploration
2. Fire fighting
3. Battle field logistic vehicle
4. Perimeter patrol
5. Under-water autonomous vehicle

Robotic submersibles are being studied and tested to be used to explore areas of the oceans that are presently too hazardous for man to explore. There is also a large potential for the use of robots in space.

All the applications listed require close-loop automatic control that typically lead to manpower reductions, improvements in stability and response.

In addition, the robotic manipulators currently installed in industry also have the potential for improvement in the areas of increase accuracy, performance, as well as weight to load capacity and productivity. The enhance performance must come with a realized savings in cost and reduction both in energy consumption and overall physical plant size.

B. BACKGROUND

Most work in the past have centered on rigid body manipulators until recently when flexible body manipulators began to show great potential in industry.

Control systems for industrial robots are currently designed using mathematical models in which the links and drive trains are assumed to be rigid [Ref. 1: p. 196]. The joint positions are controlled independently, using position and velocity feedback from sensors located at the joint actuators.

However, improvements in dynamic response and payload to weight ratio require that the flexibility effects be taken into account in the modeling stage and incorporated into the controller design. Preliminary results of studies of link structural flexibility versus drive train compliance for several industrial robots, indicated that structural flexibility accounts for 2 - 20% of total arm compliance. If the structural flexibility of the arm is small relative to the drive train flexibility, then the arm could be represented by a rigid body model with "compliance lumped between the actuators and links." [Ref. 1: p. 196]

Drive train flexibility plays a critical role in robot motion control design. It has been shown that closed loop speed response of the manipulator can be increased beyond typical industrial practices by considering the drive train compliance in the design and providing suitable feedback measurement [Ref. 1: p. 197]. Using a lumped parameter model, Forrest-Barlach and Babcock [Ref. 1: pp. 196-197] studied the effects of drive train compliance and actuator dynamics by modeling a two DOF manipulator and designing a position controller based on inverse dynamics. Simulation of various controllers were performed utilizing the Advance Continuous Simulation Language. Their inverse dynamics control law is based on the concept of "computed torque." This method decouples the motion of the arm when drive train compliance and actuator dynamics are considered. The "computed torques" concepts are utilized to determine the required input torques as functions of jerk rate, jerk, acceleration, velocity and position errors. Jerk rate is a fourth ordered term. The **ITAE** performance criteria for pole placement is used to minimize the error between the desired and the actual state

measurements [Ref. 1: p. 200]. They concluded that in general after comparative simulations, the inverse dynamics controller performance was superior to that of the other controllers they tested due to its ability to decouple the arm motion [Ref. 1: pp. 200-203].

The simulation study was conducted without considering practical limits on available motor torques. Forrest-Barlach and Babcock concluded, limitation in available torques will significantly affect system response. Therefore Forrest-Barlach and Babcock felt the effect of torque limiting on the relative performance of the controllers should be evaluated by selecting appropriate torque limits for the specific motors. [Ref. 1: pp. 203-204]

In another study, Marino and Spong [Ref. 2: p. 1030] found joint elasticity is the dominant source of compliance in most current manipulator designs. This joint flexibility may arise from gears, belts, links, bearings, and hydraulic lines and limit speed and dynamic accuracy achievable by control algorithms designed assuming perfect rigidity at the joints. The nonlinear control problem using a single link manipulator with joint elasticity were studied.

In their work, two nonlinear control techniques to control the manipulator: (1) feedback linearization design and (2) composite control design were used. It was found that feedback linearizing control required full state measurements which in their case included the velocities of both the link and the motor shaft. Whenever part of the state was not accessible for measurements, problems were created. [Ref. 2: pp.1031-1035]

Based on extensive analytical and experimental studies by Sweet and Good [Ref. 3: pp. 724-727], realistic robot dynamic models have been presented which has been validated over the frequency range from 0 to 50 Hz. These models exhibit a strong influence of drive train flexibility, producing lightly damped poles in the neighborhood of 8 Hz, 14 Hz, and 40 Hz, all unmodeled by the conventional rigid body multiple link

robot dynamic approach. They also noted the significance of drive train and mechanical flexibility had been recognized in only a few prior papers. One approach they used to improve robot motion control performance was to decouple the dynamics of the robot links through nonlinear control. The decoupling action performed by the controller was particularly significant in the same frequency range where resonant behavior occurs which was present in the robot motion control loop of electro-mechanical drives with flexibility in series with the load. Sweet and Good also realized the existence of drive train interactions did not dismiss the idea of using nonlinear or decoupling control strategies, but it required the use of realistic drive train models in the development of usable algorithms. Also they found high gear ratios employed in most drive units causes the torques resulting from cross-coupling effects as reflected back to the motors to be minimal [Ref. 3: pp. 725-726].

In a separate design study, Spong [Ref. 4: p. 312] investigated a second method of approach to control elastic joint manipulators. The second method is based on the "integral manifold formulation" of the equation of motion. One advantage of this approach as noted by Spong, is it can be applied when only the link position and velocity are available for feedback. Spong concluded at the end of his evaluation that by using global feedback linearization, the nonlinearities in the system do not have to be computed exactly but rather once the proper coordinates are found in which to represent the system, the so called matching conditions can be satisfied. In other words the nonlinearities are all in the range space of the input. He further realized realistic limitations on motor torques can prevent the arm from reaching velocities of sufficient magnitude for cross-coupling terms to become significant, but realistic trajectories for robot arms in actual manufacturing applications rarely require extremes of velocity and acceleration [Ref. 4: p. 310]. He finally concluded the integral manifold based corrective control method needed further investigation [Ref. 4: pp. 314-318].

The objectives of the above work have been the study of the nonlinear control problem for a robot manipulator with joint elasticity. Much of the past research in robotics modeled the robot manipulator as a rigid joint and did not consider joint elasticity. But recent studies have found joint elasticity is the dominant source of compliance in most current manipulator designs. It was their intention to illustrate several nonlinear control techniques to solve this control problem of joint elasticity. Their research provides the background for the investigation of a computed torque controller structure which considers drive train flexibility of a single link manipulator.

In this work, the computed torque controller will be enhanced and evaluated. The "computed torque" concept requires the values of the second and third derivatives. Since these values can not be measured from the plant, an observer or estimator will be designed as part of the controller to provide the estimates of these unmeasurable values.

C. METHOD

The flexible manipulator offers low power consumption, ease of transportation, reduced material requirement, lower mounting strength and rigidity requirement, and lower overall cost [Ref. 5]. To meet the needs of a light-weight manipulator having greater performance capabilities, certain problems must be solved in order to fully utilize the flexible manipulator.

The model must adequately describe the system and yet it must be simple enough to implement in order to design an adequate controller for the computation purpose.

The controller in this thesis is designed by using the technique called the inverse dynamics control law based on the concept of "computed torque". This control approach represents a method of decoupling the arm motion when drive train compliance and actuator dynamics are considered. A single revolute joint was modeled for this research. [Ref. 1: pp. 196-197]

First the plant will be discussed in Chapter III and the controller design procedure will be developed in Chapter IV. The parameters of the third flexible joint of the Puma 560 Robot was used in the design procedures (Figure 1). A rigid body controller is currently installed in the control loop of the Puma 560 robot. A description of the Puma 560 Robot is found in Appendix B. [Ref. 6: p. 1-27]

The **MATRIX**$_x$[1] computer software was used for the modeling of the controller and the plant and the software was installed on the Vax computer system. **MATRIX**$_x$ is a software package for modeling, simulation, engineering analysis, control design and system identification. A description of **MATRIX**$_x$ can be found in Appendix A.

---

1 **MATRIX**$_x$ is a trademark of Integrated Systems Incorporated.

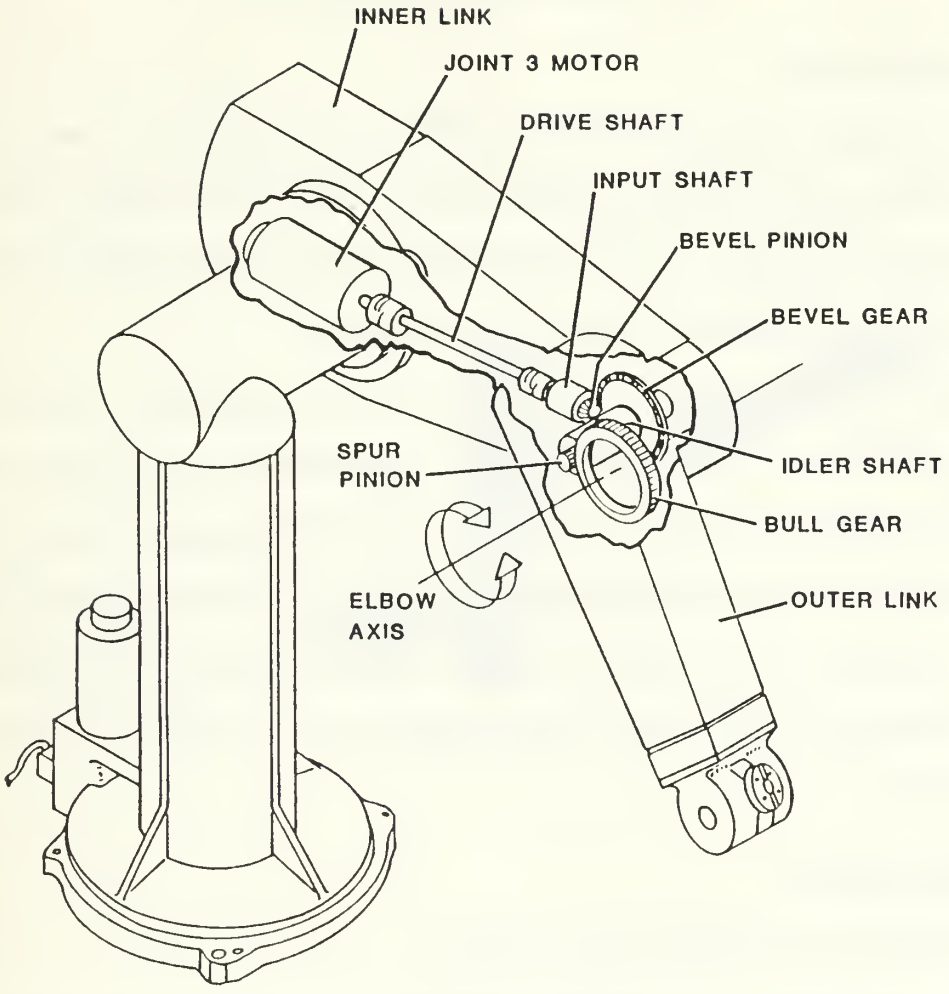

Figure 1. Joint 3 PUMA Robot Arm

II. PROBLEM STATEMENT

A. INTENTIONS

In the design of robot manipulators, controlling the tip position is of major concern. The end effector (robot tool) is attached to the tip position and through it performs the function of the robot arm. The second consideration is the small oscillation (small motion) between the arm position and the motor position.

Figure 2 shows a single-link manipulator with joint flexibility, consisting of an actuator (DC motor), a transmission line, and a rigid single link. The transmission line includes a flexible helical spring coupling and the indicated gears. The transmission line's flexibility is the cause of the difference between arm position and motor position.

It is the intent of this research to design a controller which can accurately control the tip position and also account for and minimize the small oscillation (small motion) of the system.

B. PROCEDURE

This research is conducted in three phases.

First, using Lagrangian dynamics approach, a mathematical model of the flexible-body model plant is derived. Next the flexible-body controller is designed using the concept of control law along with designing a state observer.

Second, considering the special case of rigid-body control, a comparison between the two methods of feedback, motor feedback and arm feedback, is conducted with the best method of feedback control selected to continue comparison test and analysis.

Third, after determining that the past method of control could be improved on by a flexible-body controller, comparison tests are conducted between the selected

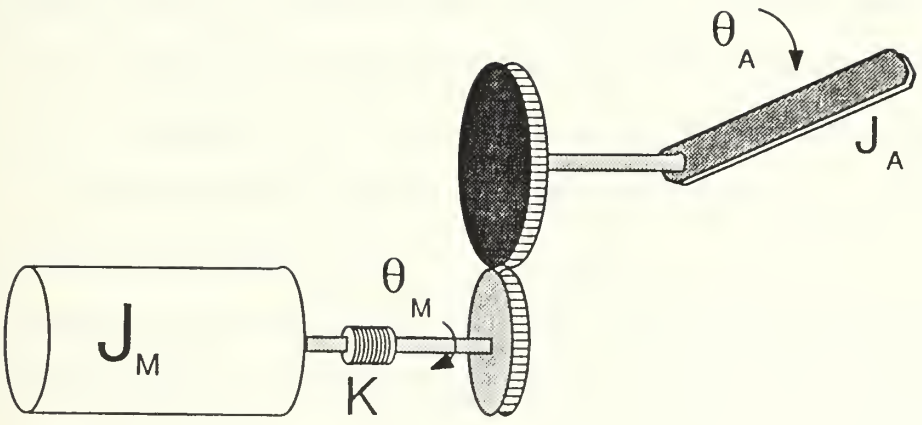

Figure 2. Single-Link Manipulator with Joint Flexibility

rigid-body controller and the flexible-body controller. A determination is made at the end to show how much the flexible-body controller improves plant operation.

Flexibility of the gear train will be considered in this research work but gear backlash will be neglected for now. Various simulation runs will be conducted with various parameters to study the dynamic flexibility behavior of the control system. An investigation of the special case of a rigid-body controller controlling a flexible body plant will be observed and compared with the simulation results of the flexible-body controller.

III. PLANT MODELING

A. EQUATIONS FOR PLANT

1. Flexible Body Model

Due to its systematic approach, the Lagrangian dynamics approach is used to derive the equations of motion. The total kinetic energy is comprised of the individual kinetic energies of the link, actuator, and any applied forces. The total potential energy of the system is comprised of the elastic strain energy of the link and the potential energy due to gravity. Generalized forces are made up of any applied forces and damping forces. Through mathematical manipulations and simplifications, two sets of coupled non-linear equations are derived. [Ref. 7: pp. 239-254]

Consider a single revolute joint (Figure 2), consisting of an actuator (DC motor) whose rotor inertia $\mathbf{J}_m$ is connected through a transmission link to a rigid link with inertia $\mathbf{J}_a$ about the axis of rotation. The transmission line consist of a flexible helical spring coupling and the gears shown. The transmission line has a spring with stiffness k and the gear ratio is equal to $\mathbf{G}_r$.

$$\mathbf{G}_r = \frac{\text{Angle in Motor Side}}{\text{Angle in Arm Side}}$$

The generalized coordinates includes the link angle θ_a and the motor shaft angle θ_m . The following relationships will apply in the derivation of the plant model:

$$\theta_a \mathbf{G}_r - \theta_m = \delta \text{ (deflection)} \tag{3.1}$$

Since the motion of the link is a pure rotation about the motor axis, the kinetic and potential energies are:

$$(KE) = \frac{1}{2} J_a \dot{\theta}_a^2 + \frac{1}{2} J_m \dot{\theta}_m^2 \tag{3.2}$$

$$(PE) = \frac{1}{2} k(\theta_a G_r - \theta_m)^2 + m_a g \frac{l}{2}(1 - \sin \theta_a) \tag{3.3}$$

Where m_a is the total mass of the arm (link) and $\frac{l}{2}$ is the distance from the axis of rotation to the center of mass of the arm.

The equations of motion are found from the Lagrangian method to be:

$$J_a \ddot{\theta}_a + k(\theta_a G_r - \theta_m) + m_a g \frac{l}{2} \cos \theta_a = 0 \tag{3.4}$$

$$J_m \ddot{\theta}_m - k(\theta_a G_r - \theta_m) = T \tag{3.5}$$

Where T is a generalized force applied to the transmission line through the actuator. [Ref 7: pp. 259-261]

See Figure 3 for a block diagram of the Flexible Body model plant.

2. Rigid Body Model

For the special case of a rigid body model, the following assumptions are made (refer to Equations 3.2 and 3.3) [Ref. 2: p. 1030]:

1. $K \rightarrow \infty$
2. The elastic displacement $\theta_a - \theta_m \rightarrow 0$

Therefore the kinetic and potential energies equations for the rigid body case reduces to:

$$\begin{aligned} KE &= \frac{1}{2}(J_a + J_m)\dot{\theta}_a^2 \\ PE &= m_a g \frac{l}{2}(1 - \sin \theta_a) \end{aligned} \tag{3.6}$$

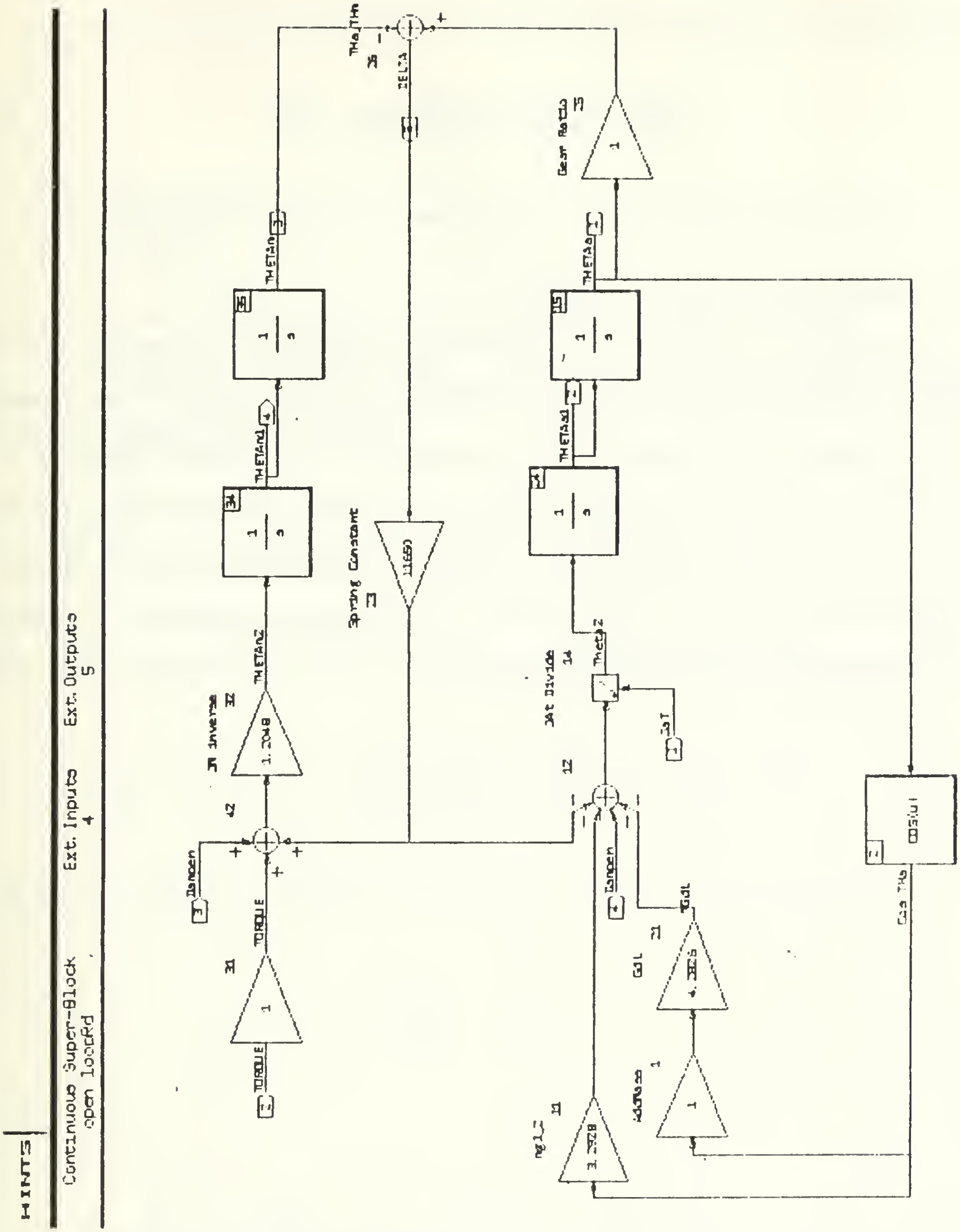

Figure 3. Flexible Body Model Plant

Referring back to Equations (3.3) and (3.4), The Lagrange equations reduces to:

$$(J_a + J_m)\ddot{\theta}_a + m_a g \frac{l}{2} \cos \theta_a = T \tag{3.7}$$

The only nonlinearity term, $\cos \theta_a$, appears in Equations (3.4) and (3.7).

B. ADDED MASS AND DAMPING

The additional special case of added mass and damping can be modeled into the plant by adding the appropriate terms to Equations (3.4), (3.5), and (3.7) (see Appendix C for an explanation and derivation of the added mass and dampening equations).

With the model of the plant, a controller for the flexible joint plant is designed as well as a a special case where the joint is considered rigid. A rigid body controller is designed to test its ability to control a plant with flexibility effects present. The design of the controller will be discussed in Chapter IV.

IV. CONTROLLER DESIGN

A. CONTROL LAW

1. Derivation

The controller is designed using the following steps [Ref. 1: p. 200]:

The dynamic equation of motion, equation (3.4), can be solved for the motor position in terms of the arm position:

$$\theta_m = \theta_a G_r + J_a \frac{\ddot{\theta}_a}{k} + \frac{m_a g l}{2k} \cos\theta_a \tag{4.1}$$

Next differentiating Equation (4.1) twice with respect to time yields the following:

$$\ddot{\theta}_m = \left[G_r - \frac{m_a g l}{2k} \sin\theta_a \right] \ddot{\theta}_a - \frac{m_a g l}{2k} \dot{\theta}_a^2 \cos\theta_a + \frac{J_a \ddot{\theta}_a}{k} \tag{4.2}$$

Substituting Equation (4.2) back into Equation (3.5) results in the following:

$$\frac{J_m J_a \ddot{\theta}_a}{k} + F = T \tag{4.3}$$

where

$$F = J_m \left[\left(G_r - \frac{m_a g l}{2k} \sin\theta_a \right) \ddot{\theta}_a - \frac{m_a g l}{2k} \dot{\theta}_a^2 \cos\theta_a \right] + J_a \ddot{\theta}_a + m_a g \frac{l}{2} \cos\theta_a \tag{4.4}$$

See Figure 4 for the block diagram of the F equation. Equation (4.3) is a fourth order differential equation in terms of the arm variables alone.

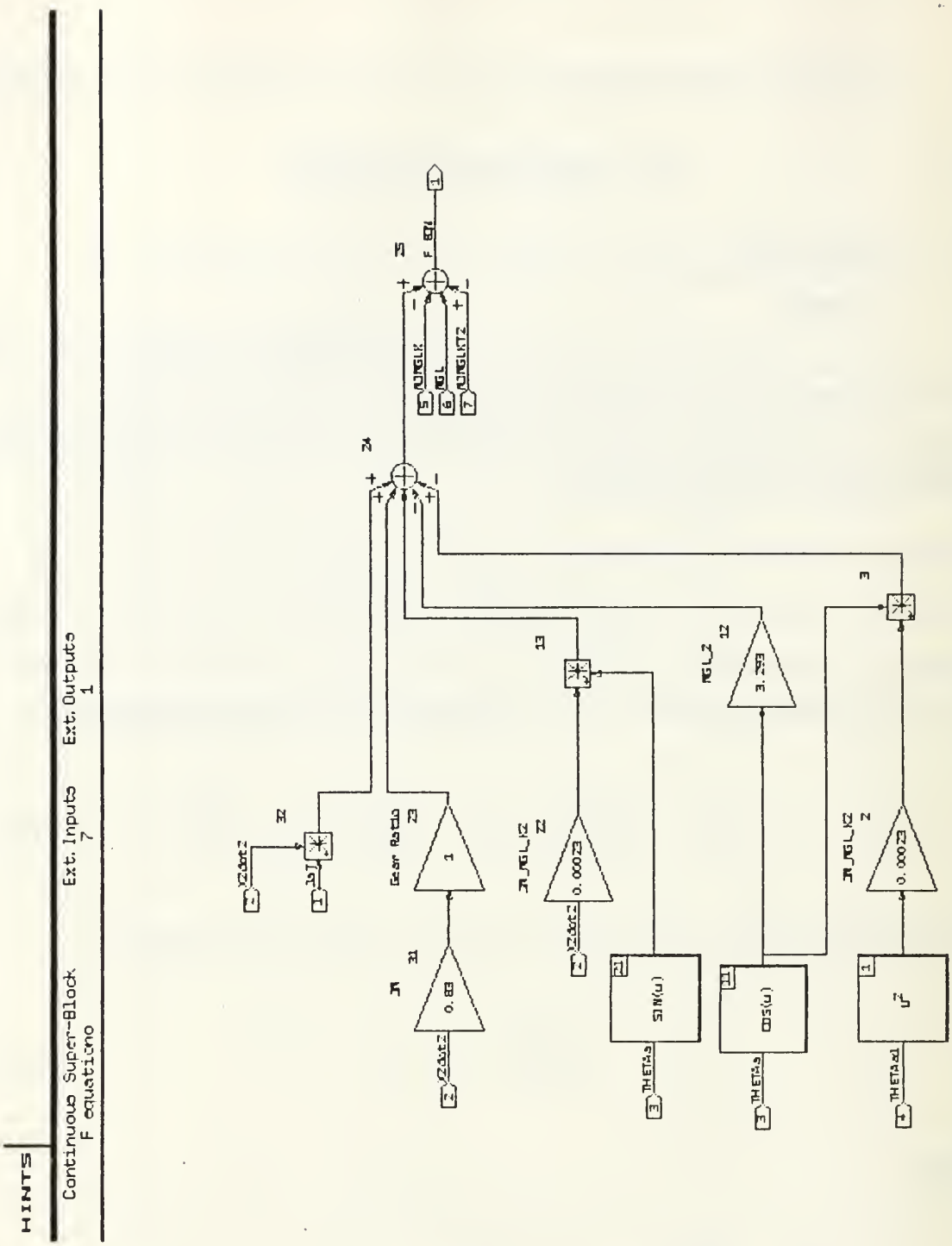

Figure 4. Flexible Body Plant F Equation Super Block

Next, the concept of computed torque is utilized to determine the desired input torques as a function of the fourth and third derivatives, acceleration, velocity, and position errors. The desired input torque can be written as:

$$T_d = \frac{J_m J_a}{k}\left[\dddot{\theta}_d + \mathbf{K}_3(\ddot{\theta}_d - \ddot{\theta}) + \mathbf{K}_2(\dot{\theta}_d - \dot{\theta}) + \mathbf{K}_1(\theta_d - \theta) + \mathbf{K}_0(\theta_d - \theta)\right] + F \tag{4.5}$$

where the **K**'s are constants representing state error feedback gains. Assuming the nonlinear F equation terms can be computed based on plant dynamics and the availability of measurements, equating Equation (4.3) and Equation (4.5) together results in:

$$\frac{J_m J_a}{k}\left[(\dddot{\theta} - \dddot{\theta}_d) + \mathbf{K}_3(\ddot{\theta} - \ddot{\theta}_d) + \mathbf{K}_2(\dot{\theta} - \dot{\theta}_d) + \mathbf{K}_1(\theta - \theta_d) + \mathbf{K}_0(\theta - \theta_d)\right] = 0 \tag{4.6}$$

Since J_m, J_a, and k are non zero, Equation (4.6) becomes:

$$\dddot{\varepsilon} + \mathbf{K}_3\ddot{\varepsilon} + \mathbf{K}_2\dot{\varepsilon} + \mathbf{K}_1\varepsilon + \mathbf{K}_0\varepsilon = 0 \tag{4.7}$$

where

$$\varepsilon = (\theta - \theta_d)$$

is the position error. As time $\rightarrow \infty$, the steady state position error $\varepsilon = (\theta - \theta_d) \rightarrow 0$ (note this is true for specific **K**'s obtained using the **ITAE** performance criteria) [Ref. 1: pp. 200-201].

ITAE performance criteria for a fourth order equation is used for the selection of the **K** values. The values are:

$$
\begin{aligned}
K_3 &= 2.1\omega_n \\
K_2 &= 3.4\omega_n^2 \\
K_1 &= 2.7\omega_n^3 \\
K_0 &= 1.0\omega_n^4
\end{aligned}
\tag{4.8}
$$

ω_n represents the selected servo input speed to the system. [Ref. 8: pp. 129-130]

A block diagram of the Flexible Body Controller is shown in Figure 5.

2. Special Case of Rigid Body Model

Referring back to equation (3.7), one can see a controller for the Rigid Body case can be developed along the same lines. Define the desired input torque equation as:

$$T_d = (J_m + J_a)\ddot{\theta}_d + K_v(\dot{\theta}_d - \dot{\theta}) + K_p(\theta_d - \theta) + F \tag{4.9}$$

where

$$F = m_a g \frac{l}{2} \cos\theta \tag{4.10}$$

Equating equations (3.7) and (4.9) together and dividing out the non zero terms, the following results:

$$\ddot{\varepsilon} + K_v\dot{\varepsilon} + K_p\varepsilon = 0 \tag{4.11}$$

To let this steady state error approach zero, K_v and K_p should be properly chosen. A block diagram of the Rigid Body Controller is shown in Figure 6. See Figure 7 for a block diagram of the Rigid Body Model F equation.

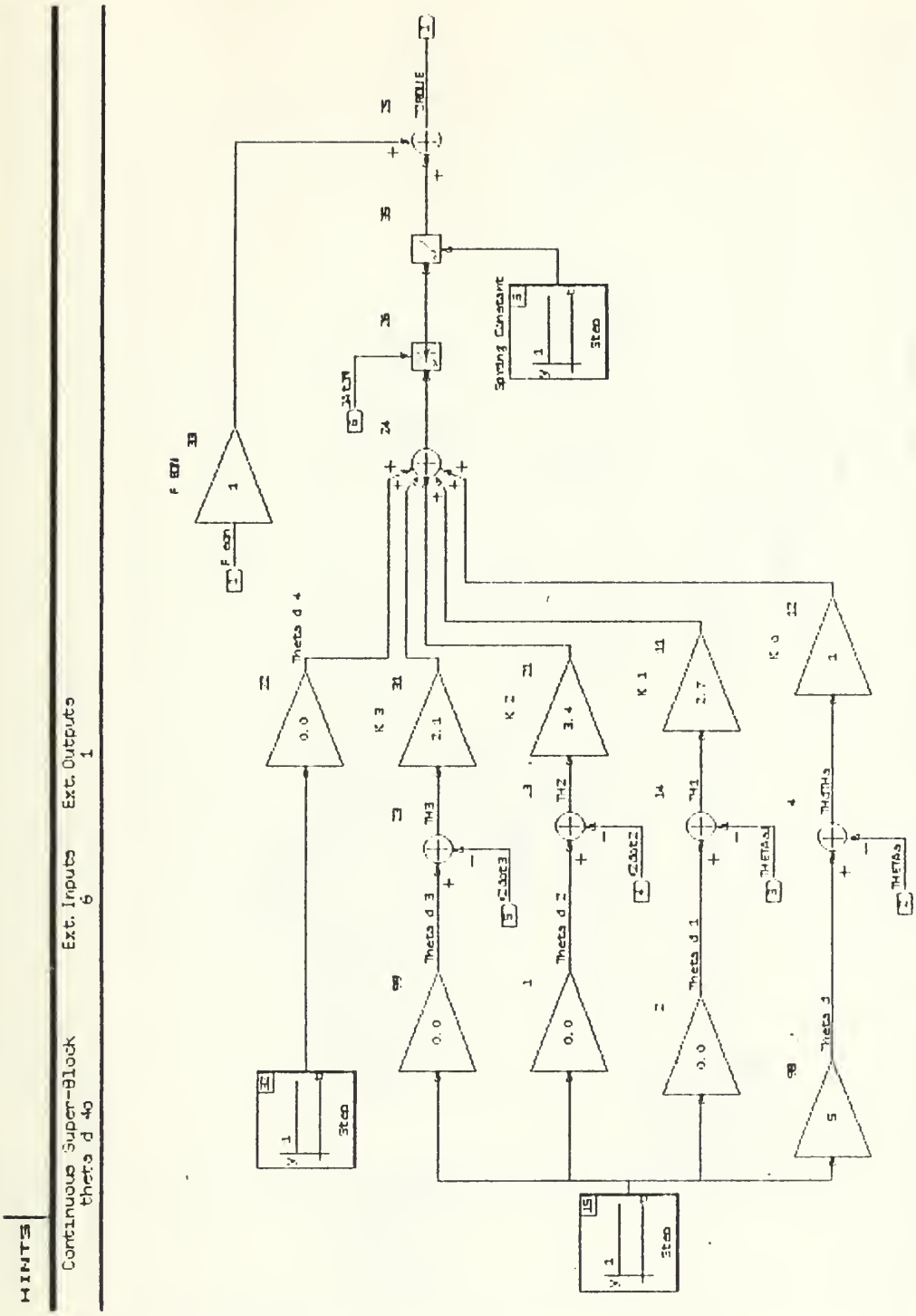

Figure 5. Flexible Body Model Controller Block Diagram

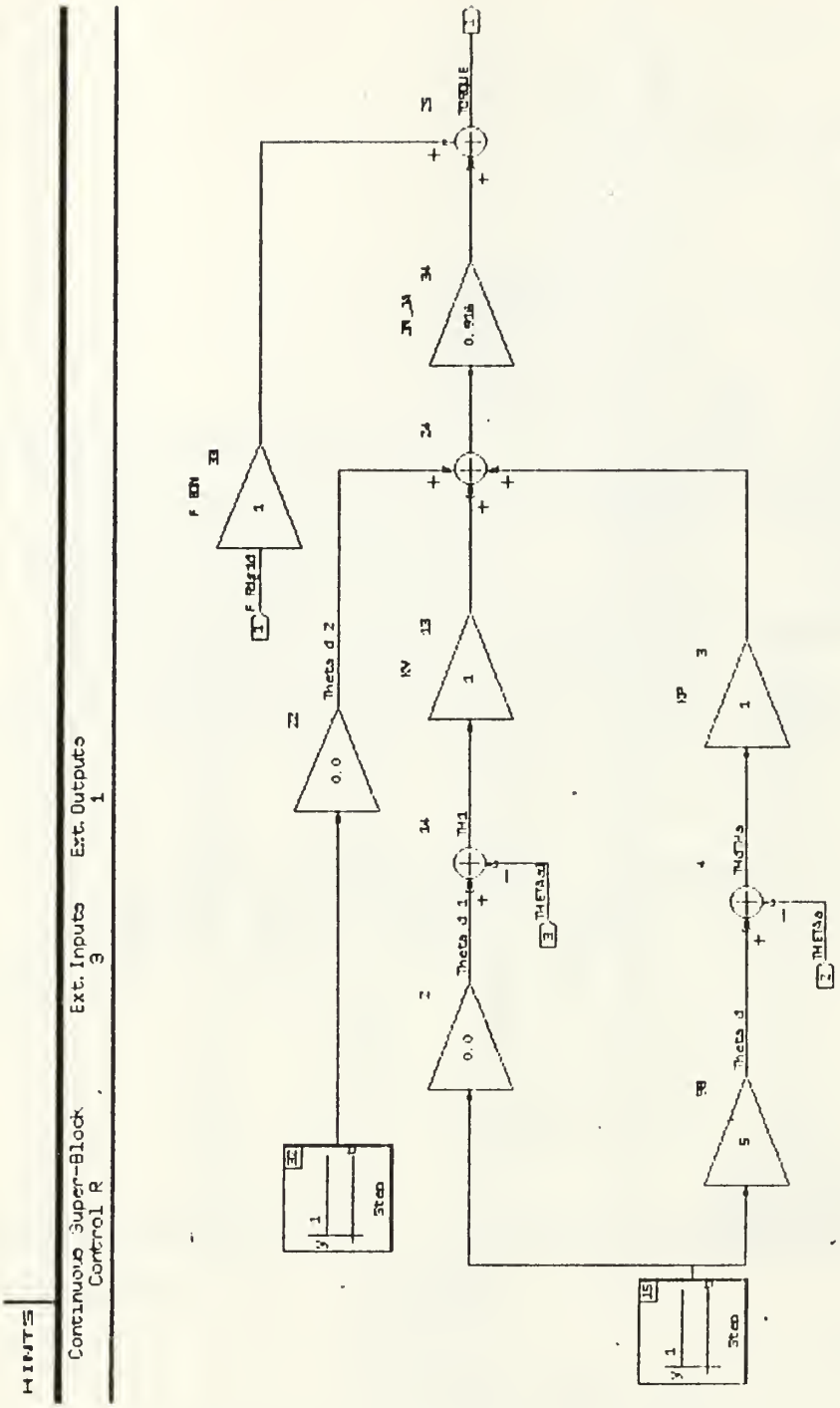

Figure 6. Rigid Body Model Controller

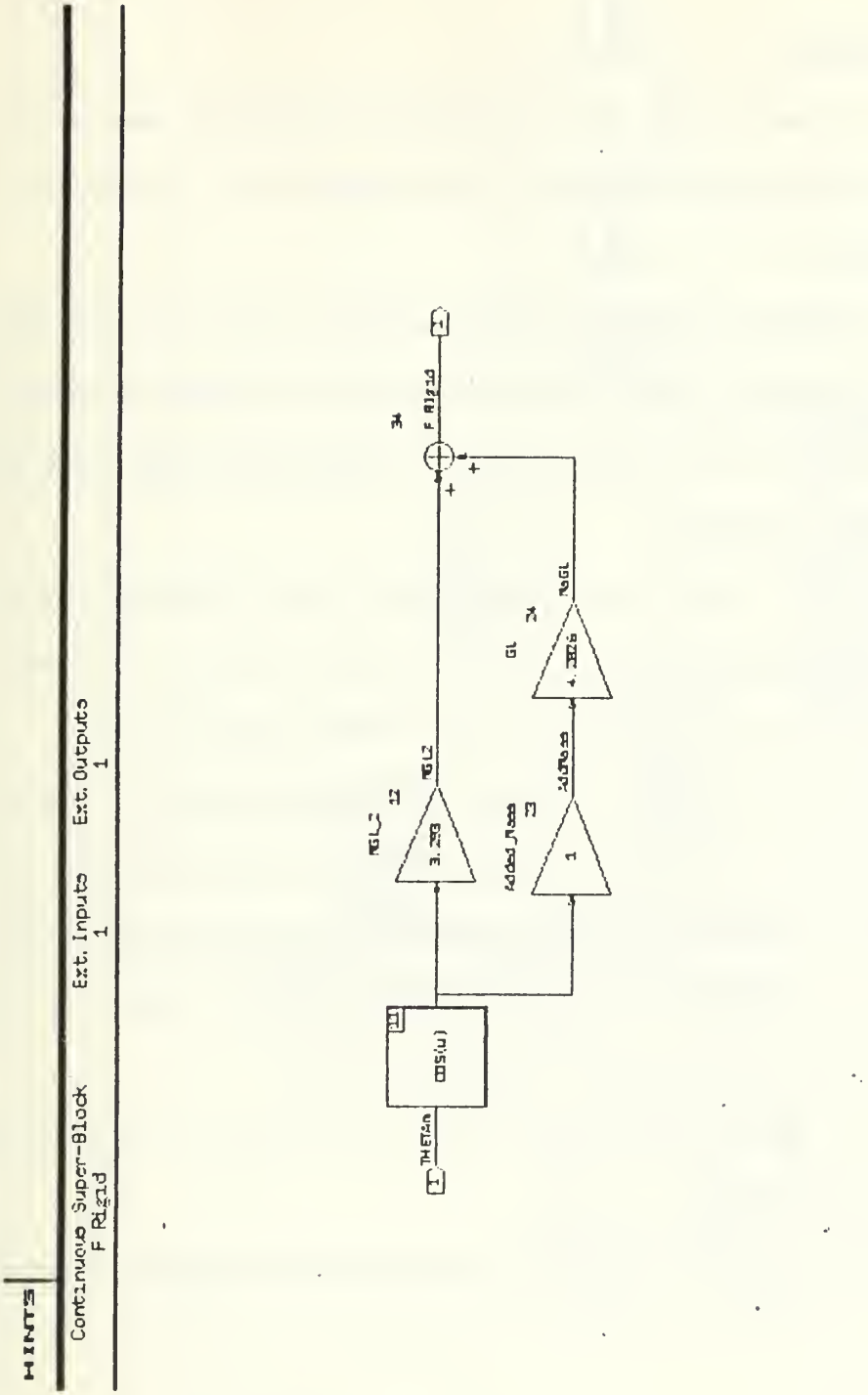

Figure 7. Rigid Body Model F Equation Block Diagram

B. OBSERVER DESIGN

Referring back to equation (4.6), this external feedback linearization series requires the values of the second and third derivatives. These values are not measurable or available from the plant.

Often it is not possible to achieve acceptable performance using only those state variables that can be measured. If the system is observable, it is possible to estimate those state variables that are not directly accessible to measurements using measuring data from those that are measurable.

State variable estimates may in some circumstances be even preferable to direct measurements, because the errors produced by the instruments that provide the measurements may be larger than errors in estimating these variables. [Ref. 9: p.259]

A dynamic system whose variables are known can be estimated with the use of an observer. Luenberger [Ref. 9: pp. 260-216] showed, that for any observable linear system, an observer can be designed having the property that the estimation error (the difference between the state variables of the actual system and the variables of the observer) can be made to go to zero as fast as one wants.

A state observer is designed to estimate the values of $\dddot{\theta}$ and $\ddot{\theta}$. The observer is shown in Figure 8 and in Figure 9.

A mathematical derivation of the observer used in this research is presented in Appendix D.

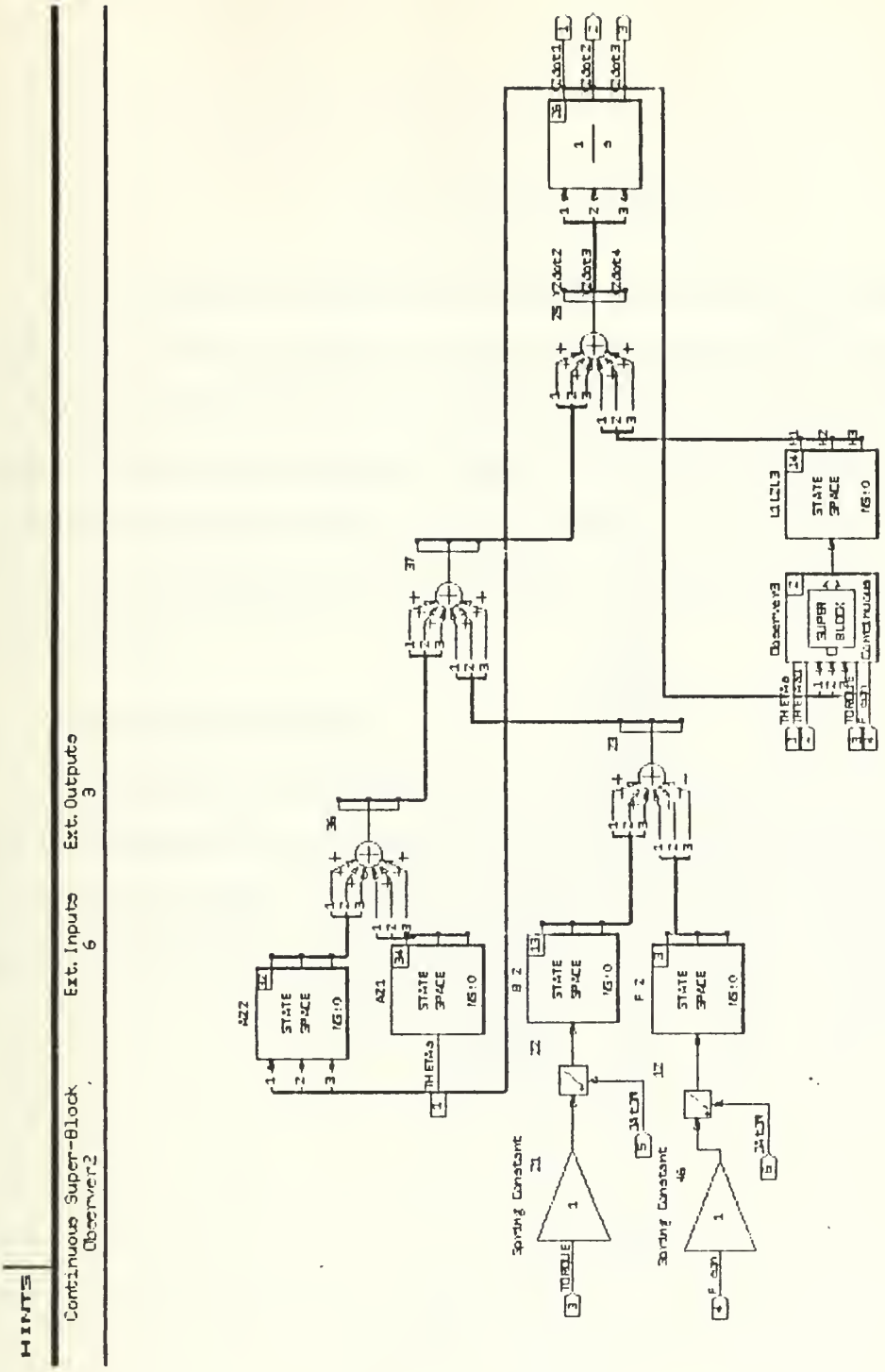

Figure 8. Observer Super Block Diagram

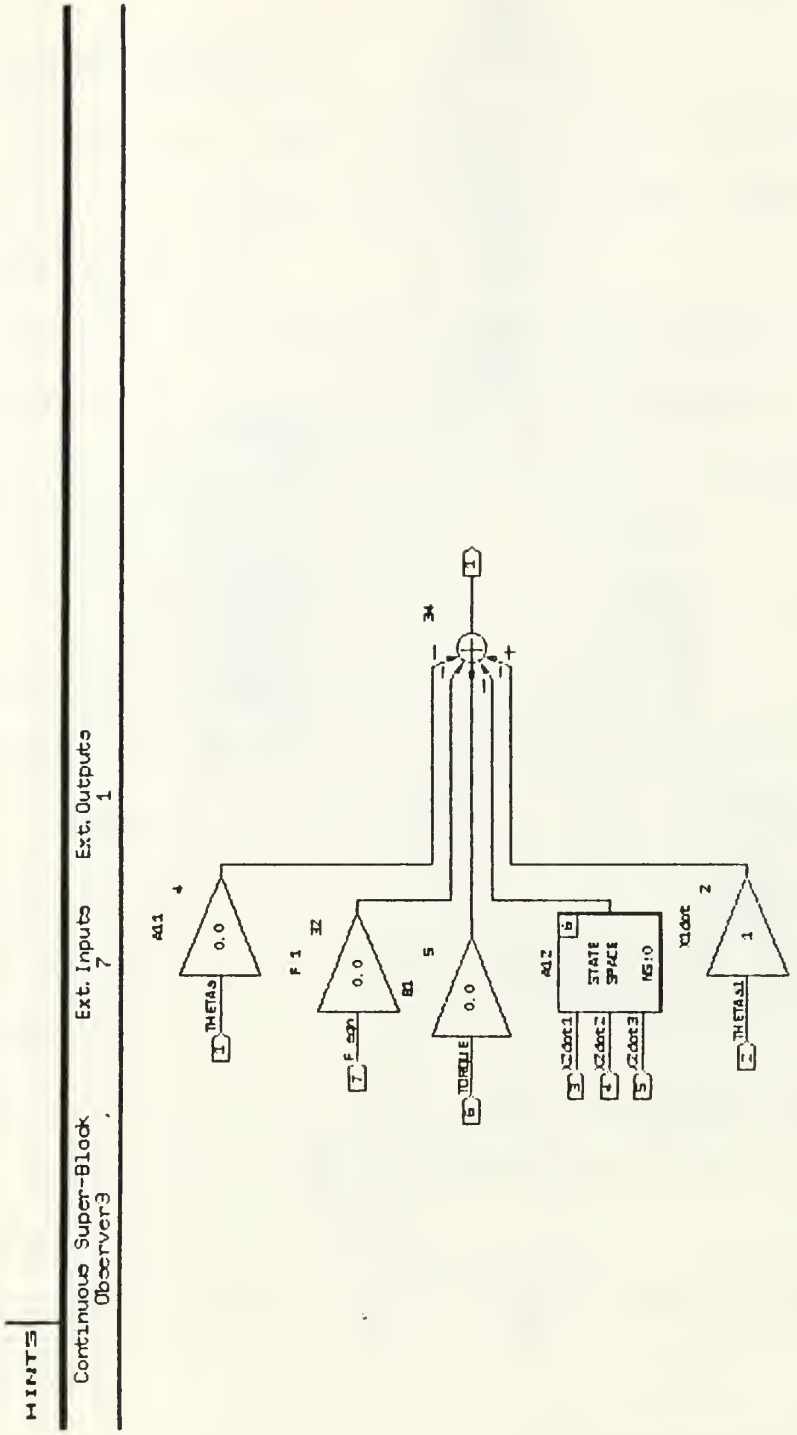

Figure 9. Observer Sub Block Diagram

V. EVALUATIONS

After designing the flexible-body controller and reviewing the special case of the rigid-body controller, a comparison will be conducted between the two controllers. The comparison will be focused on responding speed, payload capacity and torque requirement. The first set of comparisons will be between the two methods of feedback for rigid-body control (arm feedback and motor feedback). The second set of comparisons will be between the rigid-body control (using the best method of feedback) and flexible-body control.

A. RIGID-BODY CONTROL

Simulations were conducted for the special case of the Rigid-Body Controller in order to investigate its performance characteristics. The controller was used to control a plant with joint flexibility. The parameters used in the simulation were from the third joint of the PUMA 560 Robot arm.

$$
\begin{aligned}
m_a &= 4.8\ kg \\
J_a &= 0.086\ kg - m^2 \\
J_m &= 0.83\ kg - m^2 \\
k &= 11650\ \frac{N-m}{rad} \\
G_r &= 53.69 \\
\frac{l_a}{2} &= 0.007 \text{ meter} \\
L_D &= 0.439 \text{ meter} \\
M_D &= 2.5\ kg
\end{aligned}
$$

For the Rigid-Body case, there are two methods of feedback, namely, feedback from the tip (arm) position and feedback from the motor position. To demonstrate and

evaluate the rigid-body controller, both methods of feedback will be investigated. The servo input speeds used were $\omega_n = 1$ and $\omega_n = 4$. The following three outputs will be shown for each method and speed:

1. Arm position
2. Torque requirements
3. Small motion differences

Note, on the graph of small motion (the difference between the arm position and the motor position), the major line is the servo control mode which is the result of the entire system movement. The second part is the mechanical vibration superimposed onto the servo mode.

1. Rigid Body with $\omega_n = 1$

The graphs for arm feedback are shown in Figure 10, Figure 11, and in Figure 12. The graphs for the motor feedback are shown in Figure 13, Figure 14, and in Figure 15.

As shown in Figure 10, an unacceptable long settling time occurred for arm feedback. The cycle time is longer also for the arm feedback case. In the motor feedback case, the arm settles at the desired position of 5 radians after 7.4 seconds. Looking at Figure 12, and Figure 15, the servo control mode amplitude difference is similar between the two cases but the mechanical vibration (spikes) is more pronounced for the arm feedback case. Looking at Figure 11 and Figure 14, the torque is 32 times lower for arm feedback than for motor feedback. The key point here is the motor feedback provides overall superior performances but at an high torque requirement.

2. Rigid Body with $\omega_n = 4$

The servo input speed was increased to $\omega_n = 4$ to further study the effects of increased speed on performance. The graphs for arm feedback are shown in Figure 16,

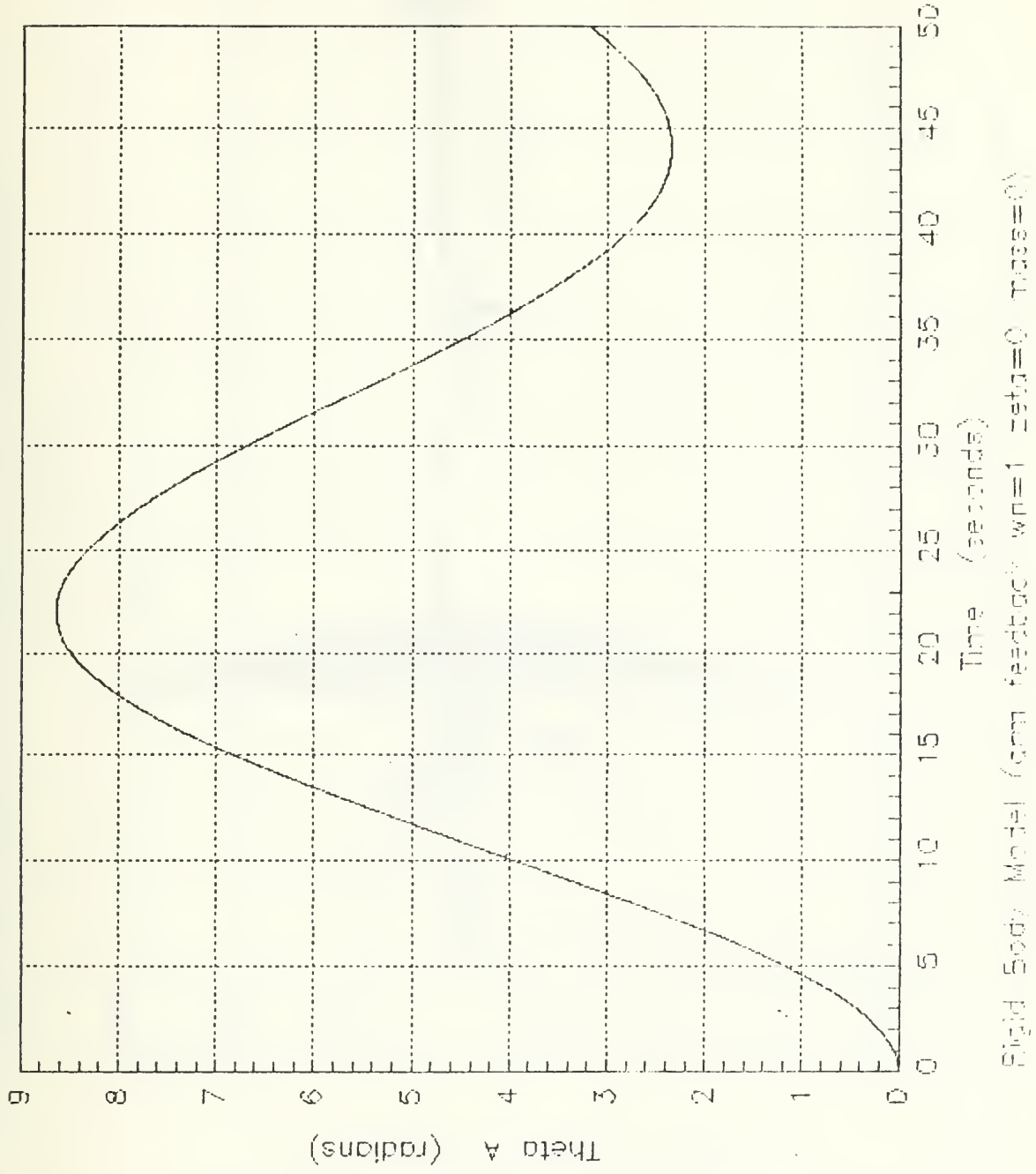

Figure 10. Rigid Body Model Arm feedBack (θ_a)

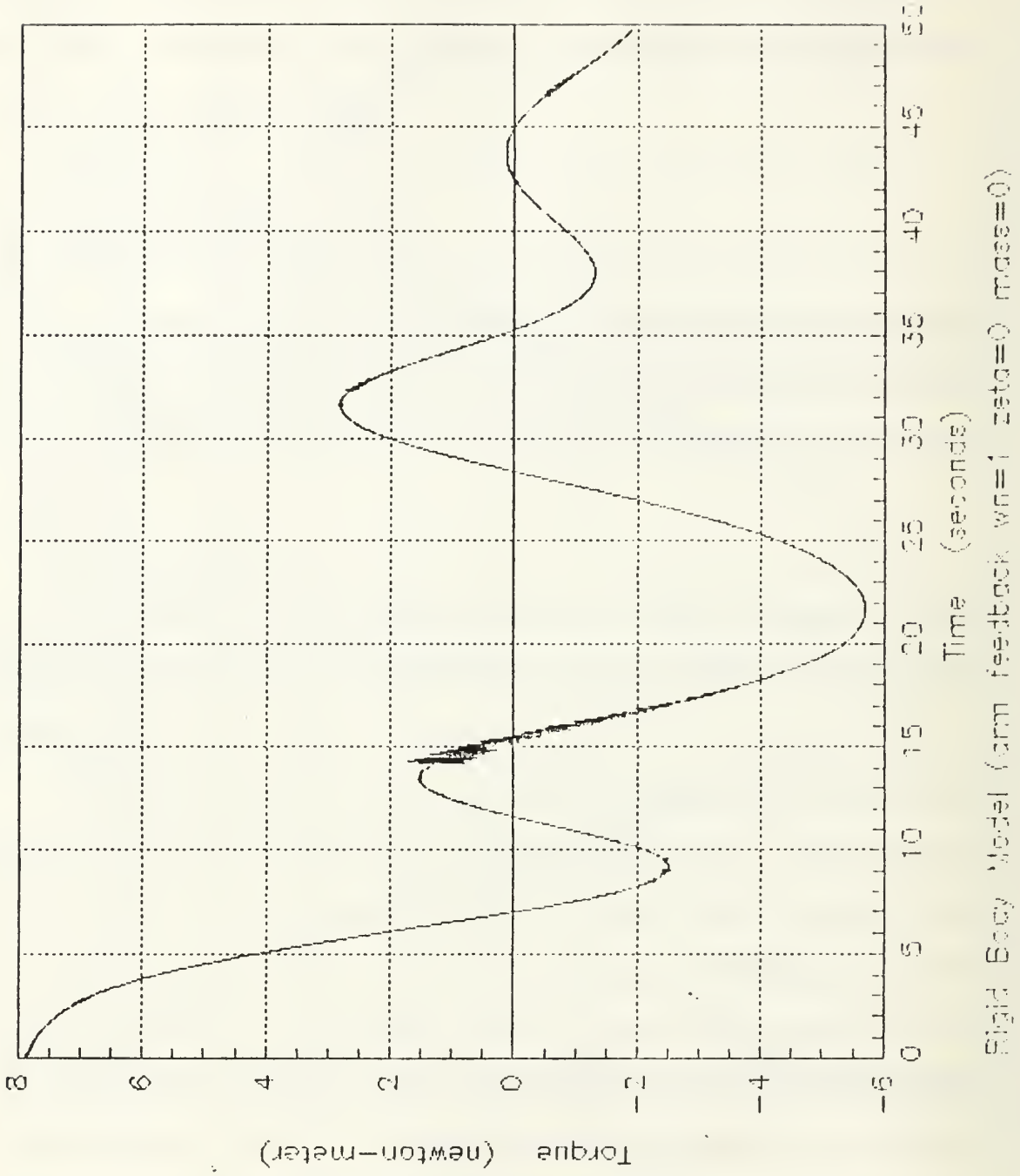

Figure 11. Rigid Body Model Arm feedBack (torque)

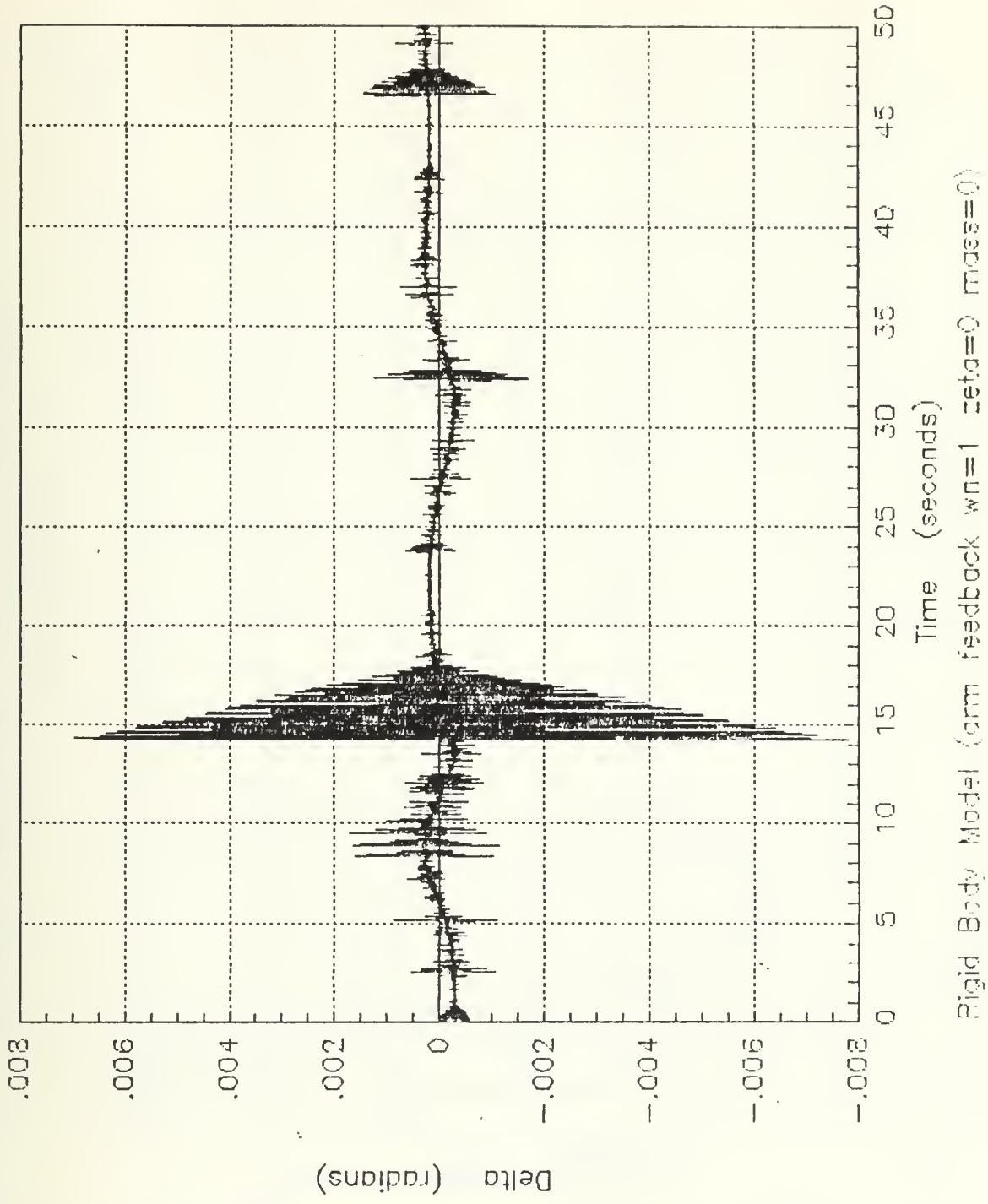

Figure 12. Rigid Body Model Arm feedBack (small motion)

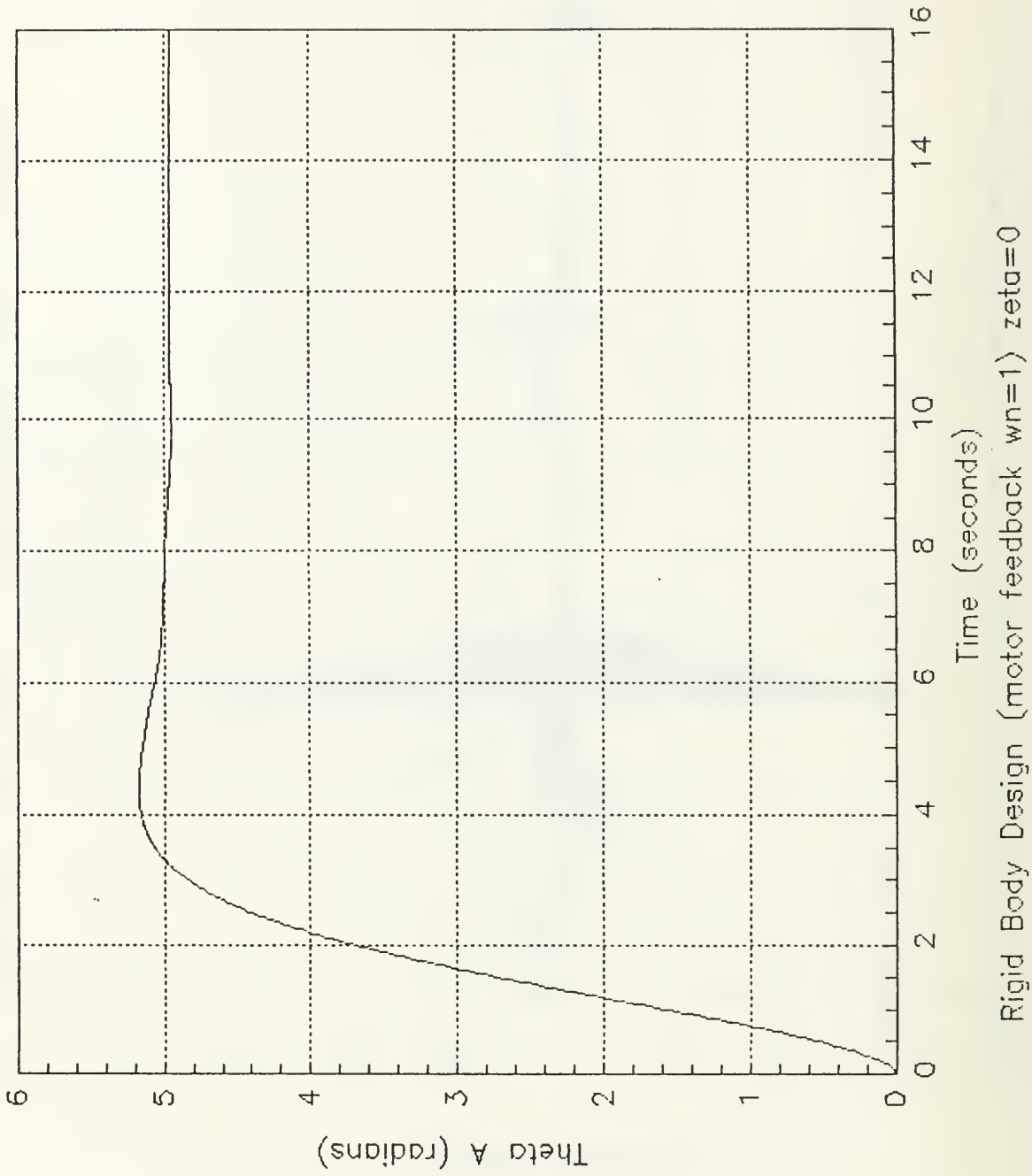

Figure 13. Rigid Body Model Motor feedback (θ_a)

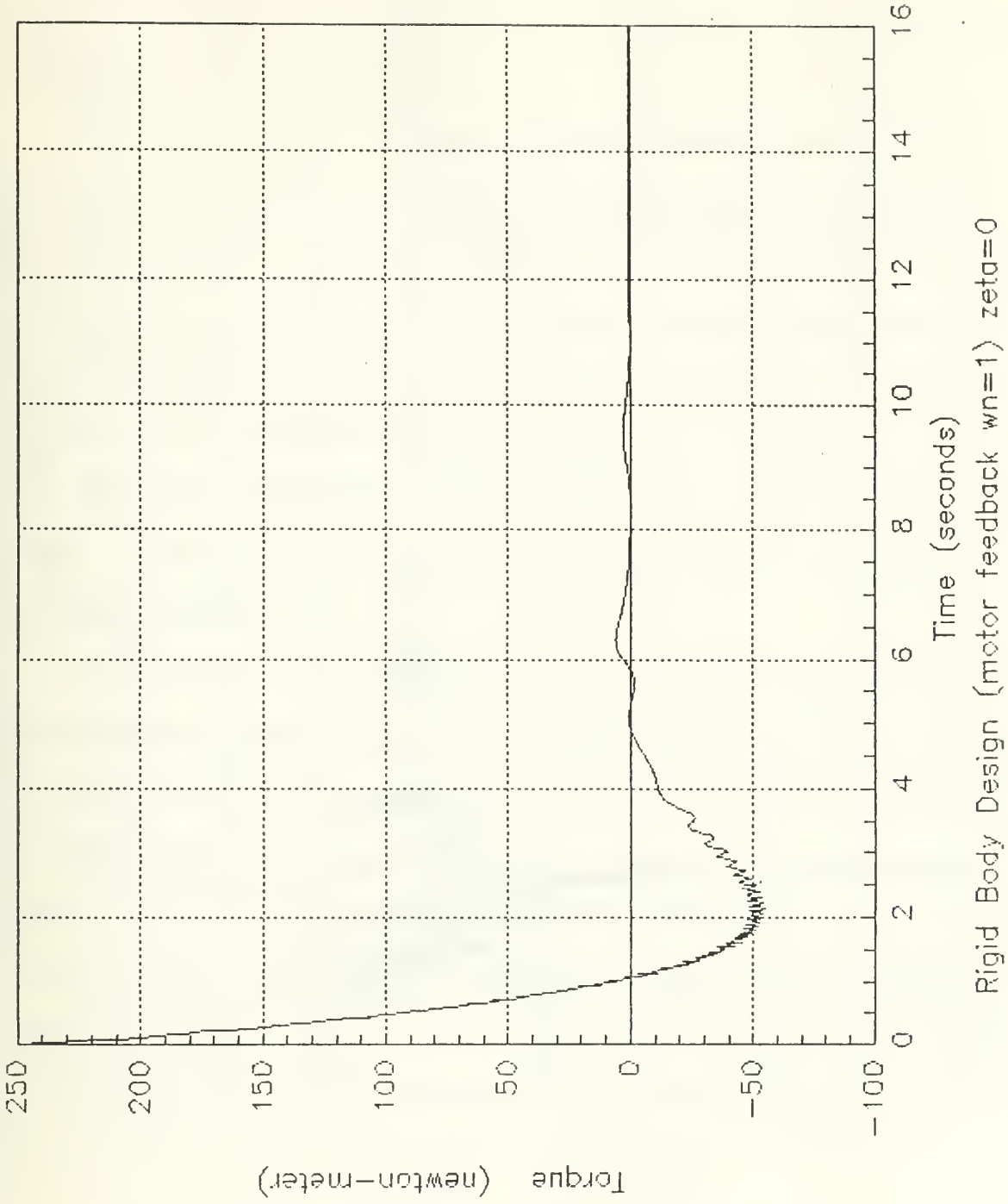

Figure 14. Rigid Body Model Motor feedback (torque)

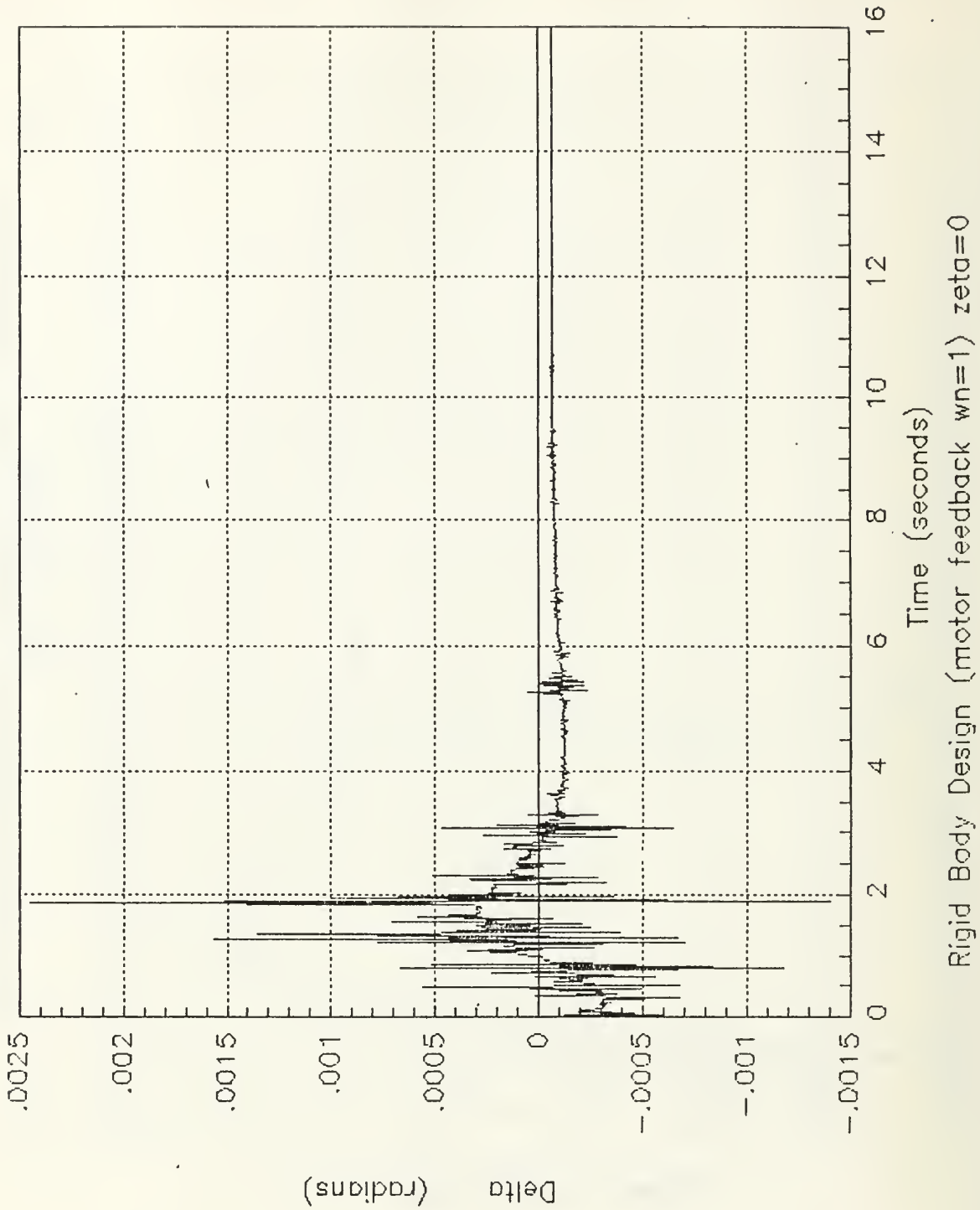

Figure 15. Rigid Body Model Motor feedBack (small motion)

Figure 17, and Figure 18. The graphs for the motor feedback are shown in Figure 19, Figure 20, Figure 21, and in Figure 22.

As shown in Figure 16, the systems response time has increased, but after 40 seconds it still has not settled out. The motor feedback settling time has decreased to 1.9 seconds (Figure 19). Another area to look at is the increased in the level of small motion (Figure 21) and (Figure 18). The mechanical vibration has increased for both cases but the level is still less for the motor feedback configuration. The torque requirements for motor feedback case (Figure 20) has increased by a factor of 14.

Appendix E presents additional simulation runs for the motor feedback configuration. In each situation a step input with a desired final position of $\theta_d = 5$ was used unless otherwise noted.

Although the controller was designed via pole placement using coefficients based on **ITAE** performance criteria, in the comparison between the two rigid body cases, the motor feedback case obviously demonstrated the best performance characteristics based on rise time, settling time, servo control mode amplitude difference, mechanical vibration and system respond time. The only weakness noted is in the area of torque requirements. The levels for the motor feedback configuration far exceeded the requirements for the arm feedback case (by 32 times for $\omega_n = 1$ and 46 times for $\omega_n = 4$). The results of the rigid body comparisons are listed in Table 1 on page 41.

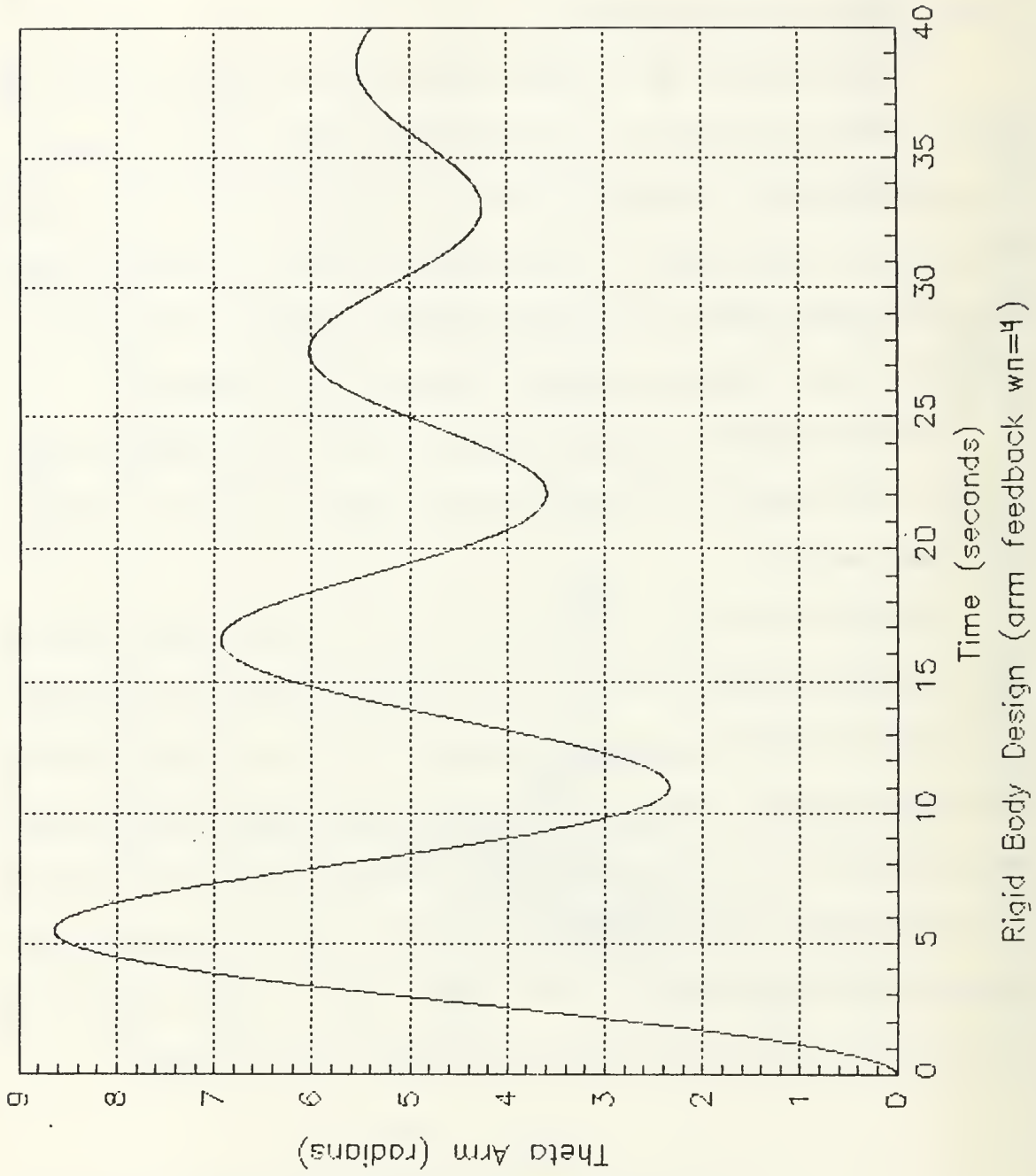

Figure 16. Rigid Body Model Arm feedBack (θ_a)

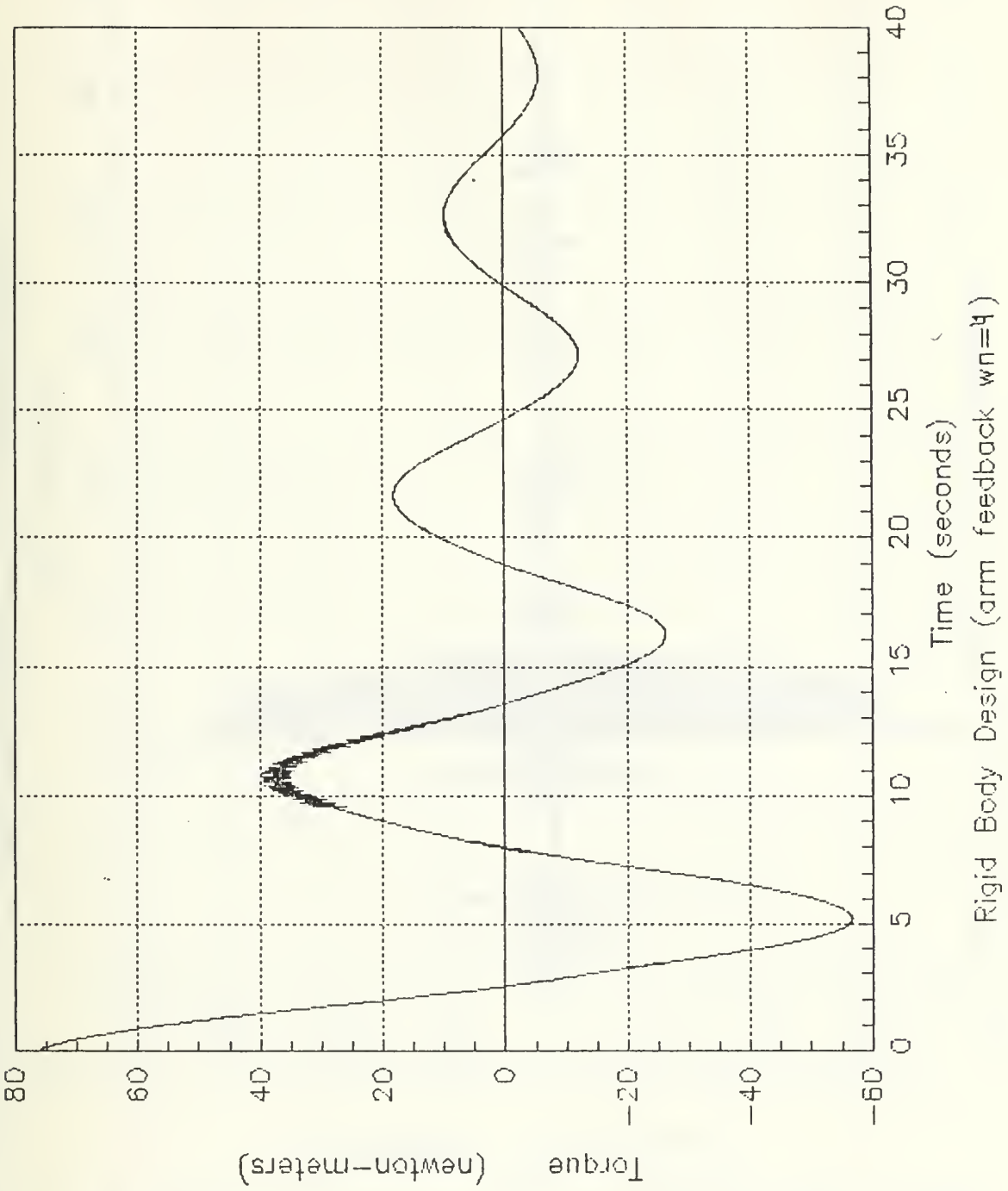

Figure 17. Rigid Body Model Arm feedBack (torque)

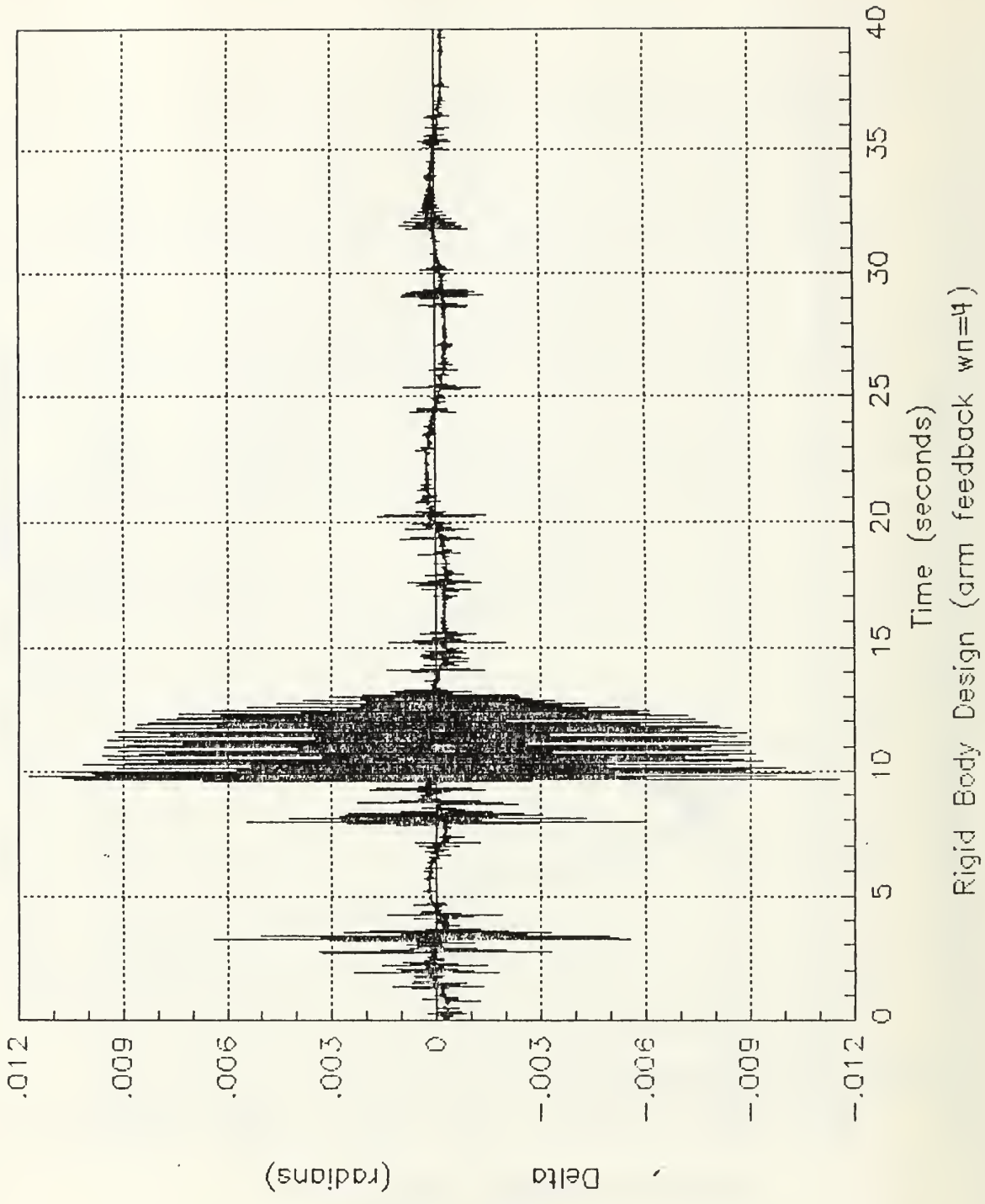

Figure 18. Rigid Body Model Arm feedBack (small motion)

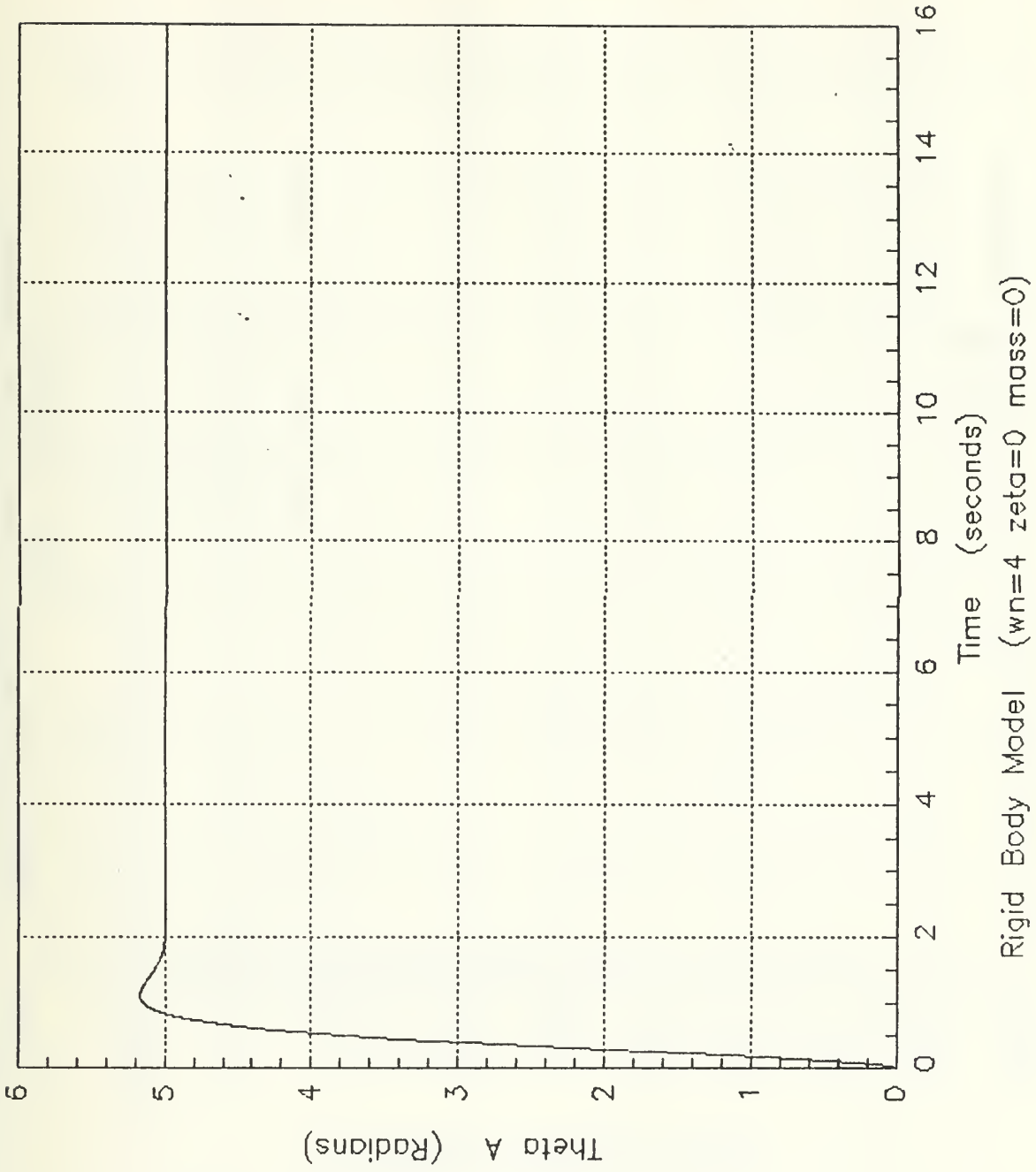

Figure 19. Rigid Body Model Motor feed back (θ_a)

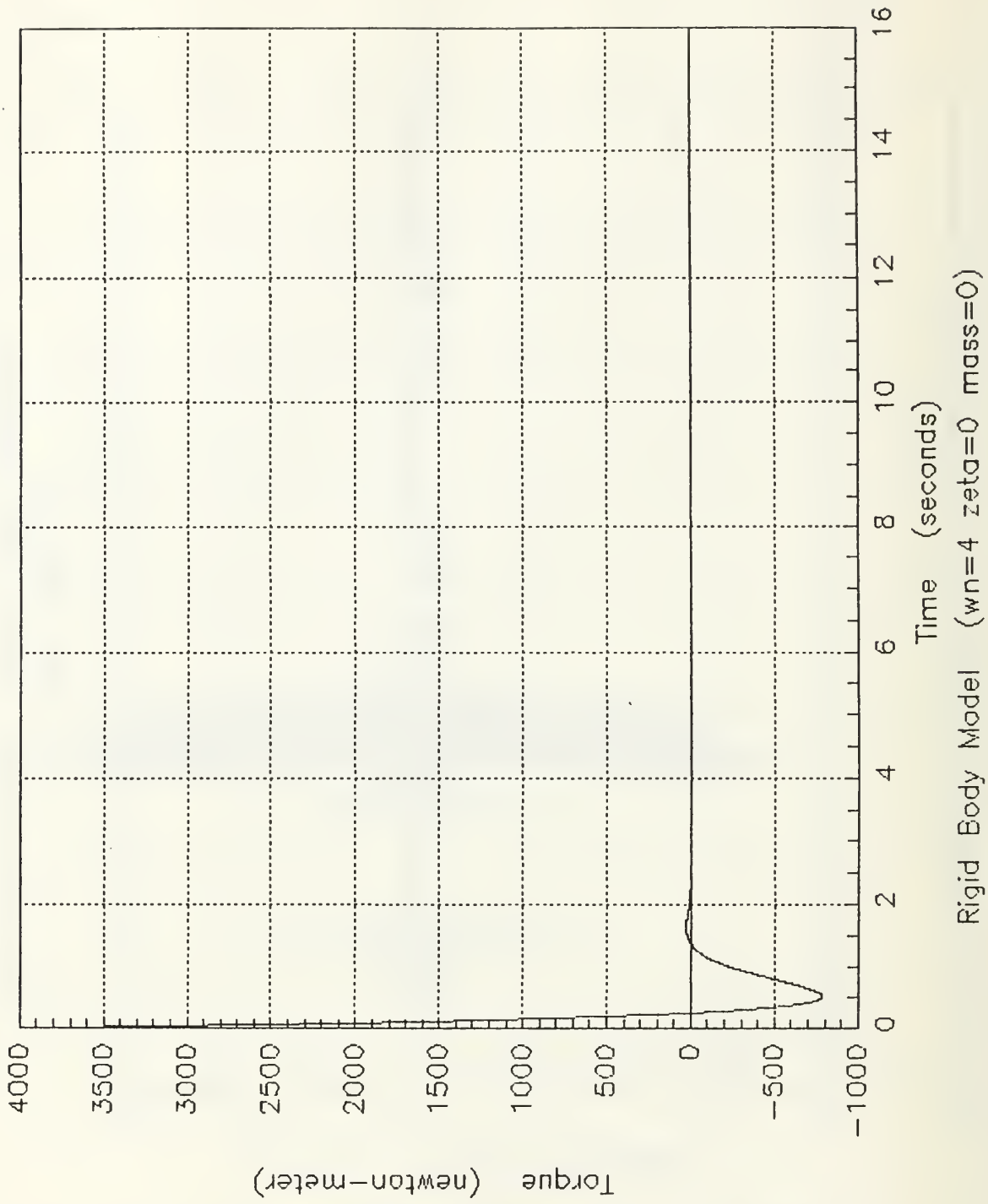

Figure 20. Rigid Body Model Motor feedBack (torque)

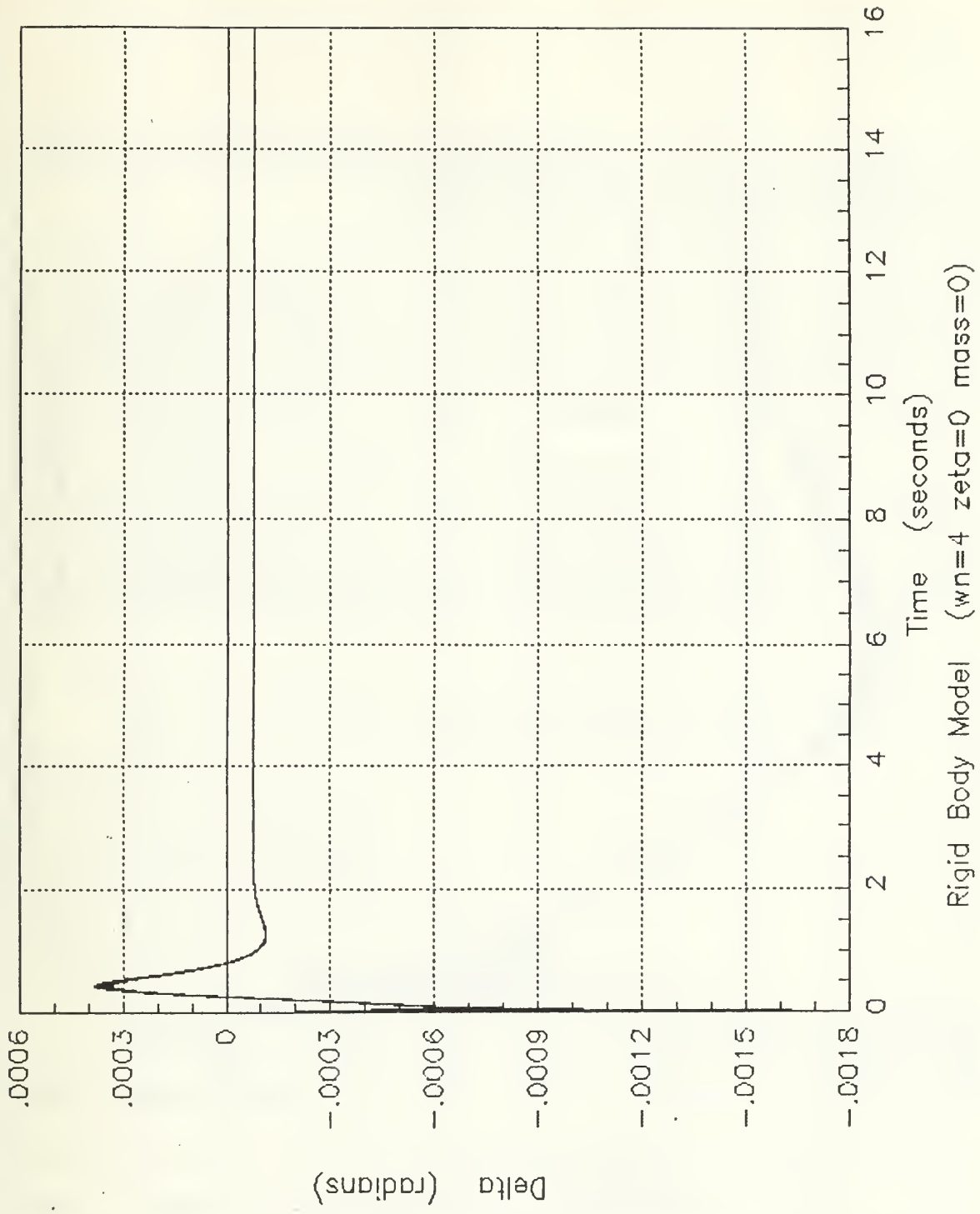

Figure 21. Rigid Body Model Motor feedBack (small motion)

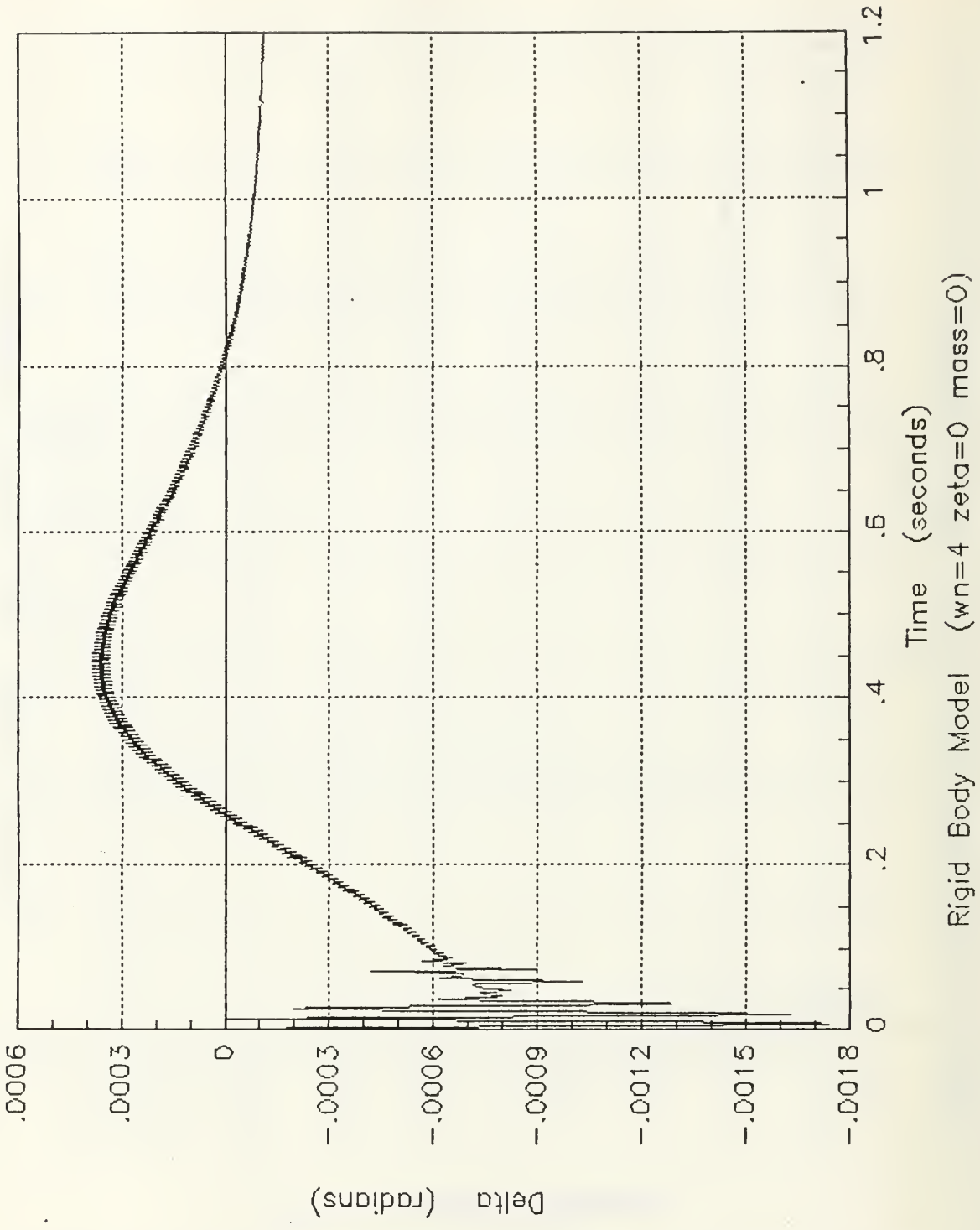

Figure 22. Rigid Body Model Motor feedBack (small motion)

Table 1. RIGID BODY MODEL COMPARISON

	ARM FEEDBACK		MOTOR FEEDBACK	
	wn = 1 ζ = 0	wn = 4 ζ = 0	wn = 1 ζ = 0	wn = 4 ζ = 0
Rise Time (seconds)	11.8	3.0	3.4	0.8
Settling Time (seconds)	*	*	7.4	1.9
Maximum Torque (N-m)	7.8	76.0	248.0	3500.0
Servo Control Mode Amplitude Absolute difference (radians)	0.0001	0.0002	0.0003	0.0004
Mechanical Vibration (major peak to peak average) (radians)	0.008	0.018	0.0010	0.0019
Slope (Speed) (rad/s)	0.46	1.66	1.47	6.67

* Note the graph had not settled out by the end of the simulation run.

While the motor feedback case seems promising, there still is a need for improvements in the areas of:

1. Lower Torque Requirements
2. Less Mechanical Vibrations
3. Lower Servo Mode Small Motion Differences
4. Less Mechanical Electric wear on actuator

Therefore the flexible-body control will be compared against the rigid-body control using motor feedback to determine if there is an improvement in performance characteristics. Due to the fact the Flexible-Body is a fourth order controller, the servo speed input will be run slightly higher in order to make realistic comparisons. A point to point and trajectory tracking control scheme were used. Added mass was analyzed in the simulations also.

B. FLEXIBLE-BODY CONTROLLER

1. Point to Point Control - No Load

The graphs for motor feedback are shown in Figure 13, Figure 14, and Figure 15. The graphs for the flexible body controller are shown in Figure 23, Figure 24, and Figure 25.

Reviewing the flexible-body graphs and the rigid-body graphs, the flexible-body controller provides improvements in all characteristic areas with a decrease in required torque. All this occurs with the flexible-body controller moving at a faster servo input speed. Other than one large spike at 0.8 seconds, the flexible-body model exhibited 6 times less mechanical vibration. The servo control mode amplitude difference was similar between the two cases. With an increase in input servo speed, the servo control mode amplitude difference and mechanical vibrations increased as expected.

The second simulation analyzed the effect of increased servo input speed on the performance characteristics of the two controllers. As seen in Table 2 on page 46, the flexible-body controller still requires less torque, generates less mechanical vibration and has a steeper slope than the rigid-body controller. The steeper slope equates to a more responsive system. The servo control mode amplitude difference was also lower than the rigid-body model. The graphs of these simulation runs are in Appendix E.

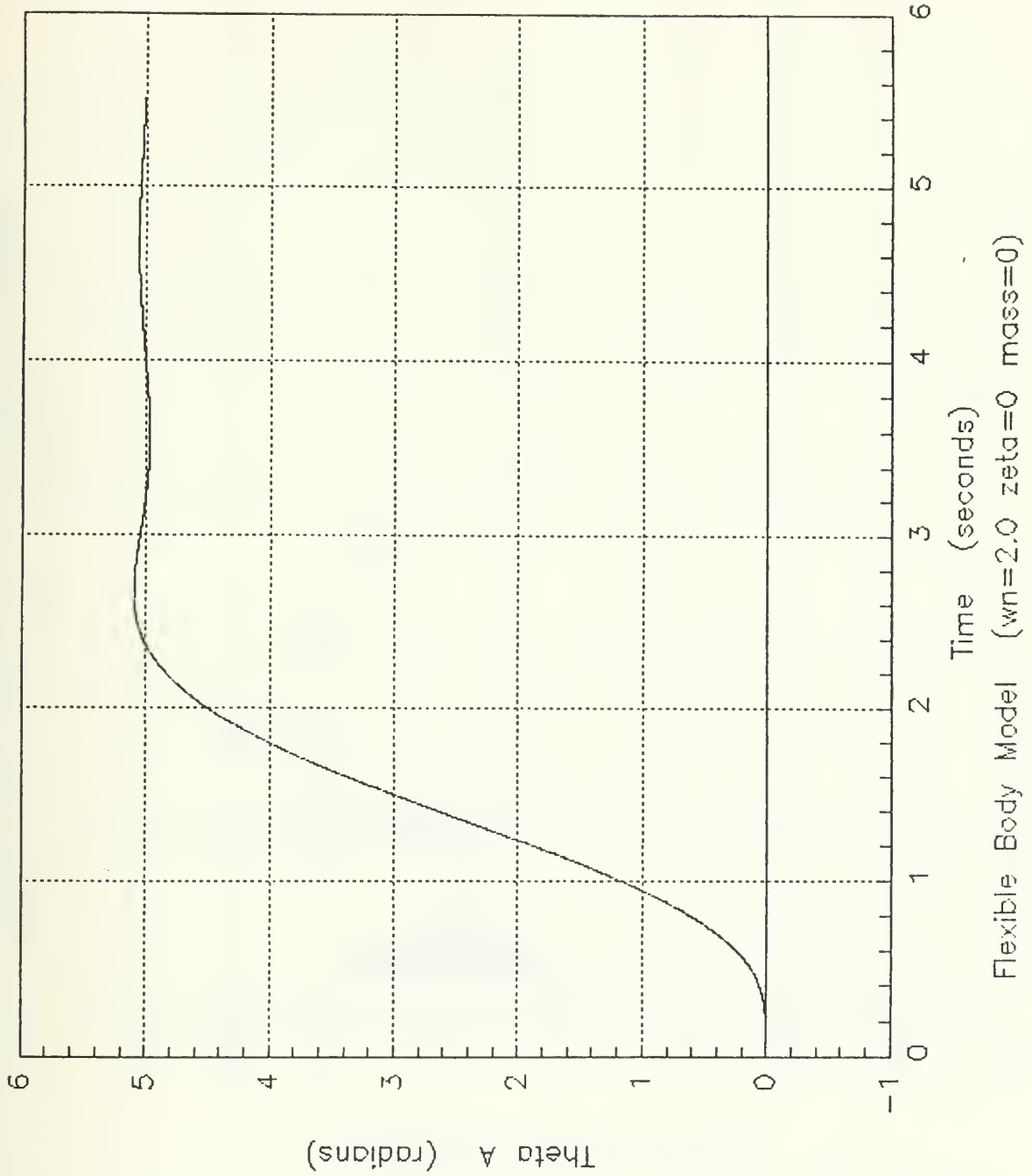

Figure 23. Flexible Body Model (θ_a)

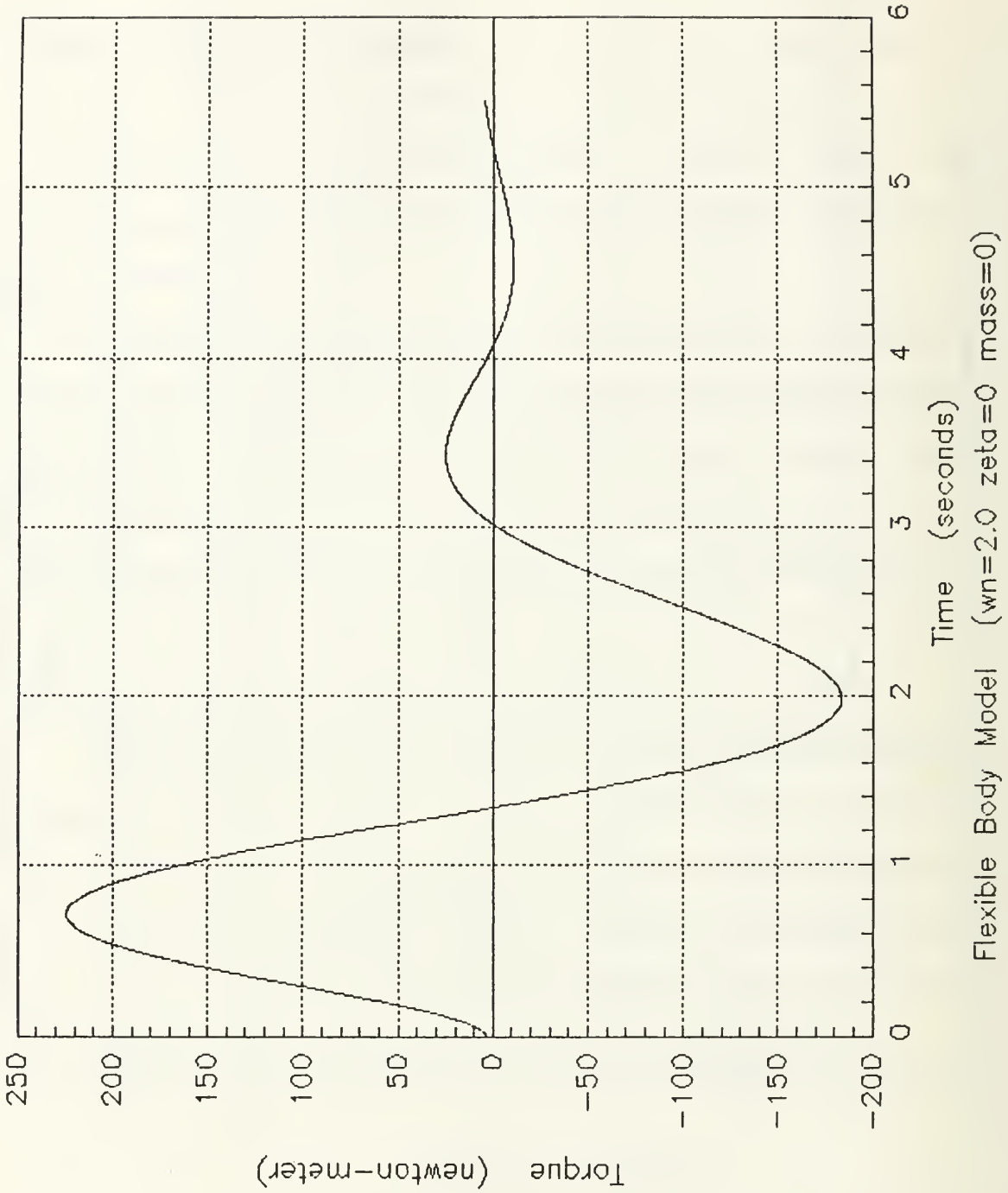

Figure 24. Flexible Body Model (torque)

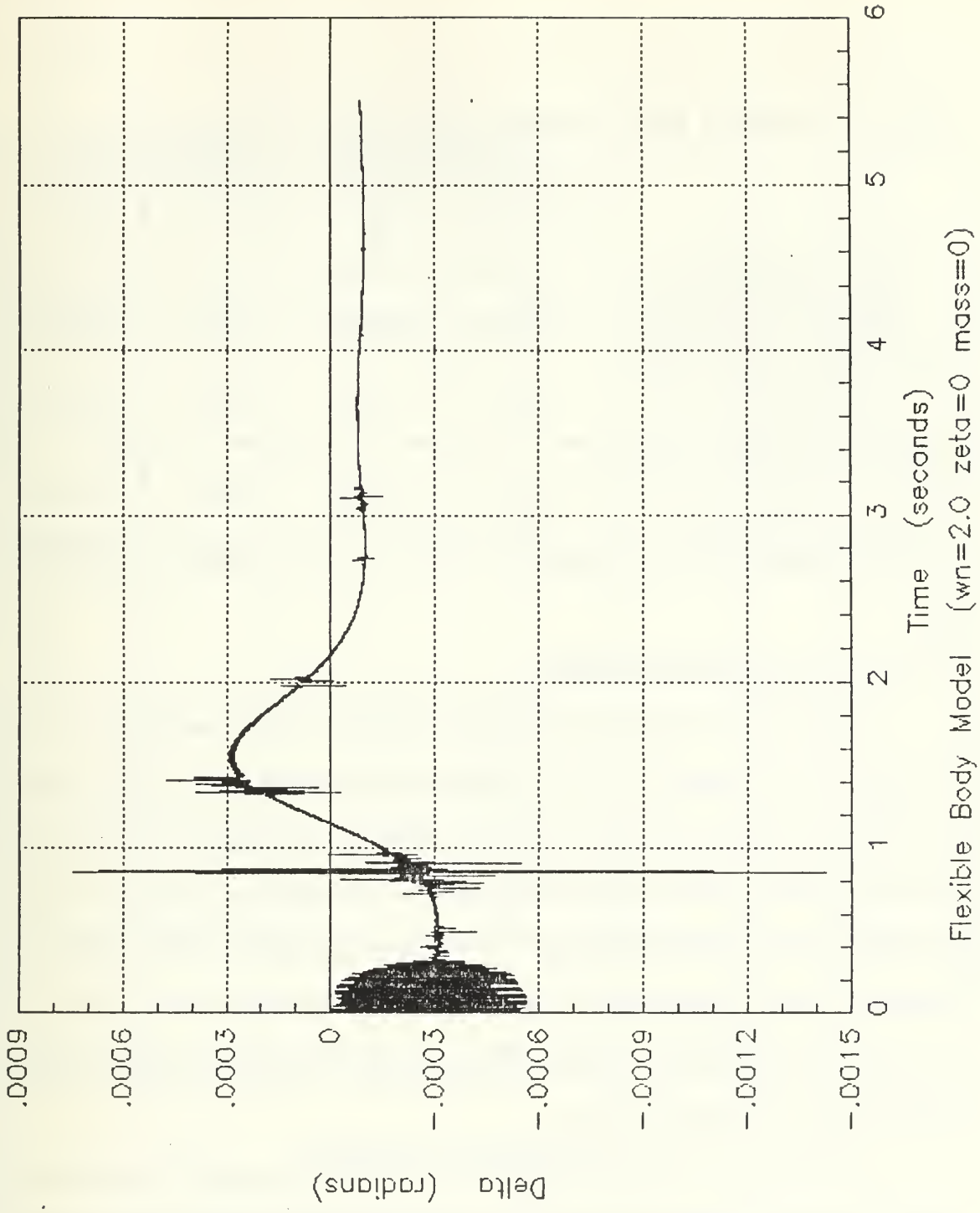

Figure 25. Flexible Body Model (small motion)

Table 2. FLEXIBLE BODY VS RIGID BODY MODEL - NO LOAD

	Flexible Body Model		Rigid Body Model	
	wn = 2 ζ = 0	wn = 4 ζ = 0	wn = 1 ζ = 0	wn = 3 ζ = 0
Rise Time (seconds)	2.2	**0.8**	3.4	**1.0**
Settling Time (seconds)	3.2	**2.1**	7.4	**2.5**
Maximum Torque (N-m)	222.0	**870.0**	248.0	**1910.0**
Servo Control Mode Amplitude Absolute difference (radians)	0.0003	**0.0003**	0.0003	**0.0003**
Mechanical Vibration (major peak to peak average) (radians)	0.0005	**0.0005**	0.0010	**0.0015**
Slope (Speed) (rad/s)	2.27	**6.25**	1.47	**5.00**

2. Load and Speed Considerations

Since the main purpose for studying a controller is to determine if it can perform its designed tasks, a comparison of two different loads (1.36 kg and 2.5 kg) and various speeds were investigated in order to study the difference in capabilities between the two methods or control. Again since the flexible-body is a fourth order controller, the servo input speed was ran slightly higher in order to allow more realistic comparisons. The comparable speeds used were ω_n = 1 and ω_n = 3 for rigid-body control and ω_n = 2 and ω_n = 4 for flexible-body control. The graphs of the robot arm positions can be seen in Figure 26 through Figure 33.

As can be seen in Table 3 on page 55 and Table 4 on page 56, as the load increases, the torque requirements has increase by a factor of 8 (from 312 N-m to 2505 N-m for 1.36 kg and 370 N-m to 2900 N-m for 2.5 kg) for the rigid-body model but the flexible-body model experienced only an increase of a factor of 3.8 (from 231 N-m to 900 N-m for 1.36 kg and 238 N-m to 900 N-m for 2.5 kg). The servo control mode amplitude

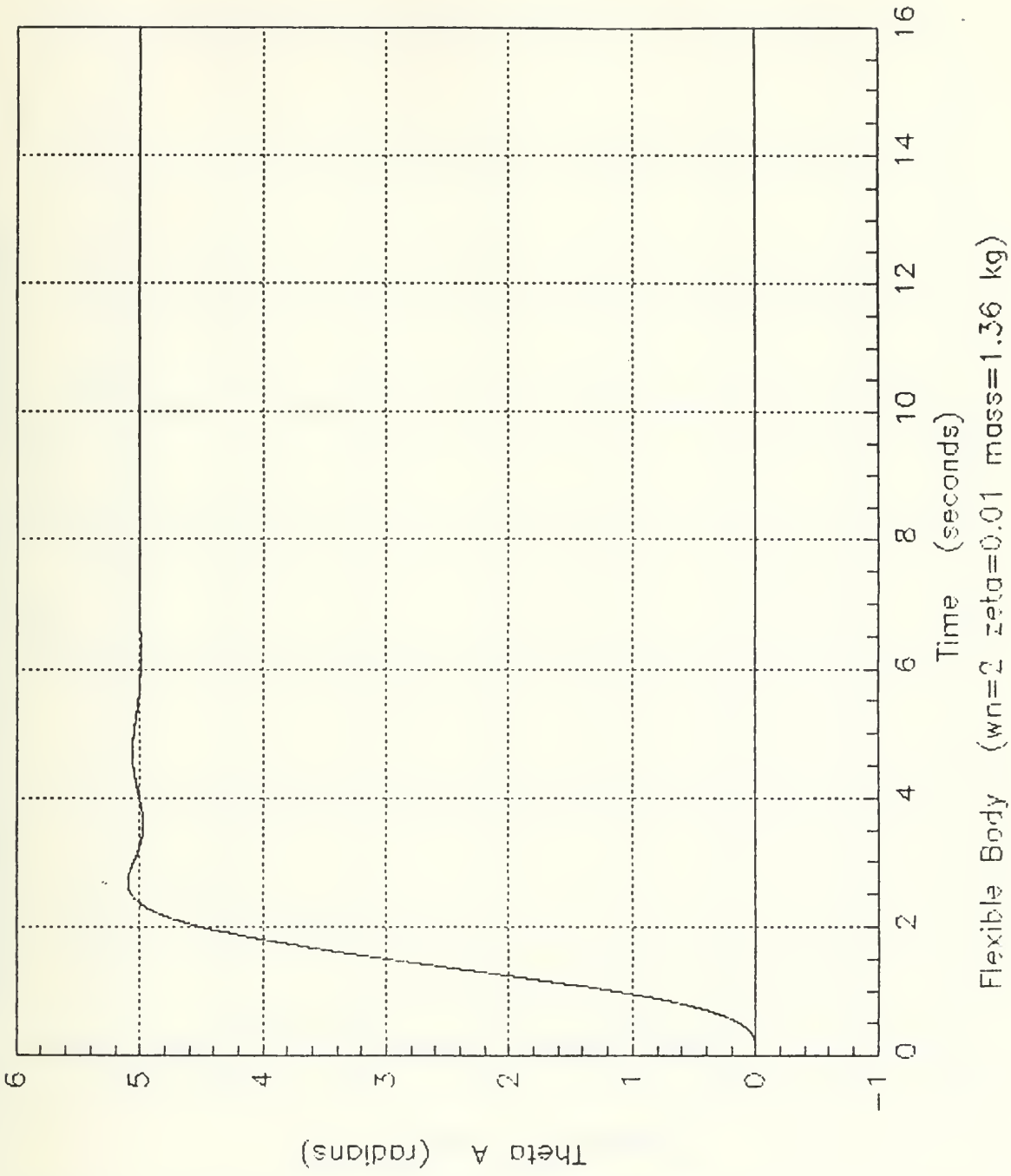

Figure 26. Flexible Body Model (θ_a)

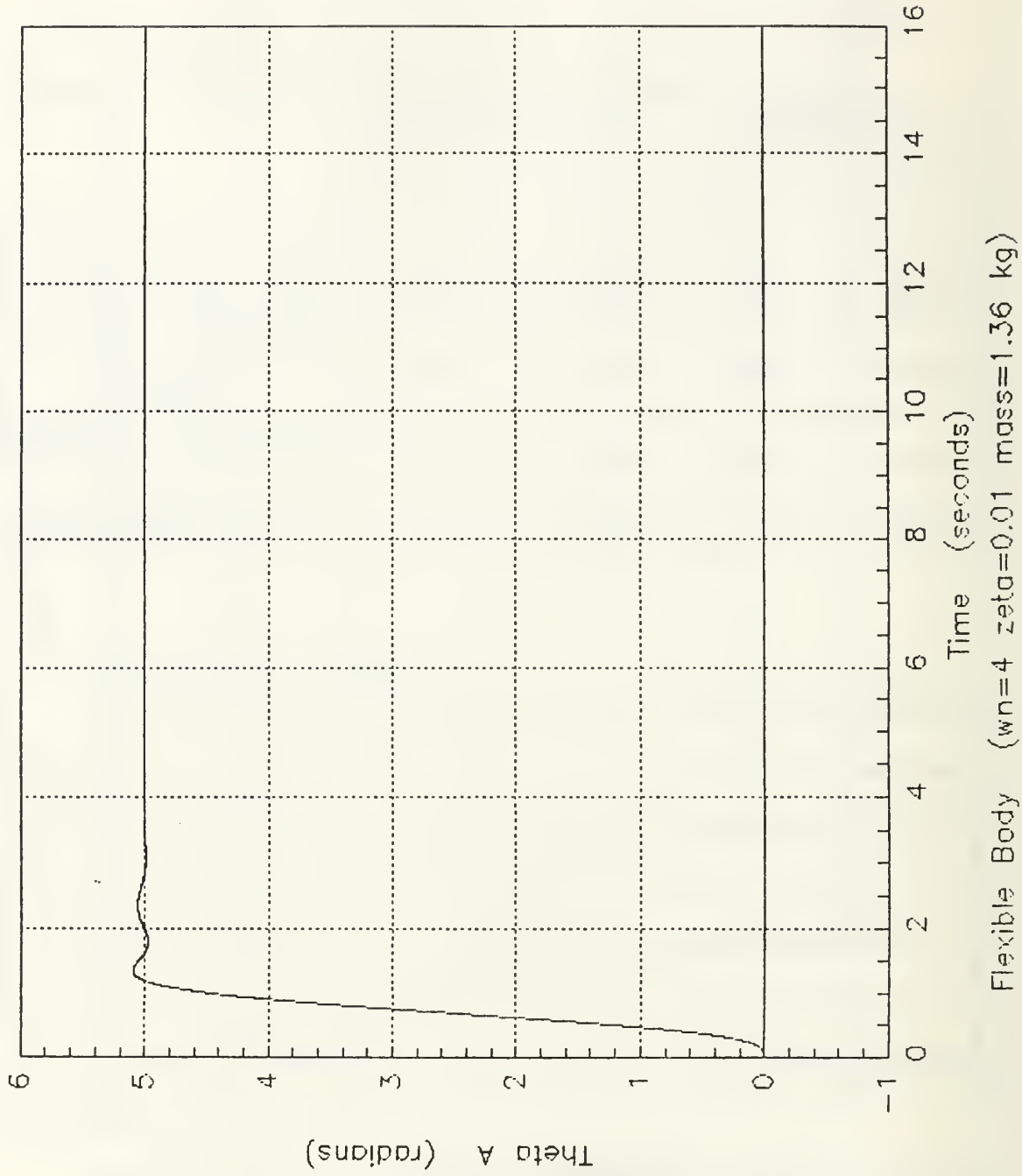

Figure 27. Flexible Body Model (θ_a)

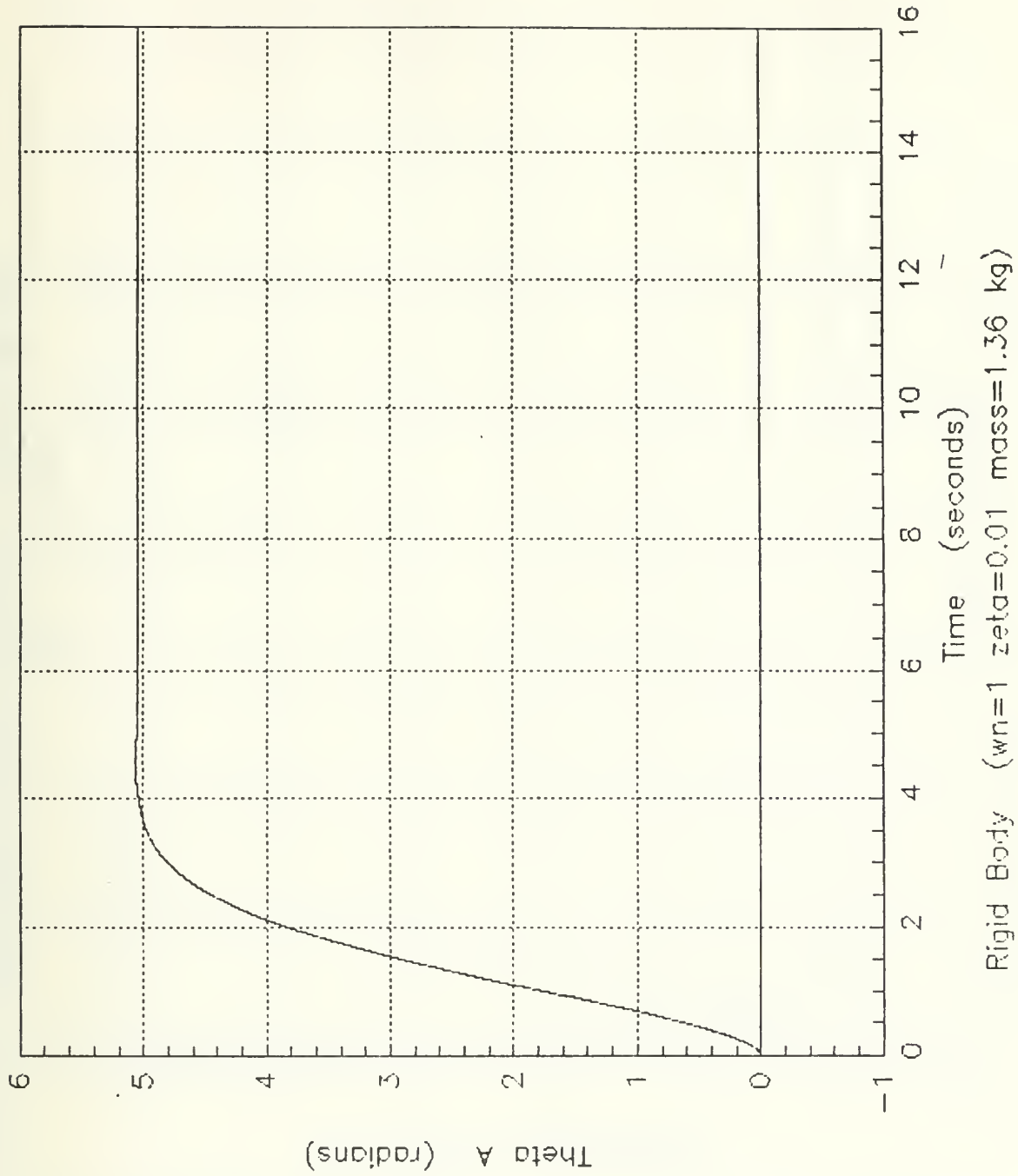

Figure 28. Rigid Body Model (θ_a)

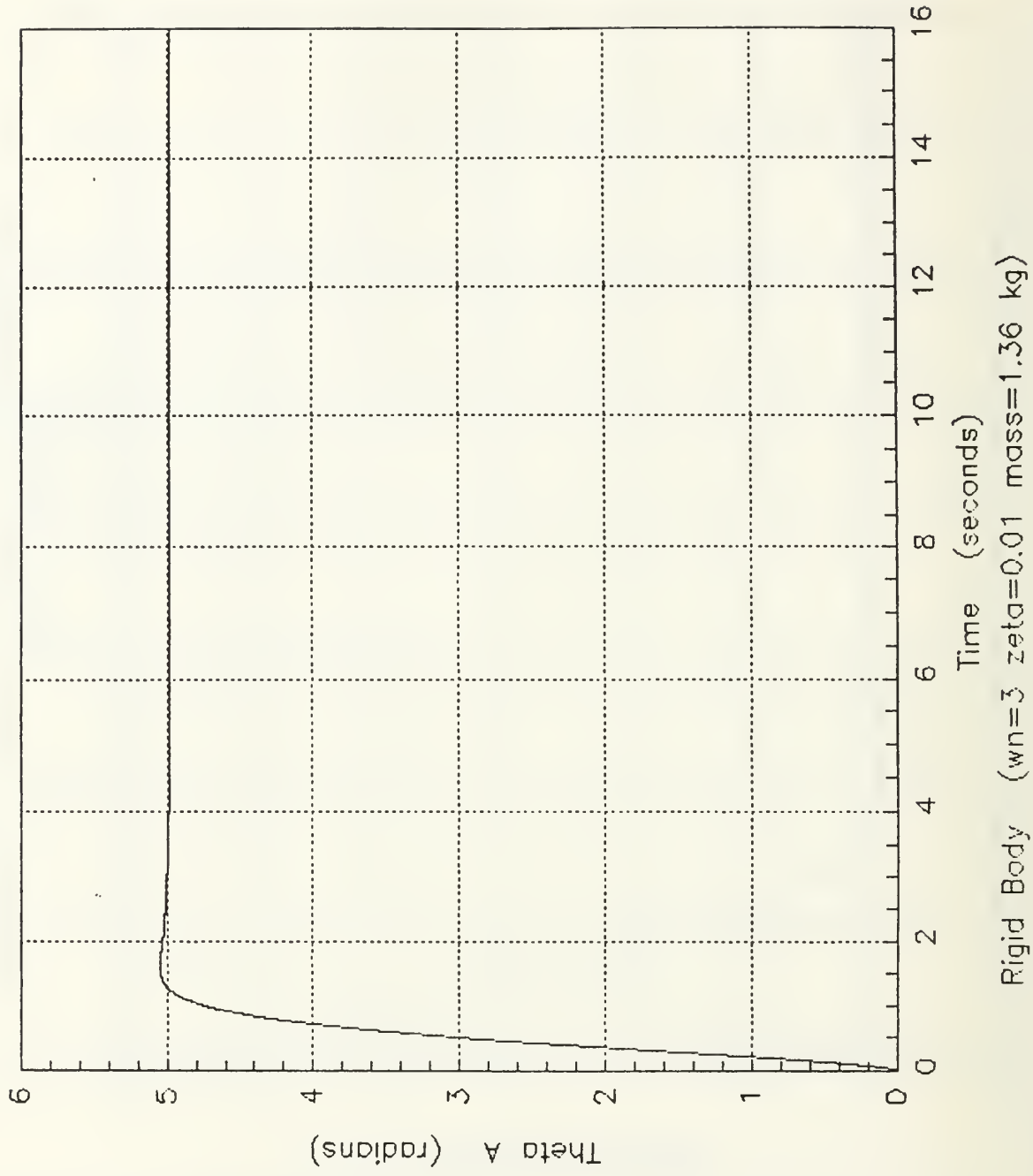

Figure 29. Rigid Body Model (θ_a)

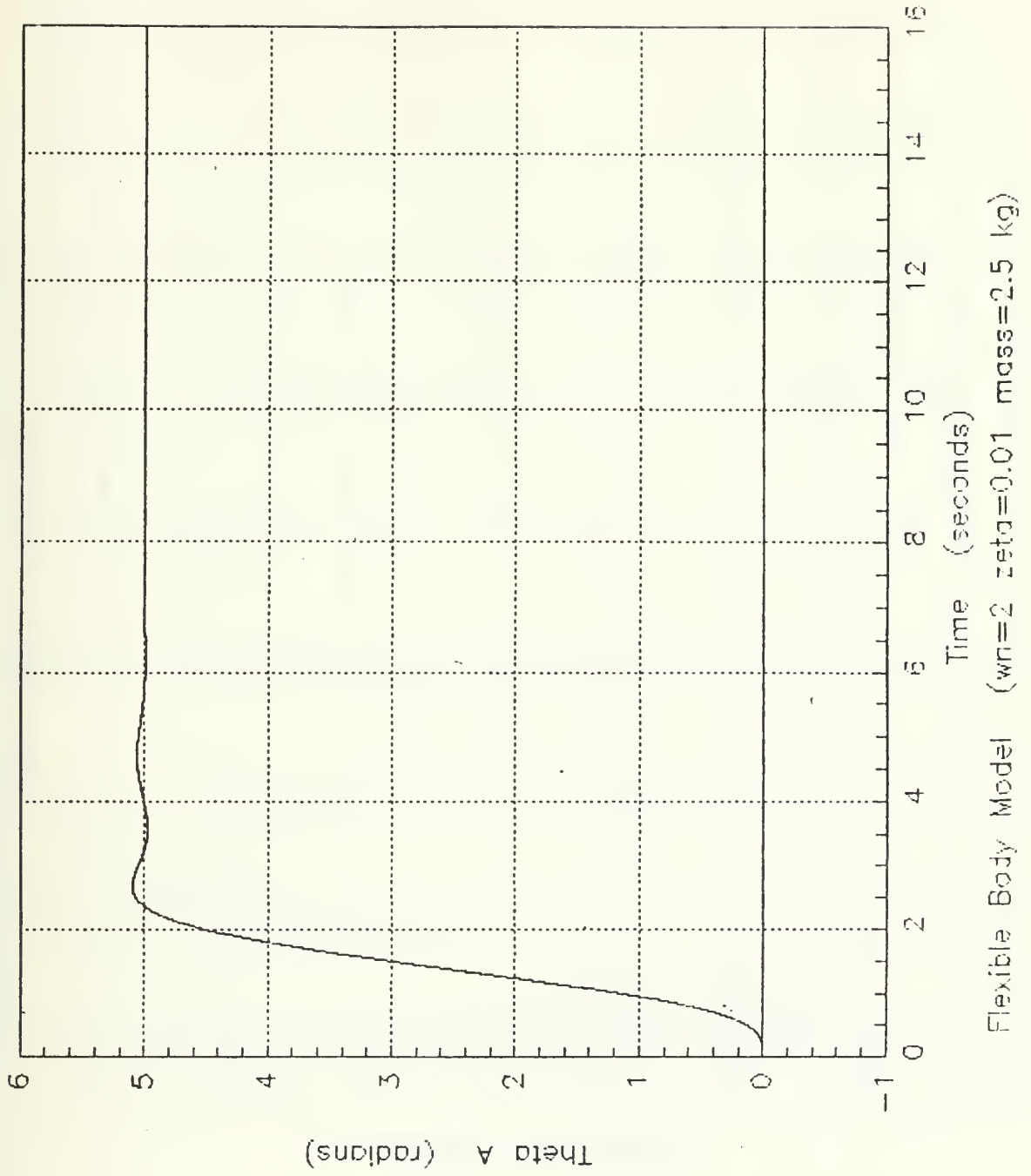

Figure 30. Flexible Body Model (θ_s)

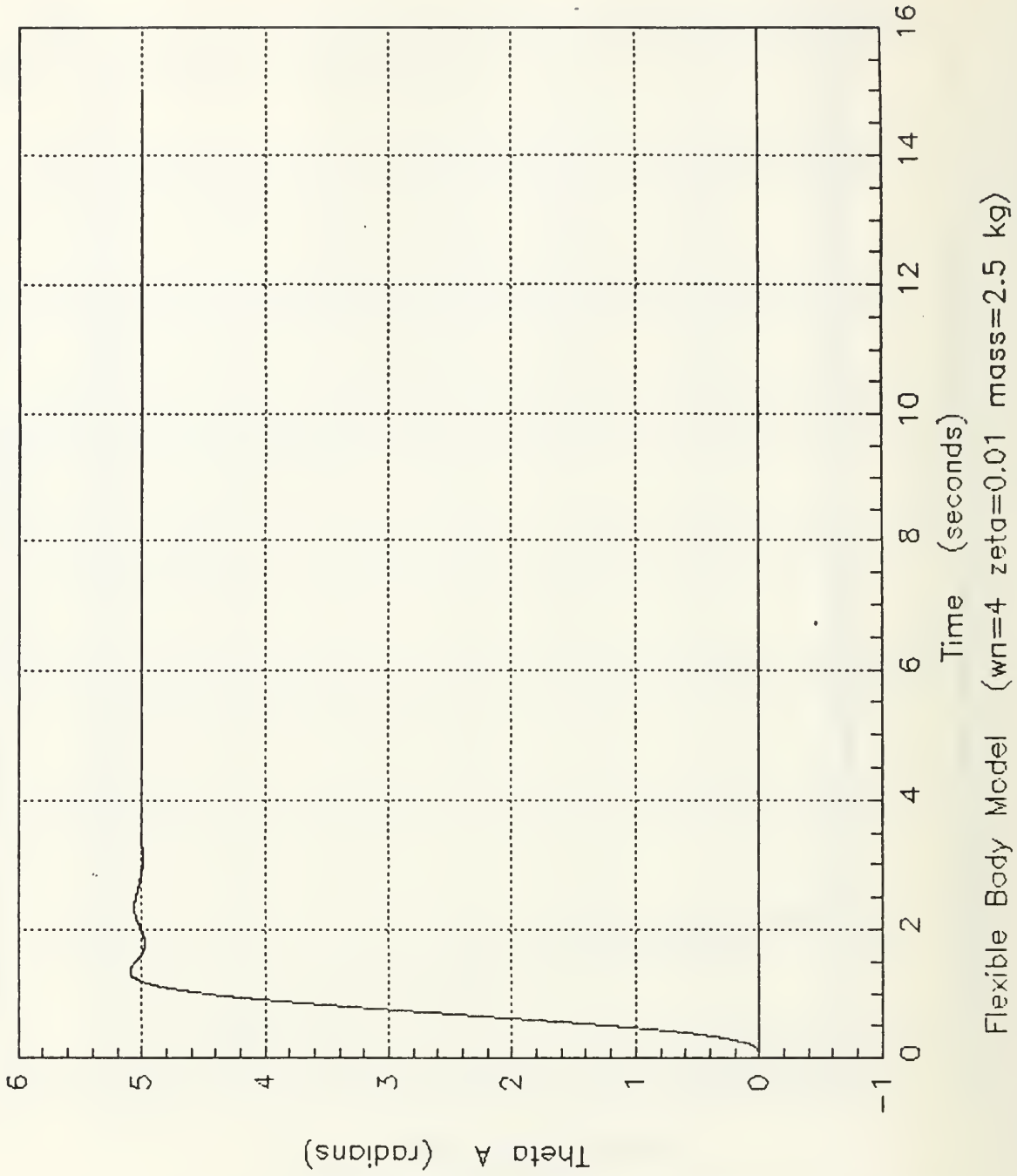

Figure 31. Flexible Body Model (θ_a)

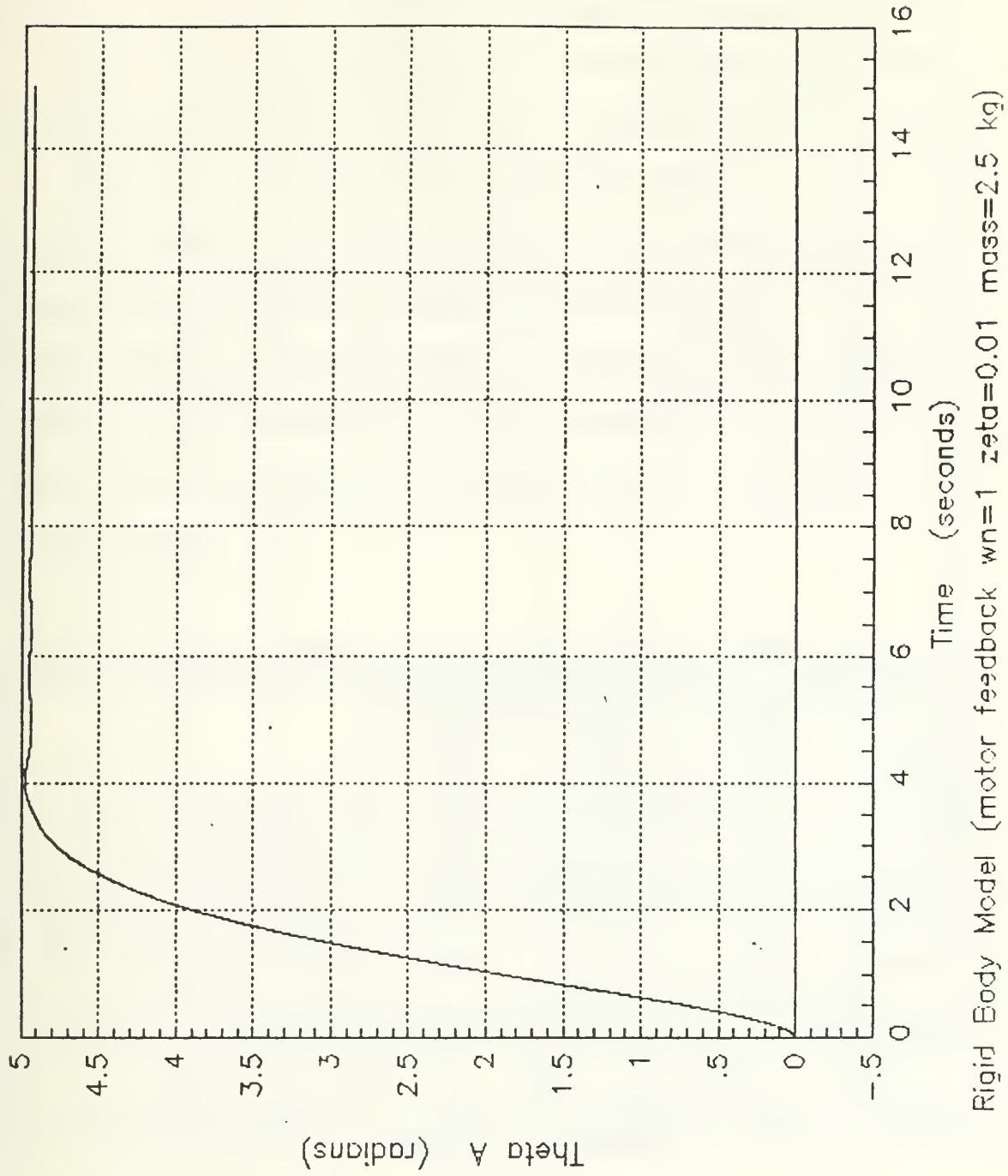

Figure 32. Rigid Body Model (θ_a)

Figure 33. Rigid Body Model (θ_s)

difference has increase by 2.5 for the rigid body model but only by 1.8 for the flexible-body controller for the same load change. The rigid-body controller experienced more mechanical vibration as can be seen in Table 3 on page 55 and Table 4 on page 56. Also the rise time has slowed down for the rigid-body controller as the load increases. As the servo speed input increases, the rigid-body control experience higher torque requirement changes, higher level of mechanical vibration and larger servo control mode amplitude differences. The flexible-body control requires less torque, experience less mechanical vibration and smaller servo control mode amplitude for a comparable speed increase. The rise time is quicker for flexible-body control for a comparable increase in servo input speed.

Table 3. FLEXIBLE BODY VS RIGID BODY MODEL - 1.36 KG

	Flexible Body Model		Rigid Body Model	
	wn = 2 ζ = 0.01	wn = 4 ζ = 0.01	wn = 1 ζ = 0.01	wn = 3 ζ = 0.01
Rise Time (seconds)	2.3	1.3	3.7	1.8
Settling Time (seconds)	5.5	2.7	5.0	3.0
Maximum Torque (N-m)	231.0	900.0	312.0	2505.0
Servo Control Mode Amplitude Absolute difference (radians)	0.0037	0.0068	0.0025	0.0062
Mechanical Vibration (major peak to peak average) (radians)	0.0015	0.0015	0.0015	0.0045
Slope (Speed) (rad/s)	2.17	3.85	1.35	2.78

Table 4. FLEXIBLE BODY VS RIGID BODY MODEL - 2.5 KG

	Flexible Body Model		Rigid Body Model	
	wn = 2 ζ = 0.01	wn = 4 ζ = 0.01	wn = 1 ζ = 0.01	wn = 3 ζ = 0.01
Rise Time (seconds)	2.3	1.1	4.0	1.5
Settling Time (seconds)	5.5	2.8	6.0	4.0
Maximum Torque (N-m)	238.0	900.0	370.0	2900.0
Servo Control Mode Amplitude Absolute difference (radians)	0.0050	0.0090	0.0034	0.0080
Mechanical Vibration (major peak to peak average) (radians)	0.0020	0.0025	0.0028	0.0070
Slope (Speed) (rad/s)	2.20	4.54	1.25	3.33

The mass increase had little effect on the performance of the flexible-body controller but the rigid-body controller stability has decrease. The robot arm position graphs for the rigid-body case exhibit little or no overshoot as required by the ITAE criteria used to design the controller. The mechanical vibration of the rigid-body control system has increased also for both a speed increase as well as a mass increase.

From the stand point of desirability, the flexible-body controller moves the added mass faster with less vibration or system wear, and with less torque. The flexible-body controller still continues to demonstrate superior performance characteristics even with a load placed at the tip position and a comparable speed increase.

The torque and small motion graphs can be viewed in Appendix E.

As shown by the graphs, the flexible-body controller again outperformed the rigid-body controller. The flexible-body controller requires less torque to move the added mass and does it at a faster speed. The mechanical vibration is less for the

Flexible-Body case even though the servo control mode difference is similar between the two controllers.

3. Trajectory Motion

The next simulation involved a trajectory tracking with and without an added mass. The trajectory tracking was a combination of a steady ramp input with a leveling off at 4 seconds and a desired arm position of five radians. Next, after holding the input at a constant value in order to maintain an arm position of five radians, a negative ramp input at 10.5 seconds was used to bring the arm back to its starting position at approximately 16 seconds. The results of the simulation are listed in Table 5. The graphs of the robot arm motion can be seen in Figure 34 through Figure 37. The other graphs are in Appendix E.

Table 5. FLEXIBLE BODY VS RIGID BODY MODEL - TRAJECTORY

	Flexible Body Model		Rigid Body Model	
	wn = 2 ζ = 0 no mass	wn = 2 ζ = 0 added mass 2.5 kg	wn = 1 ζ = 0 no mass	wn = 1 ζ = 0 added mass 2.5 kg
Desired Rise Time (seconds)	4.0	4.0	4.0	4.0
Settling Time (seconds) *	6.5	6.3	7.5	7.0
Maximum Torque (N-m)	92.0	110.0	98.00	140.0
Servo Control Mode Amplitude Absolute difference (radians)	0.00029	0.0026	0.0004	0.0080
Mechanical Vibration (major peak to peak average) (radians)	0.00020	0.00060	0.0010	0.0050
Desired Slope (Speed) (rad s)	1.25	1.25	1.25	1.25

* For the level portion of the trajectory between the two ramps only

As seen in Figure 34 through Figure 37, there is a more pronounced overshoot than found on the point to point control. This is due to the momentum left over in the

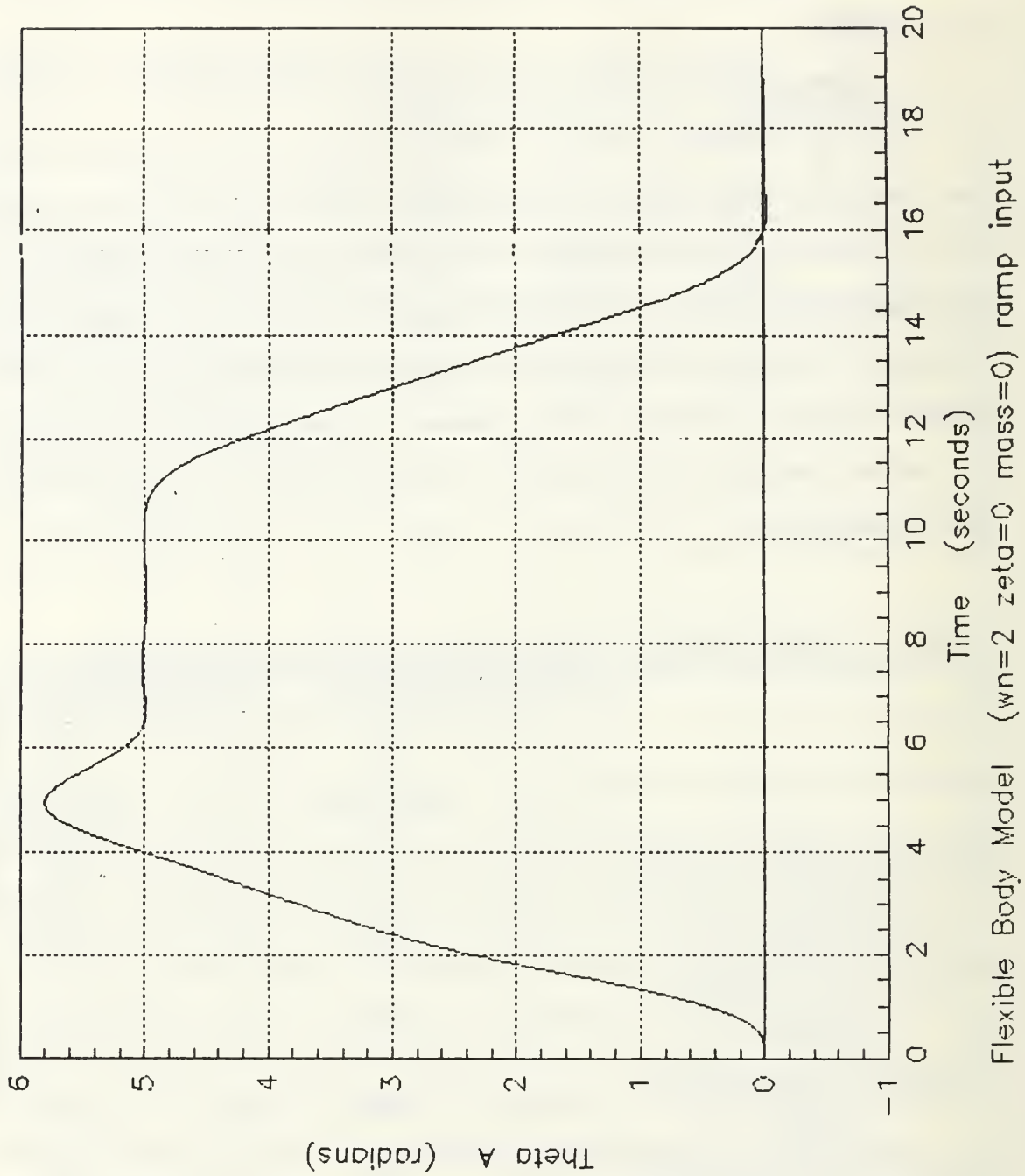

Figure 34. Flexible Body Model Trajectory (θ_a)

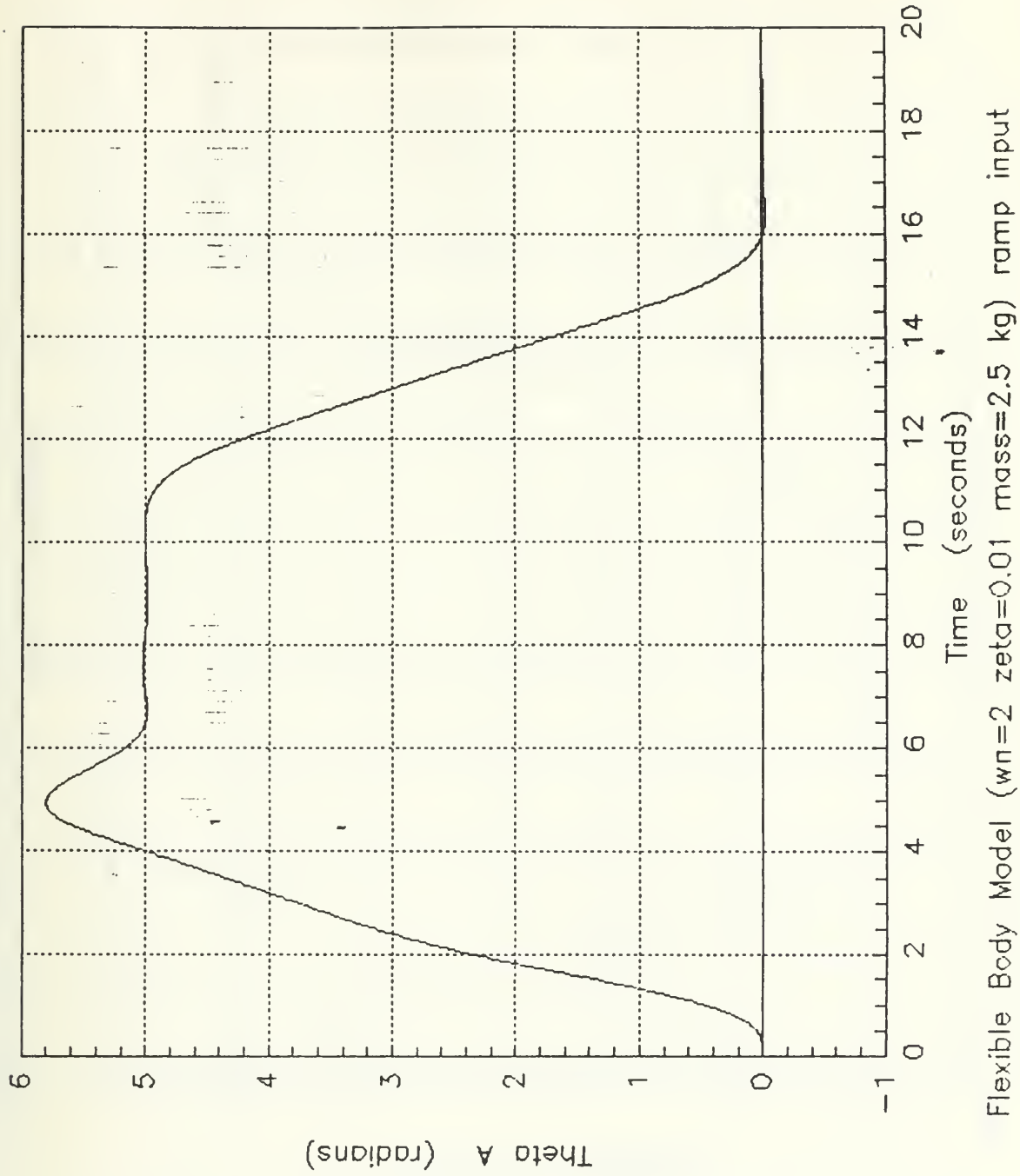

Figure 35. Flexible Body Model Trajectory (θ_a)

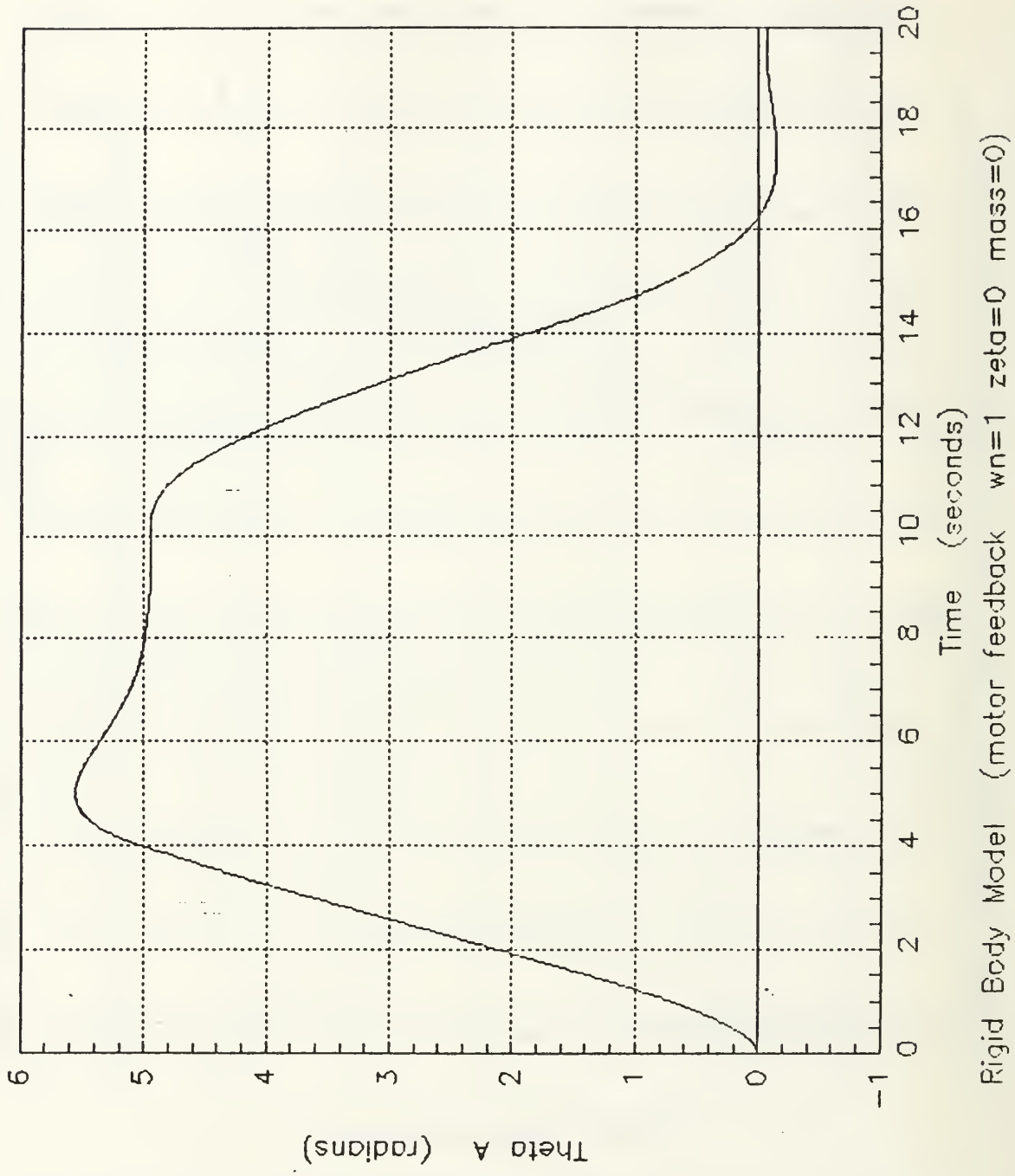

Figure 36. Rigid Body Model Trajectory (θ_a)

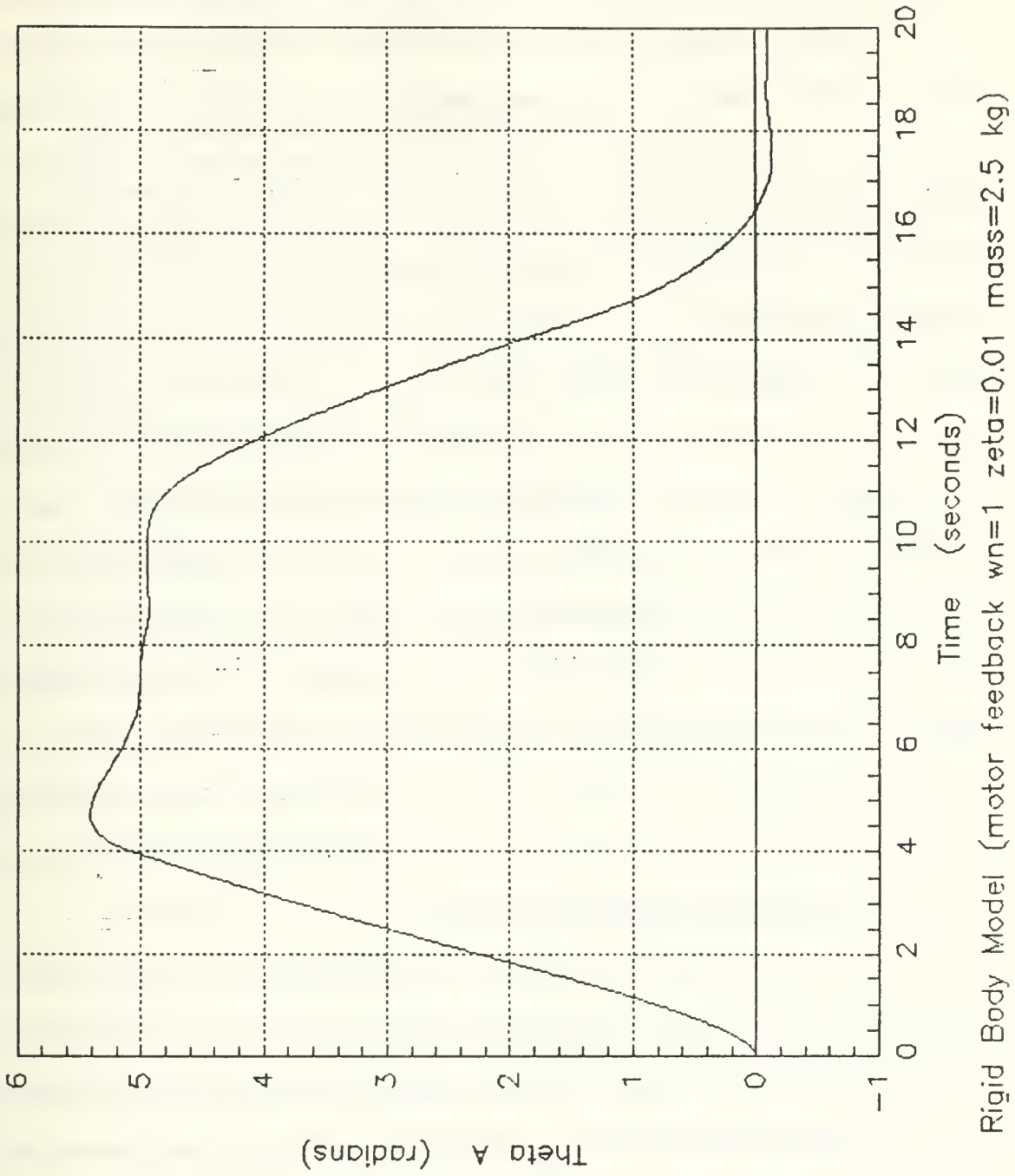

Figure 37. Rigid Body Model Trajectory (θ_a)

system as it reaches the desired position. It overshoots the position and gradually settles down to the final position. Due to the fact the controller gradually rises the arm to its desired position instead of a sudden jump similar to point to point control, less torque is required to perform the same movement. As a result less mechanical vibration is detected and the servo control mode amplitude is less. The desired trajectory was designed to lower the speed response to the desired trajectory at the saving of wear and tear on the equipment. With less torque required, this tracking method would consume less energy. The flexible-body controller still was able to outperform the rigid-body controller. With an increase in load, the flexible-body control servo control mode amplitude was less than the rigid-body control experiencing the same load increases. Also the mechanical vibration and the torque requirements were less for the flexible-body control. But even still the trajectory tracking allows larger masses to be handled at a lower required torque than do the point to point control method. For comparable speed increases, similar results were obtained. The level of mechanical vibration and the servo control mode amplitude were greater for the rigid-body control. The torque requirements were also greater for the rigid-body control. The the relative stability were similar for both the flexible-body and rigid-body control.

Overall observation is the trajectory tracking required less torque to move a mass than the point to point control required to move the arm with no mass attached. Also the loaded condition reached a relative stability condition faster than the unloaded case. An increase in load from 0 kg to 2.5 kg and comparable increases in servo input speeds resulted in an increase in the mechanical vibration and servo control mode amplitude for both controllers, with the rigid-body controller level of vibration being slightly higher than the flexible-body controller. But the overall level of mechanical vibration and servo control mode amplitude difference for the trajectory tracking method

is less than the vibration level and servo control mode amplitude difference for the point to point control method.

C. TORQUE SATURATION CONSIDERATIONS

The simulation analysis up to this point has not considered an input torque limitation on the motor for the actuator. Since the PUMA Robot arm is used as the model for this research work, the limitation of the model should be included in the analysis of the flexible body controller. The PUMA Robot arm was designed as a rigid body device which restricts any flexibility in its operation.

A saturation device was included in the design in order to study the performance characteristics of the controller controlling the PUMA Robot arm. A value of 49.2 newton-meters was used as the torque saturation point (49.2 newton-meters is the torque limit of the third joint motor on the PUMA arm).

First the performance of the Rigid Body case will be looked at and finally the Flexible Body case will be reviewed.

1. Rigid Body Saturation Case

For the graphs of the Rigid Body case with saturation included, see Figure 38 for point to point control and Figure 39 and Figure 40 for trajectory control. For the Rigid Body case, when the the torque value exceeded the preset limit of 49.2 newton-meters, the curve flattened out until the torque decreased below the preset limit. The servo control mode amplitude and the mechanical vibration results are similar to the cases without torque limitation included. The rise time for the saturation case is slower and the settling time is longer. For a summary of the rigid body simulations see Table 6 on page 67.

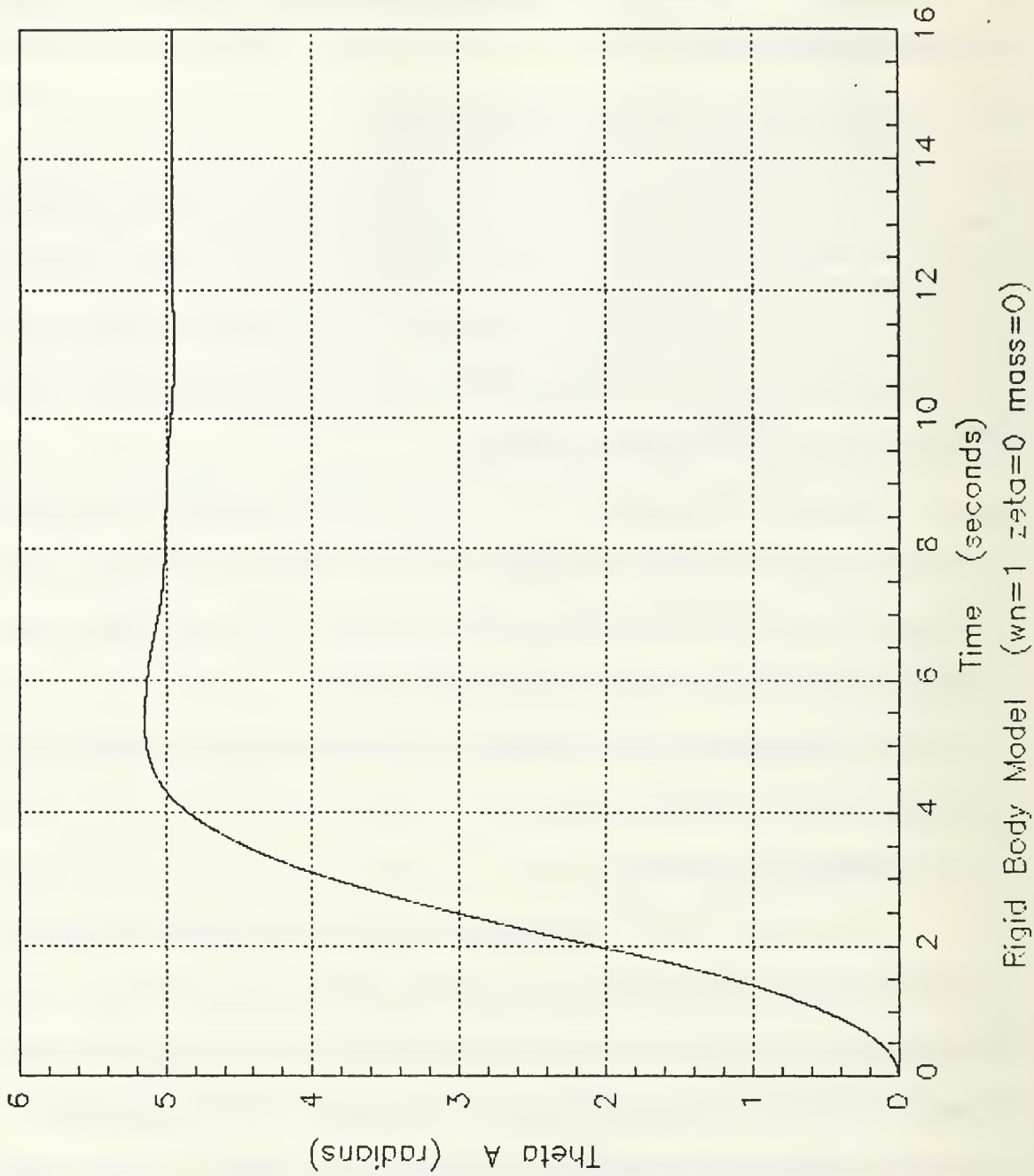

Figure 38. Rigid Body Model (saturation)

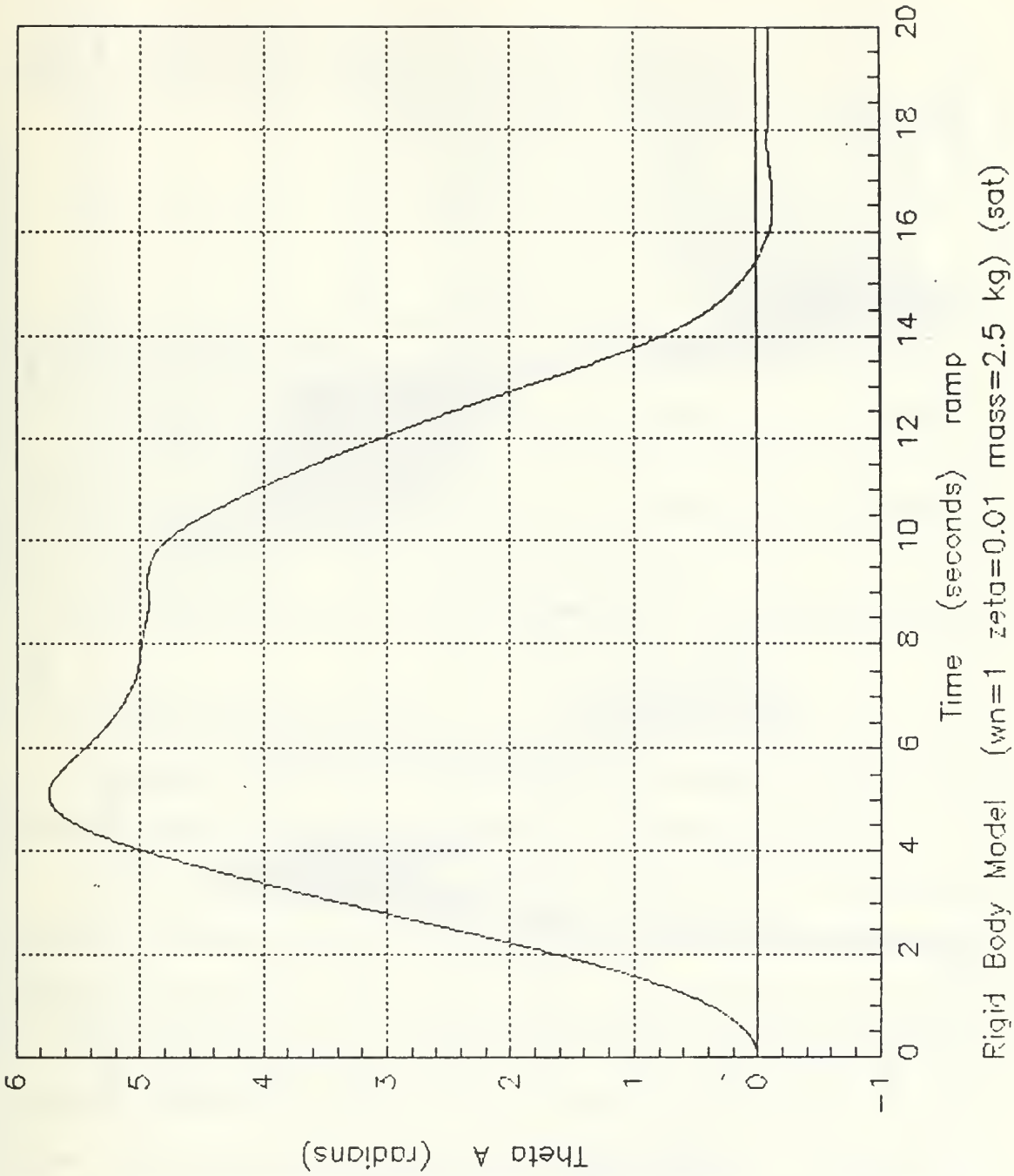

Figure 39. Rigid Body Model (saturation)

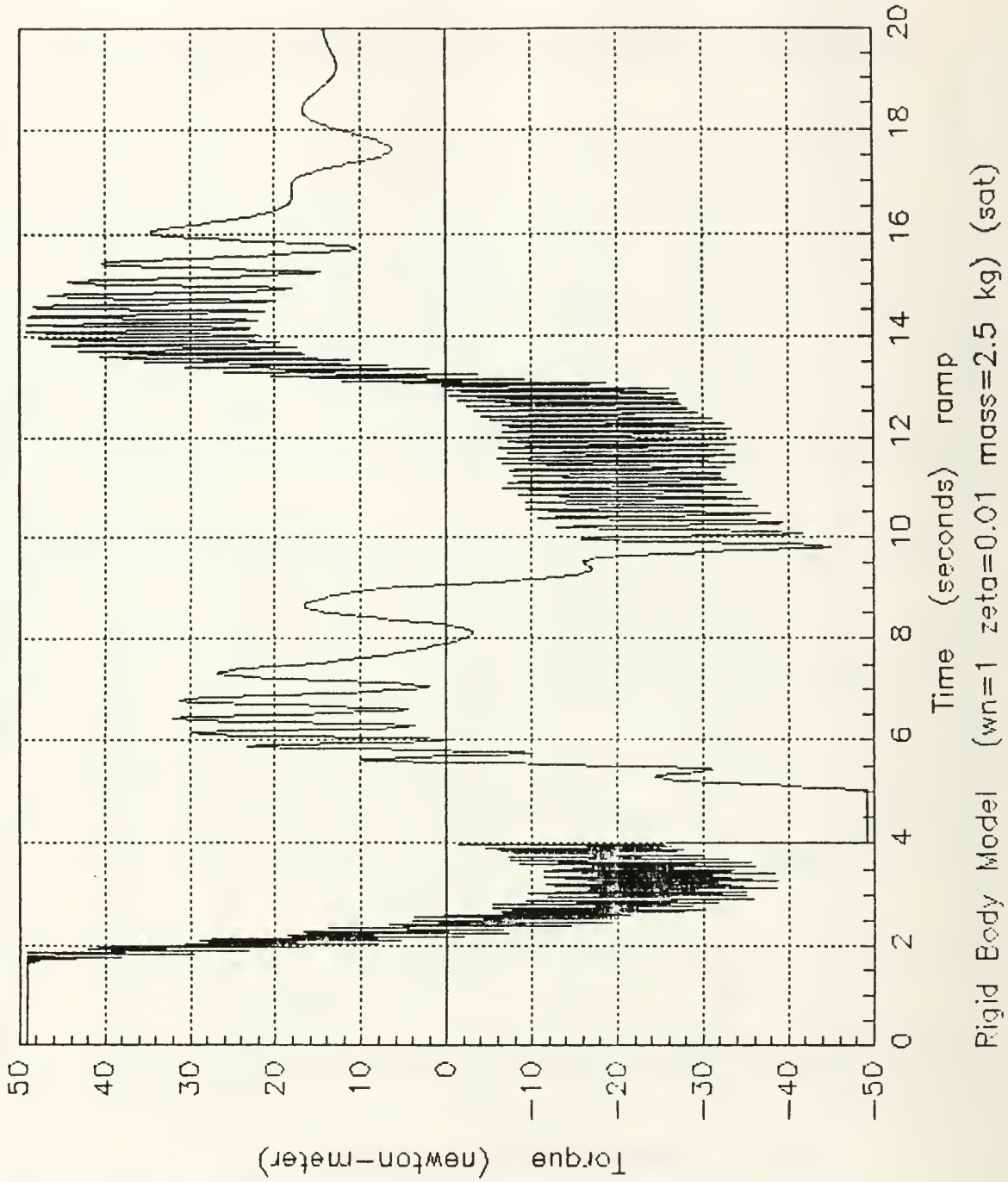

Figure 40. Rigid Body Model (saturation)

Table 6. RIGID BODY TORQUE LIMITATION RESULTS

	Point to Point Tracking Control	Trajectory Tracking Control	Trajectory Tracking Control
	wn = 1 ζ = 0 no load	wn = 1 ζ = 0 no load	wn = 1 ζ = 0 mass = 2.5 kg
Maximum Torque (N-m)	49.2	49.2	**49.2**
Servo Control Mode Amplitude Absolute difference (radians)	0.0003	**0.0004**	**0.003**
Mechanical Vibration (major peak to peak average) (radians)	0.0055	0.0024	**0.0070**
Maximum Overshoot (radians)	5.2	5.7	**5.6**

2. Flexible Body Saturation Case

For graphs of the flexible body case with saturation included, see Figure 41 and Figure 42 for point to point control and Figure 43 for trajectory control.

For the point to point control with input servo speed of $\omega_n = 2$, the torque curve had a secondary frequency mode superimposed on it during the time input torque exceeded the imposed limit. This was present only at ω_n greater than one. Overshoot of the final desired position was higher for the saturation cases. This was due to the momentum which was still present in the system after the torque limitation was reached. The servo control mode amplitude differences are similar to the non saturation cases but the mechanical vibration was higher for the torque saturation cases. Using the trajectory tracking method with added mass (Figure 43), the controller was still able to move the mass to the desired arm position but at a reduced level of performance when compared to the case where motor torque limitations are not considered.

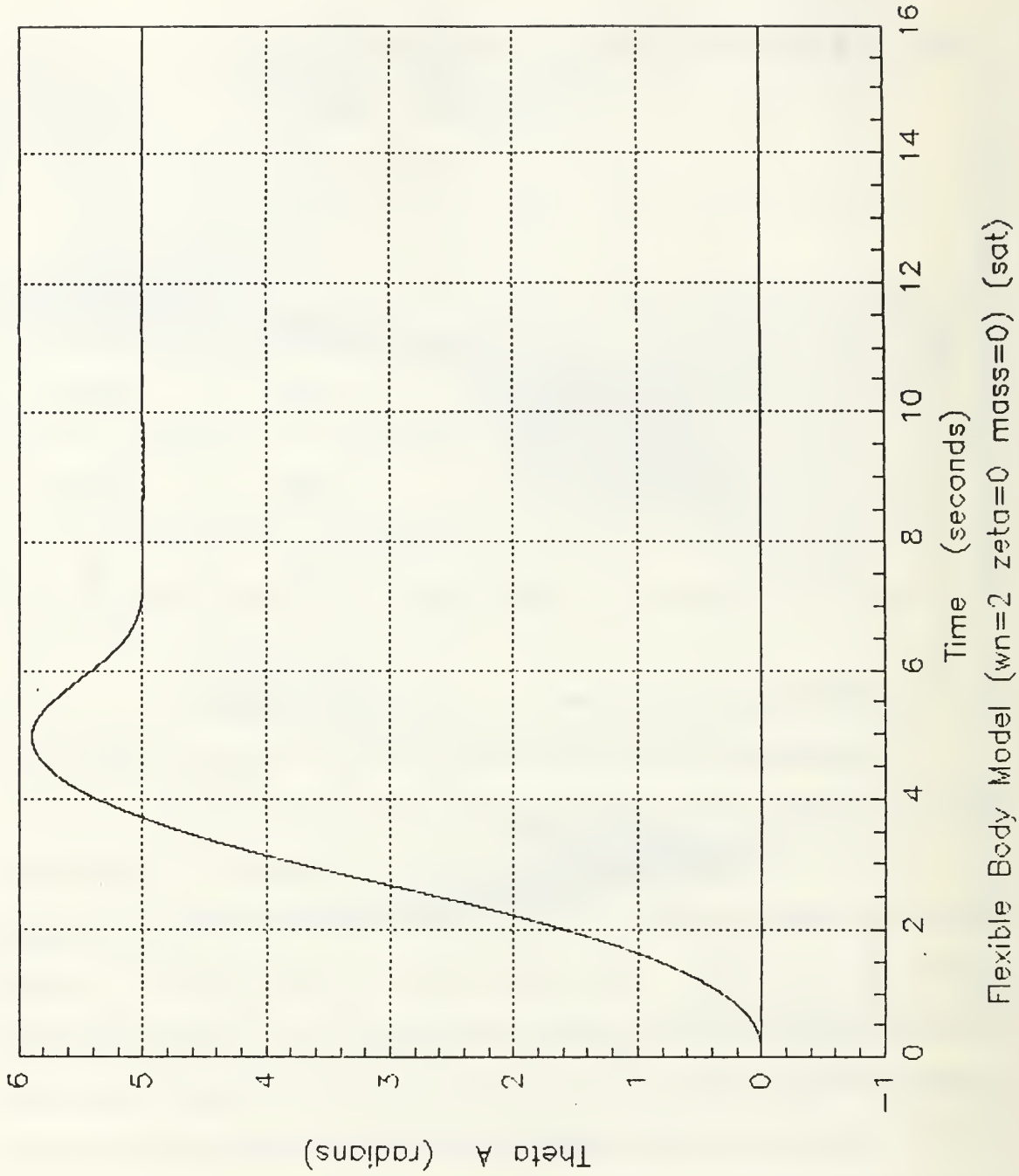

Figure 41. Flexible Body Model (saturation)

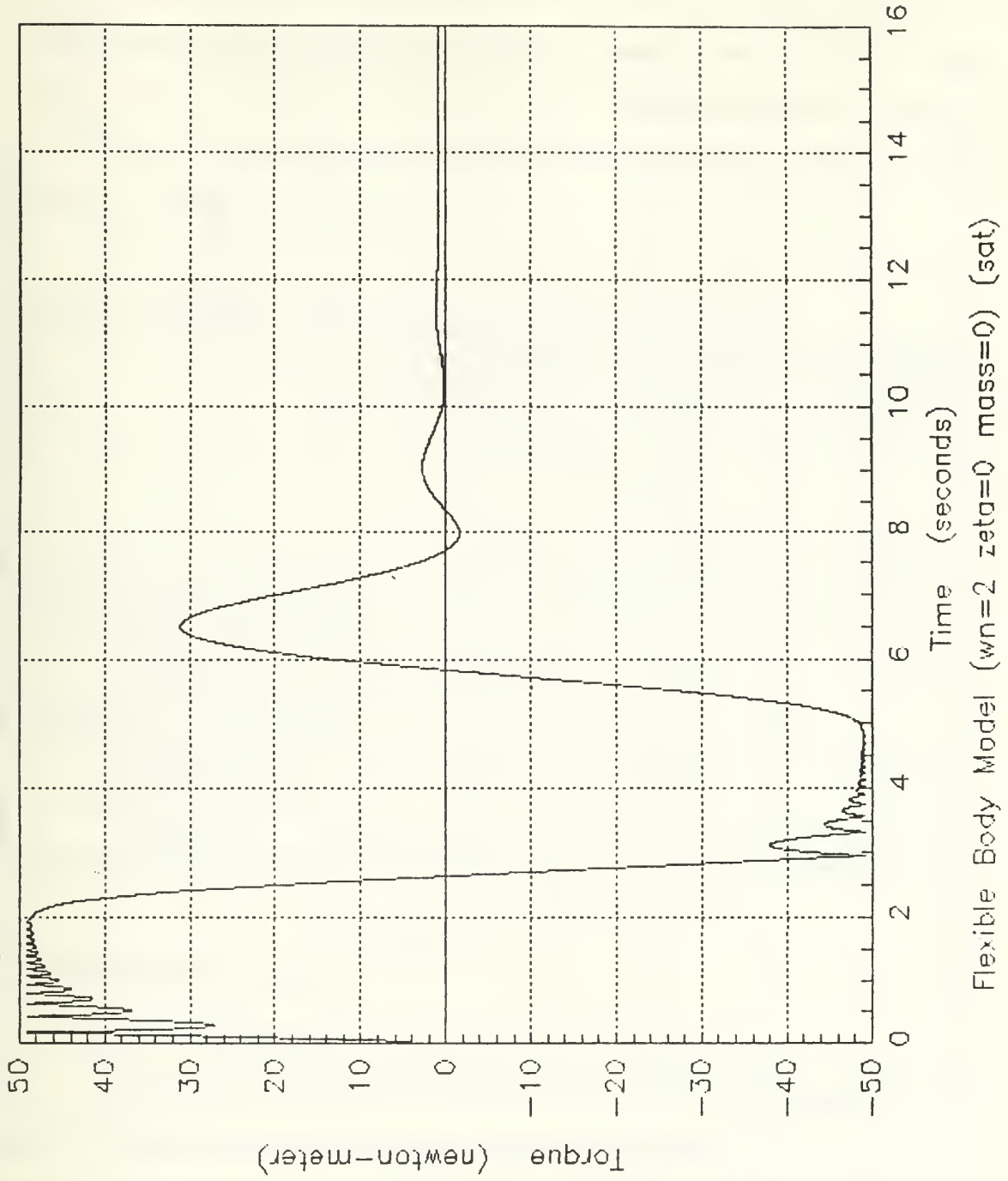

Figure 42. Flexible Body Model (saturation)

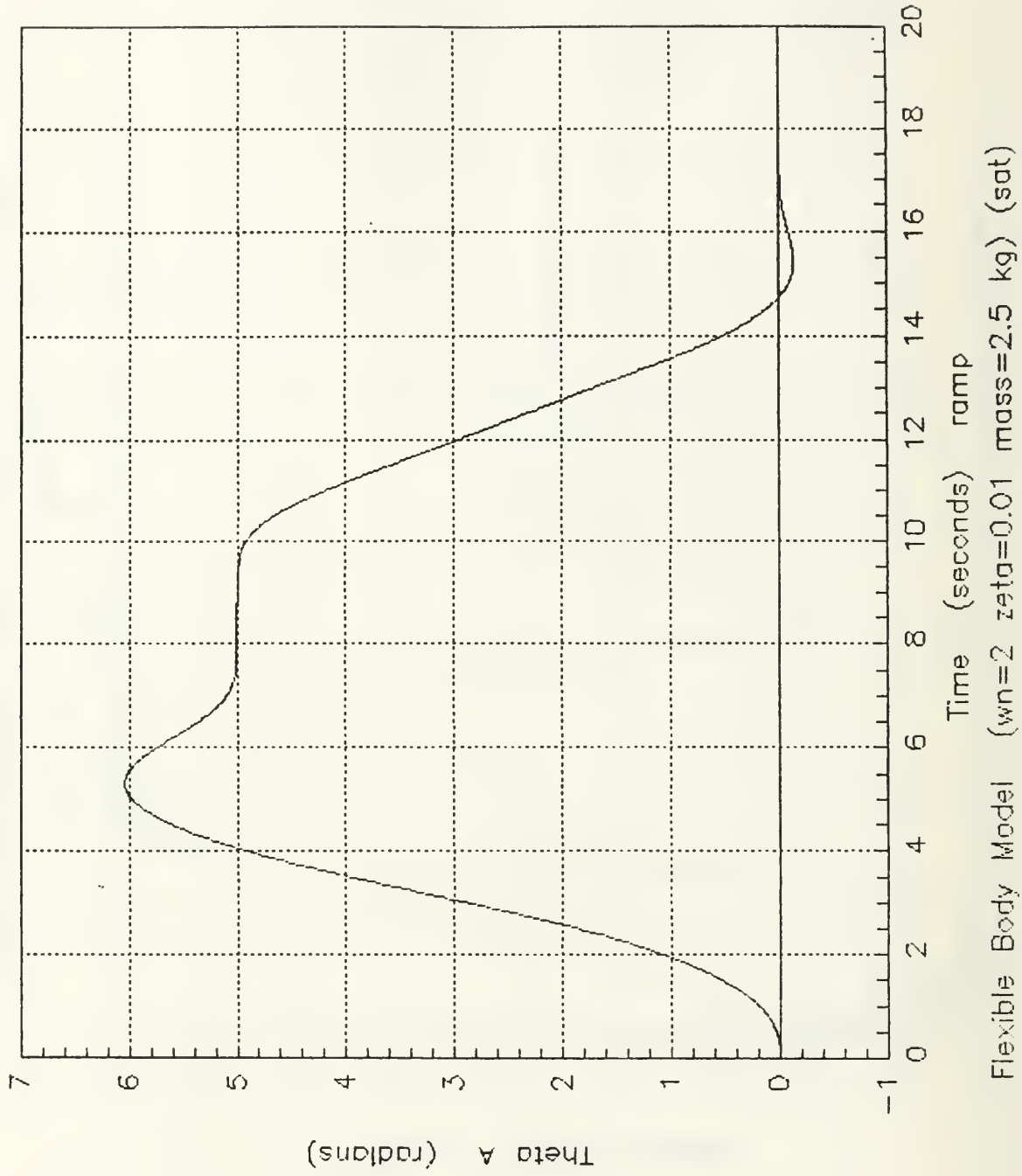

Figure 43. Flexible Body Model (saturation)

The Flexible-Body controller was still able to control the plant at a greater performance level than the Rigid-Body controller in the areas of less mechanical vibration, smaller servo mode amplitude differences and quicker settling times, but its performance was degraded due to the limitation of the torque motor input. For a summary of flexible body model simulations see Table 7.

Table 7. FLEXIBLE BODY TORQUE LIMITATION RESULTS

	Point to Point Tracking Control	Trajectory Tracking Control	Trajectory Tracking Control
	wn = 2 ζ = 0 no load	wn = 2 ζ = 0 no load	wn = 2 ζ = 0 mass = 2.5 kg
Maximum Torque (N-m)	49.2	49.2	49.2
Servo Control Mode Amplitude Absolute difference (radians)	0.0003	0.0003	0.0034
Mechanical Vibration (major peak to peak average) (radians)	0.0005	0.0008	0.0020
Maximum Overshoot (radians)	5.8	6.0	6.02

D. DISCUSSION

1. Rigid Body Results

The performance of the motor feedback method of control remains superior to the arm feedback method for all servo bandwidths. With its long settling time, the arm feedback is unacceptable as a method of control. This poor performance is due to the fact the sensors and actuators used for control are separated by the flexible structure of the transmission line and gears. The flexibility of the system introduces noise in the feedback loop which in turn produces erroneous or inaccurate signals to be received by

the controller. The motor feedback, on the other hand, is not faced with this predicament. Its sensor and actuator are located together and is not faced with this unwanted disturbance or noise.

Another key point are the two parts of the small motion (the difference between the arm position and the motor position) graph. The major line is the servo control mode which is the result of the entire system movement. The second part is the mechanical vibration superimposed onto the servo mode. As the servo input frequency is increased, the servo mode motion increased with a slight increase in mechanical vibration. This is due to the fact the servo frequency ω_n moves towards the systems natural frequency ω_o When damping is introduced, the mechanical vibration decreases slightly while the servo mode increases. With the addition of ζ , the system's natural frequency decreases to ω_d. With this decrease in natural frequency which relates to a movement towards the servo input frequency, the excitation of the system increases due to this closer position of ω_d to ω_n.

2. Flexible Body Results

The Flexible Body Model has demonstrated improved characteristics in each of the areas which were measured. One superior quality was the ability of the controller to move at a faster rate yet use less torque while the Rigid Body controller required more torque while moving at a slower speed. This means the Flexible controller has the capability to control greater payloads, provide more accuracy and could possibly consume less energy. The results of the simulations are listed in the tables on the pages to follow. The results of the Rigid Body Model comparison is listed in Table 1 on page 41 below. To see the Flexible Body Model vs Rigid Body Model results see Table 2 on page 46. To review the effects of damping on the Rigid Body and Flexible Body Model both with input speed increases and added mass increases see Table 3 on page 55 and Table 4 on

page 56. To see the results of trajectory tracking effects on the Flexible Body Model and Rigid Body Model see Table 5 on page 57.

3. Saturation Case Results

For the cases where torque saturation was considered, the Flexible Body controller performance characteristics deteriorated as the result of the limitation of the rigidity of the PUMA Robot arm. The level of mechanical vibration increased and the servo mode level increased also. At an input servo speed of ω_n greater than one, secondary frequencies of the servo system were superimposed on the torque curves where the level exceeded the preset torque limit (since the Flexible Body controller is a fourth order equation, is has an additional frequency mode which is not present in the Rigid Body controller). For the added mass case, the flexible body controller was still able to control the plant. The performance characteristic were superior to the Rigid Body controller in the areas of less mechanical vibration, smaller servo control mode amplitude differences and quicker settling times. However, the performance of the controller was still degraded. The controller needs to operate with a plant designed with flexibility. The PUMA plant is designed to be a rigid plant and therefore restricts the capability of the flexible body controller. The controller stability has decreased as a result of this restriction in motor torque. The results of saturation effects on the Rigid Body Model can be seen in Table 6 on page 67 and the results of the Flexible Body Mode experiencing torque limitation can be reviewed in in Table 7 on page 71.

In Figure 44 is the Super Block diagram of the entire system of the Flexible Body Model. In Figure 45 is displayed the Super Block diagram of the Rigid Body Model system.

Additional simulations were run at various input speeds, with and without damping. These runs without explanation can be reviewed in Appendix E. The graphs are self explanatory. The desired final position of 5 radians was used in all cases.

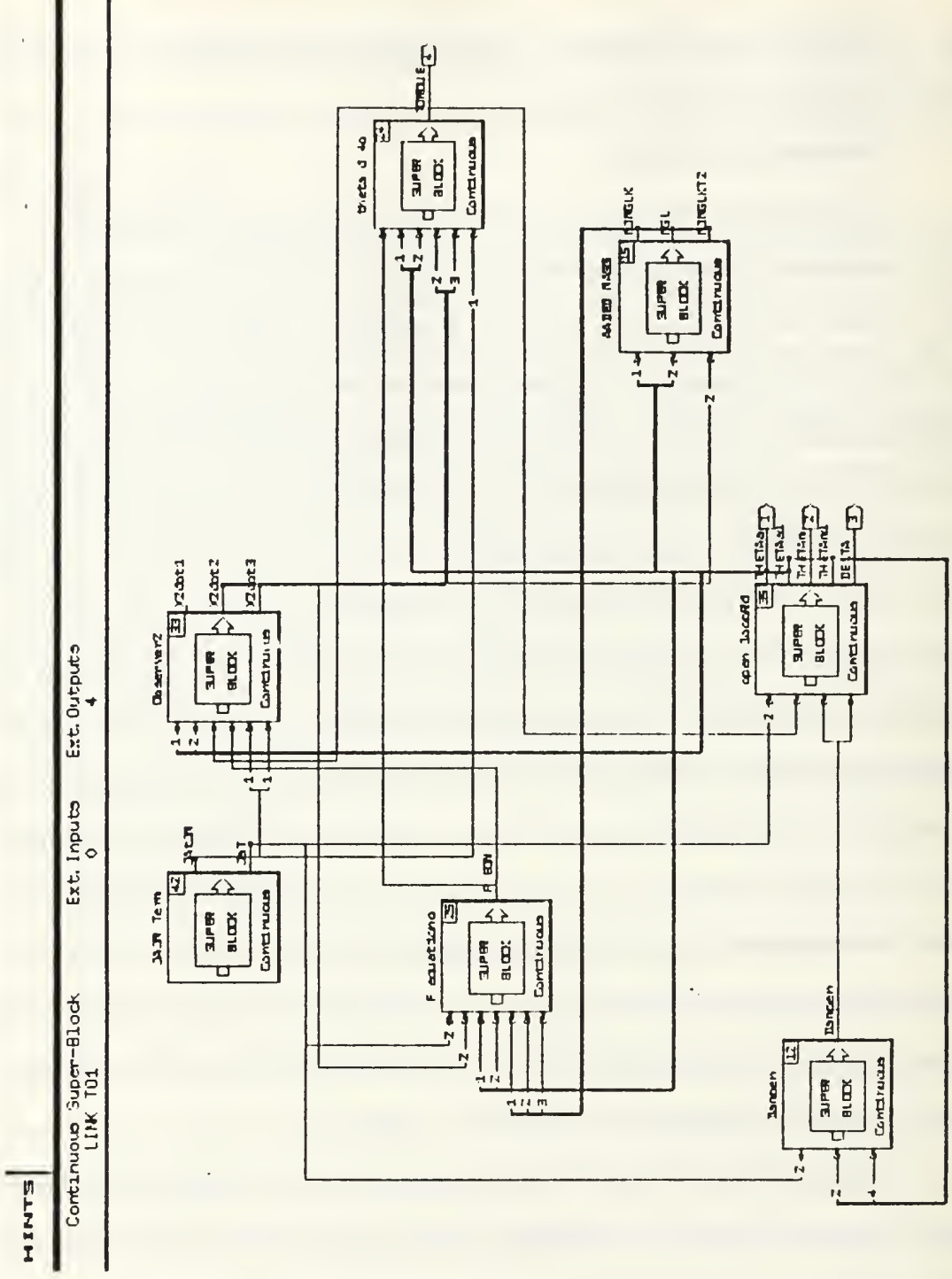

Figure 44. Flexible Body Model Super Block

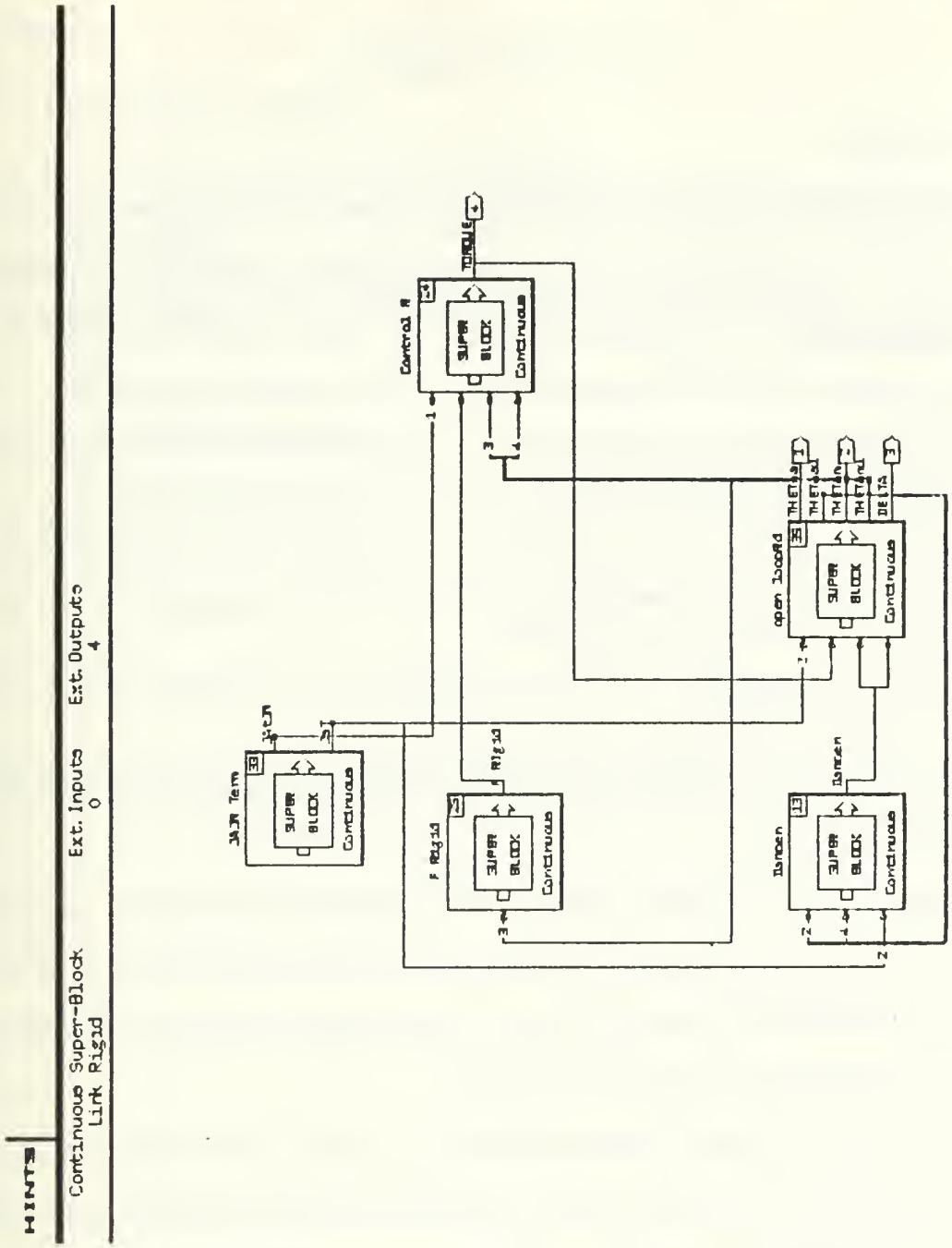

Figure 45. Rigid Body Model Super Block

VI. CONCLUSIONS

A. INSIGHTS

The flexible-body controller performance was superior to the rigid body controller. The results of the comparisons between the two controllers are summarized as follows:

1. With an increase in input servo speed, the rigid body had a higher Mechanical vibration level
2. The flexible body model required less torque even at a higher input speeds
3. The flexible body model proved to be a responsive robust system over the range of speeds and conditions tested
4. The torque requirement for the added mass case was less for the flexible-body controller
5. The flexible body model performance characteristics were superior to a rigid body for both an increase in load and speed
6. A ramp input requires a lower torque requirement with no increase in servo mode or mechanical vibration
7. The flexible-body controller using a ramp trajectory was able to handle a greater load with an improvement in all performance characteristics except rise time which increased slightly

It appears the results obtained points towards selecting the flexible body controller. However, since the results are based on simulations, more comparisons should be conducted at more speeds and a variety of loads. This research considered the the flexibility in the gear coupling and neglected gear backlash.

The case of the torque limitation did point out some of the limitations of the flexible-body controller. The performance characteristics deteriorated as the result of the limitation of available input servo torque. The level of mechanical vibration increased and the servo mode level increased also. At input servo speeds greater than $\omega_n = 1$, secondary frequencies of the servo system were superimposed on the torque curve where the torque required exceeded the preset level. Results in the simulations indicate that

actuator saturation may be the only significant nonlinearity in the robot motion design problem.

B. RECOMMENDATIONS

The following recommendations are submitted:

1. Continue further study of the Flexible Body Model under varies simulated conditions and load.
2. Build a Flexible Body Controller and test it on the PUMA Robot.
3. Extend the present study of the Flexible Manipulator to include more than one joint.

Additional suggestions are:

1. The flexible body controller be used at input speeds which do not exceed the saturation level or the actuator.
2. The flexible body controller be tested on plants which were design to be flexible.

APPENDIX A. MATRIX$_X$

A. MATRIX$_X$

MATRIX$_X$ is a Computer Aided Engineering software package for modeling, simulation, engineering analysis, control design, signal processing, and system identification.

MATRIX$_X$, is a programmable, matrix solving software package with emphasis on controls applications. Scalar functions as well as complex, large-scale matrix problems can be solved using the state-of-the art matrix analysis functions built into **MATRIX$_X$** . **MATRIX$_X$** can be used to solve complex, large-scale matrix problems in an engineering discipline. However, it is bested used in the analysis of control engineering related problems. **MATRIX$_X$** was designed to have a complete set of design and analysis functions for input/output (classical) control and state-space (modern) control." [Ref. 10]

Control systems are concerned with the control of specific variables. The interrelationship of the controlled variables to the controlling variables is required. This relationship is typically represented by the transfer function of the subsystem relating the input and output variables. Therefore, the transfer function is an important relation for control engineering. The importance of the cause and effect relationship of the transfer function is evidence by representing the relationship of the system by use of diagrams called **block diagrams**.

The block diagram representation of a system's relationships is prevalent in control system engineering. Block diagrams consist of unidirectional, operational blocks that represent the transfer function of the variables of interest. Once the block diagram is developed, a transfer function relation is defined, and the system is analyzed using the

transfer function. *MATRIX$_x$* has a feature called SYSTEM_BUILD[2] which solves linear or non-linear control problems directly from block diagrams.

B. SYSTEM_BUILD

SYSTEM_BUILD is an interactive,menu-driven graphical environment for building, modifying computer simulation models. Any combination of linear, non-linear, continuous-time or discrete-time models that describe a system can be constructed from a library of more that 70 distinct block types. Simulating system performance under both nominal and constrained environments is easily accomplished with SYSTEM_BUILD. [Ref. 11: pp. SB P-1-SB P-2]

Systems are modeled by dividing them into individual components, and each components is described by a specific type of functional block. A group of functional blocks are called Super Blocks, and Super Blocks can be nested together within another Super Block. Once a system is modeled in SYSTEM_BUILD, The system is analyzed in the **MATRIX$_x$** interpreter. Any system modeled in SYSTEM_BUILD can be simulated, linearized, and analyzed through the use integration algorithms, built into the **MATRIX$_x$** interpreter, which are suitable for simulating a variety of systems. [Ref. 11: pp. SB P-1]

---

2 SYSTEM_BUILD is a trademark of Integrated Systems Incorporated.

APPENDIX B. PUMA 560 ROBOT DESCRIPTION

The Puma 560 Robot is an industrial robot system with six degrees of freedom. It is comprised of a robot arm (Figure 46) [Ref. 6: p. 1-20], a controller, software, and other peripherals. It is designed to manipulate nominal end-effector load of 2.5 kilograms. With a positional repeatability of 0.1 milli-meters. It has a spherical work envelope of 0.92 meters (Figure 47) [Ref. 6: p. 2-2]. Its drive is an electric DC servomotor. The maximum tool acceleration is 1 G with a maximum tool velocity of 1.0 meter per second (with maximum load within the primary work envelope). The maximum static force at the tool is 58 newtons. The arm assembly is driven by a permanent-magnet DC servomotor driving through its associated gear train. The motor contains an incremental encoder and a potentiometer driven through a 116 to 1 gear reduction. The motor is housed in the upper arm. The gear train is housed in the elbow end of the upper arm and is connected to the motor by a drive shaft. A bevel pinion on the input shaft drives a bevel gear on one end of an idler shaft. A spur pinion at the other end of the idler shaft engages a bull gear fixed to the forearm, and so rotates the forearm around the elbow axis. [Ref. 6: pp. 1-22-1-25]

The PUMA 560 Robot is controlled by a closed-loop control system. Incremental encoders and potentiometers at each drive motor provide the positional feedback for the control system. Each of the joint encoders provides a resolution of approximately 0.005 degree/bit . The PUMA 560 robot can also be positioned using transformations. [Ref. 12]

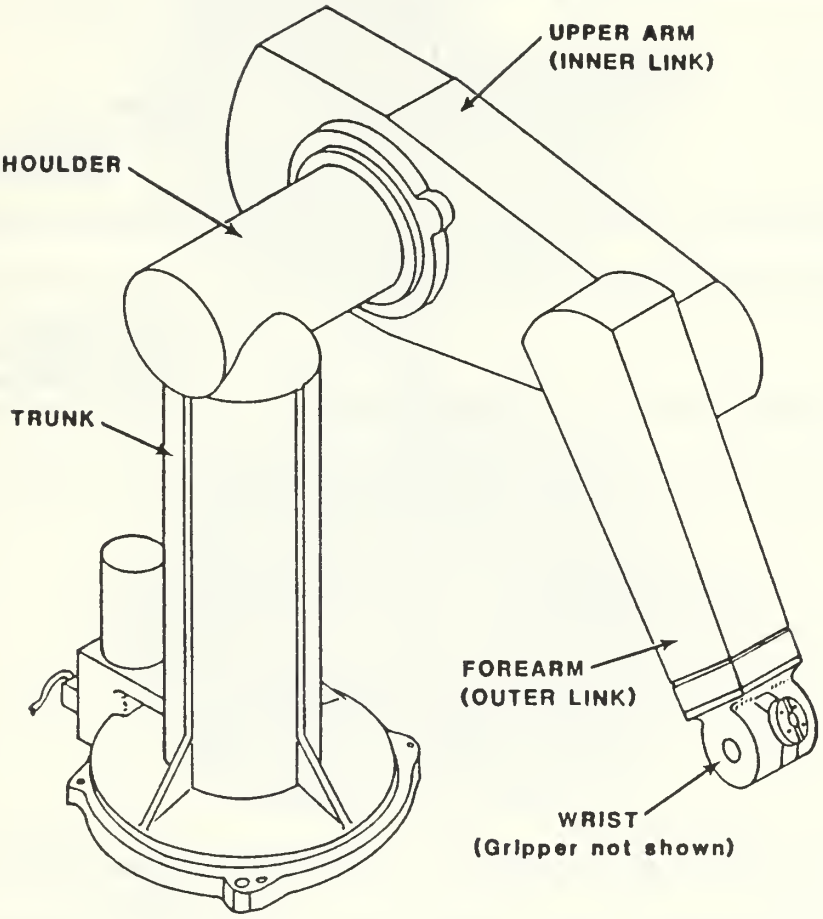

Figure 46. PUMA60 Robot Arm

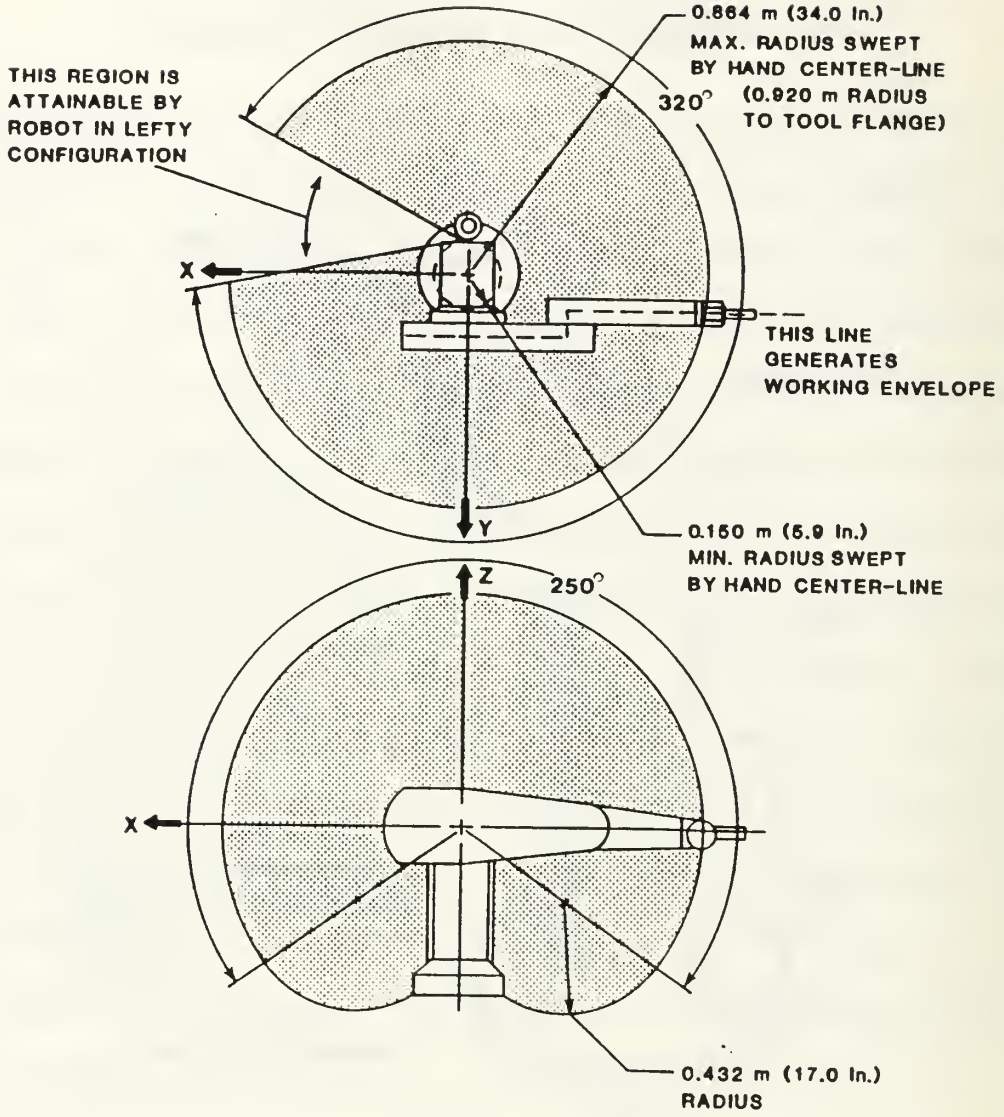

Figure 47. Robot Arm Operating Envelope

APPENDIX C. ADDED MASS AND DAMPING

A. ADDED MASS EQUATIONS

For added mass, the J_A term is revised to include the additional mass which is placed at the arm tip position. The appropriate term is:

$$M_D L_D g \cos\theta_a \tag{C.1}$$

which is added to Equations (3.4) and (3.7). The following term $M_D L_D^2$ is added to the J_A term which results in a new term $J_a T$, which represents the moment of inertia for the link (arm) and the added mass (see Figure 48).

Now performing the derivation for the controller as presented in Chapter Four with the additional added mass terms, the revised **F** equation (Equation 4.4) will be:

$$\begin{aligned} F = J_m \Bigg[\left(G_r - \frac{m_a g l}{2k} \sin\theta_a - \frac{M_D g L_D}{k} \sin\theta_a \right) \ddot{\theta}_a \\ - \left(\frac{m_a g}{2k} + \frac{M_D g L_D}{k} \right) \dot{\theta}_a^2 \cos\theta_a \Bigg] + J_A T \ddot{\theta}_a \\ + (m_a g l + M_D g L_D) \cos\theta_a \end{aligned} \tag{C.2}$$

Figure 49 illustrates the block diagram elements which are added to the **F** equation inorder to revise the Flexible Body Model overall system equations. By setting mass equal to zero (for no added mass) these terms do not effect the simulation of the plant. See Figure 4 for a block diagram of the **F** equation.

For the special case of the Rigid Body Model, the **F** equation (Equation 4.9) is modified as shown:

$$F = m_a g \frac{l}{2} \cos\theta + M_D g L_D \cos\theta \tag{C.3}$$

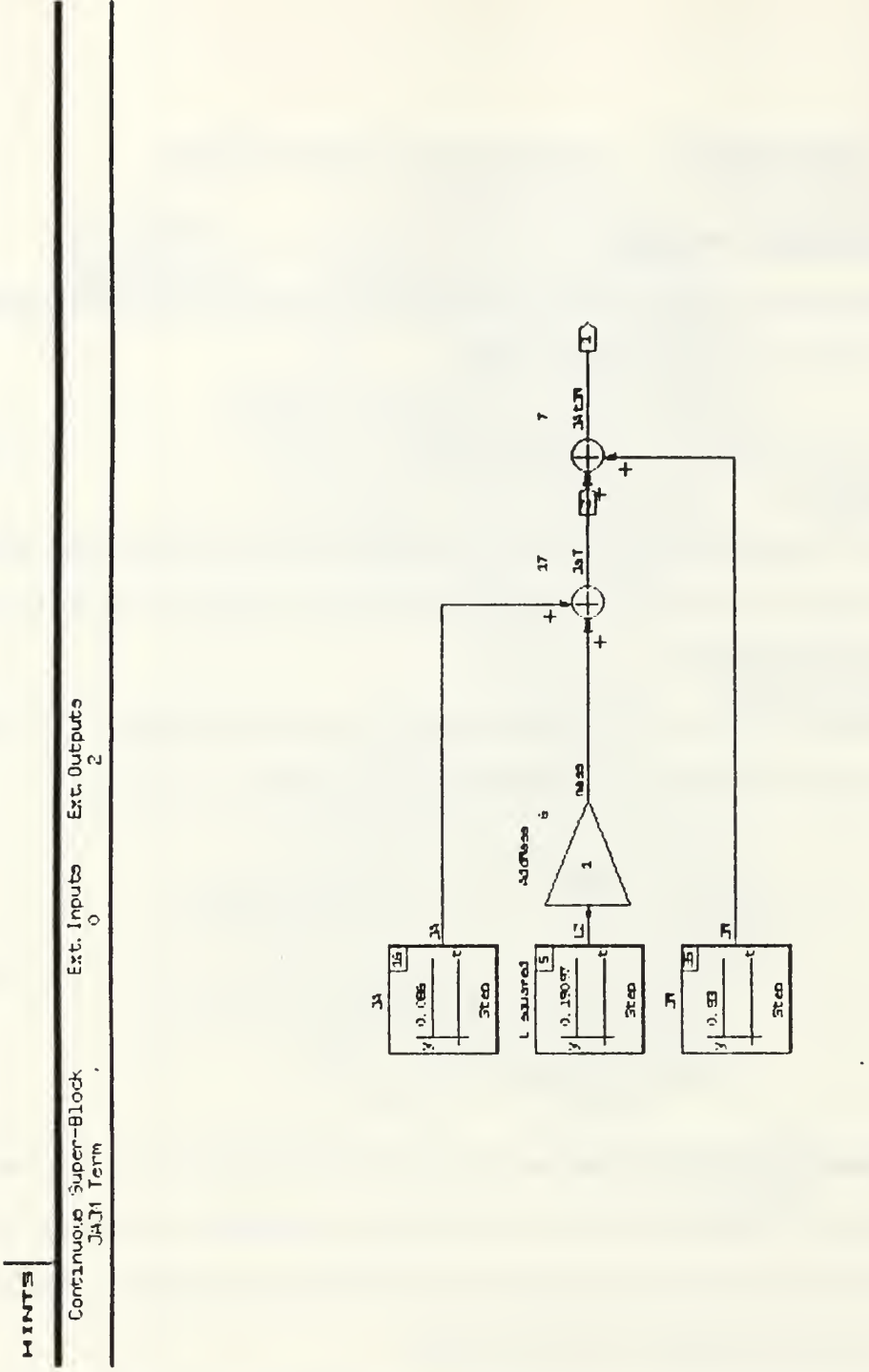

Figure 48. J,T Added Mass Terms

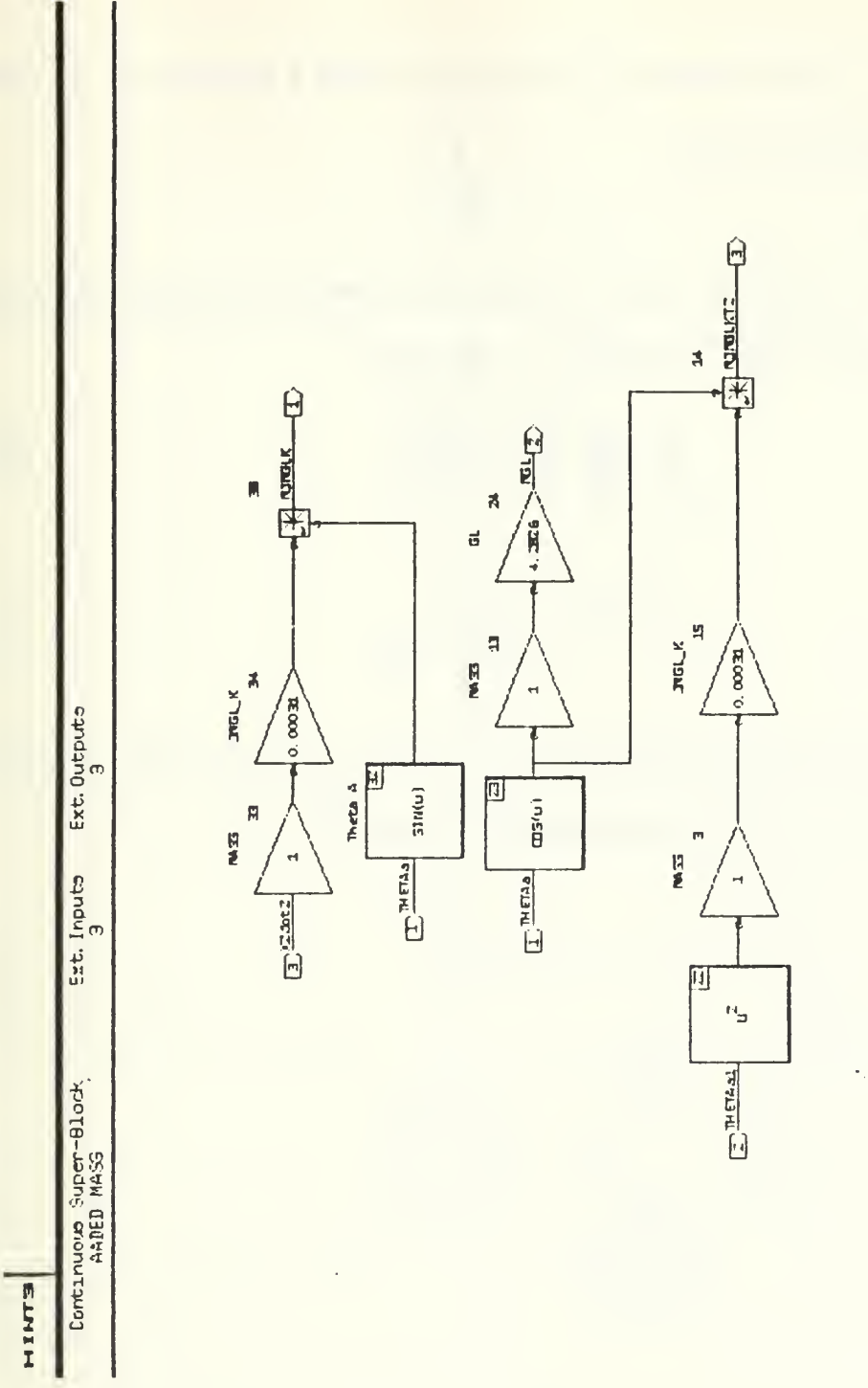

Figure 49. Flexible Body Model Added Mass Block

See Figure 7 for a block diagram of the Rigid Body Model F equation with the placements of the added mass terms.

B. DAMPING

Damping is considered in both the Flexible Body Model and the Rigid Body Model. The following term is added to equations 3.4, 3.5, and 3.7

$$C = 2\zeta\sqrt{\frac{k\,J_a J_m}{(J_a + J_m G_r)}} \tag{C.4}$$

$$\begin{aligned} Damping &= C(\dot{\delta}) \\ \dot{\delta} &= (\dot{\theta}_a - \dot{\theta}_m) \end{aligned} \tag{C.5}$$

in order to observe the performance characteristics of the two models with and without damping. See Figure 50 for a block diagram of the damping term.

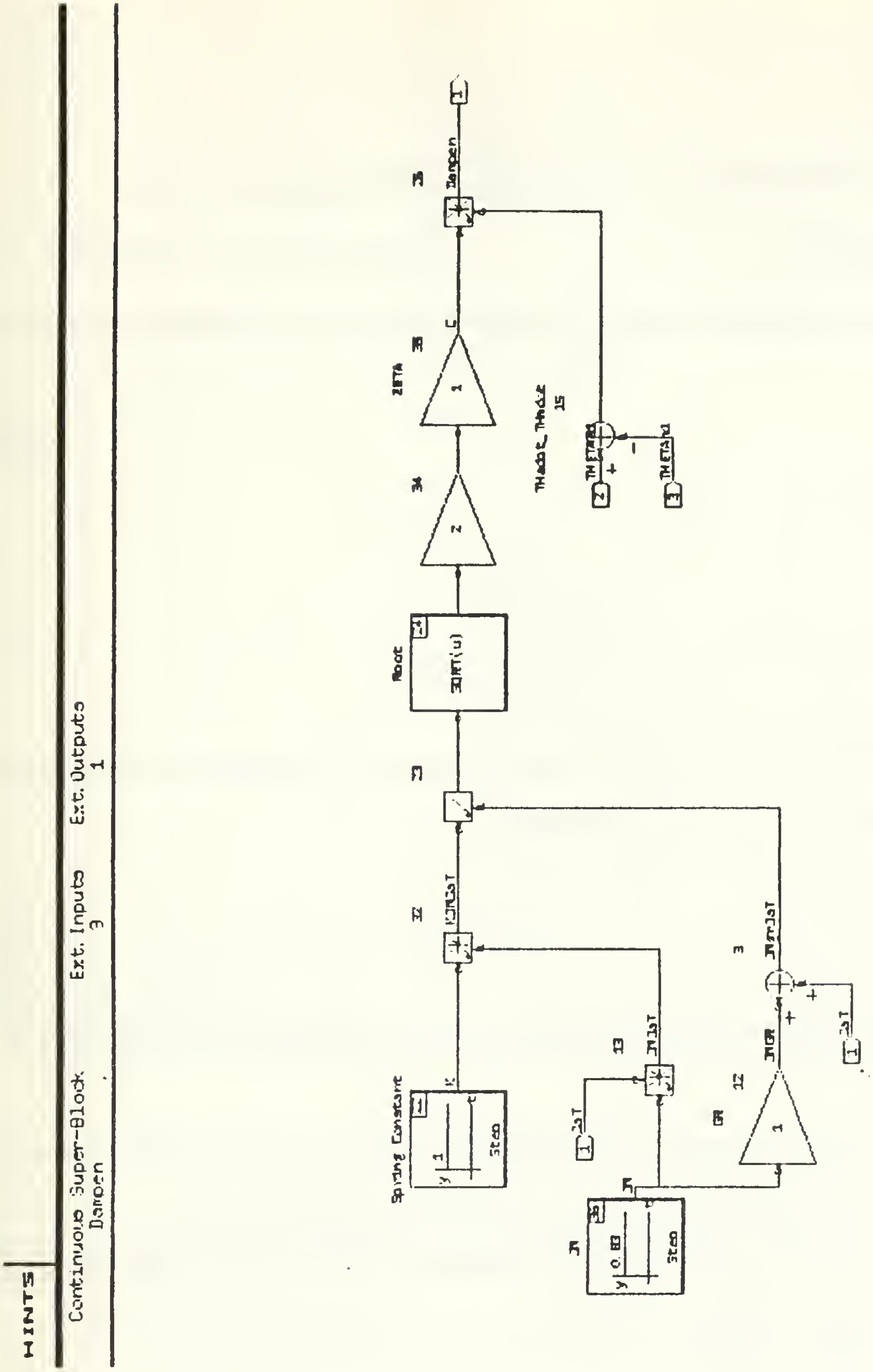

Figure 50. Damping Block Diagram

APPENDIX D. STATE OBSERVER DERIVATION

A. BACKGROUND

A dynamic system can be represented in state-space form by the following equation:

$$\dot{x} = Ax + bu \tag{D.1}$$

A control law of

$$\begin{aligned} u &= -Gx \\ \dot{x} &= (A - bG)x \end{aligned} \tag{D.2}$$

can be assumed if 'x' is accessible for measurements. But instead of being able to measure the state 'x', one can only measure

$$y = Cx \tag{D.3}$$

where the dimension m of the observation vector y is less than the dimension of x [Ref. 9: p.260].

Errors inevitably will be present in the measurement of y(t). These errors mean only an estimate for $\hat{x}(t)$ of x(t) can be made and never x(t) itself. [Ref. 13]

A better procedure for obtaining an estimate of $\hat{x}(t)$ is to make the estimate, the output of a dynamic system.

$$\dot{\hat{x}} = \hat{A}\hat{x} + \hat{B}u + Ky \tag{D.4}$$

The system is excited by 'y' and input 'u'. By selecting the matrices $\hat{A}$, $\hat{B}$, and K, the error can be made equal to

$$e = x - \hat{x}$$
$$\text{or} \qquad (D.5)$$
$$\tilde{x} = x - \hat{x}$$

Let a differential equation be equal to

$$\dot{e} = (A - KC)e \qquad (D.6)$$

where

$$K = \begin{bmatrix} k_1 \\ k_2 \\ . \\ . \\ k_k \end{bmatrix} \qquad (D.7)$$
$$C = [c_1, c_2, ., ., c_k]$$

[Ref. 9: pp. 260-261].

Pole placement is to place poles of the feedback system at desired locations. Assume

$$\lambda_1, \lambda_2, \lambda_k, \ldots . \qquad (D.8)$$

are desired eigenvalues, and the characteristic polynomial is

$$(S - \lambda_1)(S - \lambda_2) \ldots (S - \lambda_k) = S^k + \hat{a}_1 S^{k-1} + \ldots + a_k \qquad (D.9)$$

In other words, pole placement lets

$$|SI(A - bG)| = S_k + \hat{a}_1 S^{k-1} + \ldots + \hat{a}_k \qquad (D.10)$$

multiple input multiple output systems, G has l x k unknowns (l is the number of inputs). The solution of G is not unique. Next a matrix N will be defined as

$$N = [C', A'C', \ldots, A'^{k-1}C'] \qquad (D.11)$$
$$C' = \text{transpose of matrix } C$$

Matrix 'W' equals

$$W = \begin{bmatrix} 1 & a_1 & . & a_{k-1} \\ 0 & 1 & . & a_{k-2} \\ 0 & . & . & 1 \end{bmatrix} \qquad (D.12)$$

Now a term K' will be defined as

$$K' = (\hat{a} - a)(NW)^{-1} \qquad (D.13)$$

where

$$\hat{a} = [\hat{a}_1 \hat{a}_2 \ldots \hat{a}_k] \qquad (D.14)$$
$$a = [a_1 a_2 \ldots a_k]$$

â terms are the desired coefficients of the characteristic polynomial. 'a' coefficients are obtained from the ITAE criteria for a third order equation since 'a' is a 1 x 3 matrix.

B. OBSERVER FOR FLEXIBLE JOINT ROBOT

The system in this research will be described by the following state space representation:

$$\begin{Bmatrix} \dot{x}_1 \\ \dot{x}_2 \end{Bmatrix} = \begin{bmatrix} A_{11} & A_{12} \\ A_{21} & A_{22} \end{bmatrix} \begin{Bmatrix} x_1 \\ x_2 \end{Bmatrix} + \begin{Bmatrix} B_1 \\ B_2 \end{Bmatrix} u + \begin{Bmatrix} f_1 \\ f_2 \end{Bmatrix} \qquad (D.15)$$

Now make the following relationships:

$$\begin{aligned} z_1 &= \theta & \dot{z}_1 &= z_2 \\ z_2 &= \dot{\theta} & \dot{z}_2 &= z_3 \\ z_3 &= \ddot{\theta} & \dot{z}_3 &= z_4 \\ z_4 &= \dddot{\theta} \end{aligned} \qquad (D.16)$$

From Equation (4.3)

$$\dot{z}_4 = \dddot{\theta} = \frac{K}{J_M J_A} T - \frac{K}{J_M J_A} f \qquad (D.17)$$

$$x_1 = \{z_1\} = \{\theta\}$$

$$x_2 = \begin{bmatrix} z_2 \\ z_3 \\ z_4 \end{bmatrix} = \begin{bmatrix} \dot{\theta} \\ \ddot{\theta} \\ \dddot{\theta} \end{bmatrix}$$

Substituting values into equation (D.15), results in the following equation:

$$\begin{bmatrix} \dot{z}_1 \\ \dot{z}_2 \\ \dot{z}_3 \\ \dot{z}_4 \end{bmatrix} = \begin{bmatrix} 0 & 1 & 0 & 0 \\ 0 & 0 & 1 & 0 \\ 0 & 0 & 0 & 1 \\ 0 & 0 & 0 & 0 \end{bmatrix} \begin{bmatrix} z_1 \\ z_2 \\ z_3 \\ z_4 \end{bmatrix} + \begin{bmatrix} 0 \\ 0 \\ 0 \\ \frac{K}{J_M J_A} \end{bmatrix} T - \begin{bmatrix} 0 \\ 0 \\ 0 \\ \frac{K}{J_M J_A} \end{bmatrix} f \qquad (D.18)$$

Referring back to equation (D.15),

A_{11} is a 1 x 1 matrix
A_{12} is a 1 x 3 matrix
A_{21} is a 3 x 1 matrix
A_{22} is a 3 x 3 matrix

Expanding equation (D.15) results in the following

$$\begin{aligned} \dot{x}_2 &= A_{22}x_2 + A_{21}x_1 + B_2u + f_2 \\ -f_1 + \dot{x}_1 - A_{11}x_1 - B_1u &= A_{12}x_2 \end{aligned} \tag{D.19}$$

An observer is designed as

$$\begin{aligned} \dot{\hat{x}}_2 &= A_{22}\hat{x}_2 + [A_{21}x_1 + B_2u + f_2] \\ y &= C\hat{x}_2 \\ \text{where } y &= -f_1 + \dot{x}_1 - A_{11}x_1 - B_1u \\ C &= A_{12} \end{aligned} \tag{D.20}$$

Redefining equation (D.19) results in

$$\begin{aligned} \dot{\hat{x}}_2 &= A_{22}\hat{x}_2 + A_{21}x_1 + B_2u + f_2 \\ &+ L[\dot{x}_1 - A_{11}x_1 - B_1u - f_1 - A_{12}\hat{x}_2] \end{aligned} \tag{D.21}$$

$$\begin{aligned} \tilde{x}_2 &= x_2 - \hat{x}_2 \\ \dot{\tilde{x}}_2 &= [A_{22} - LA_{12}]\tilde{x}_2 \end{aligned} \tag{D.22}$$

As 't' $\rightarrow \infty$ $\tilde{x}_2 \rightarrow 0$.

C. NUMERICAL SOLUTION

Using the values provided in equation (D.18), the solution to equation (D.10) is

$$\begin{aligned} |sI - \bar{A}| &= s^3 + 0 + 0 - 0 - 0 - 0 \\ a_1 = 0 \quad a_2 &= 0 \quad a_3 = 0 \end{aligned} \tag{D.23}$$

where

$$C^T = \begin{bmatrix} 1 \\ 0 \\ 0 \end{bmatrix} \quad A^T = \begin{bmatrix} 0 & 0 & 0 \\ 1 & 0 & 0 \\ 0 & 1 & 0 \end{bmatrix}$$

From equation (D.11) and equation (D.12)

$$N = \begin{bmatrix} 1 & 0 & 0 \\ 0 & 1 & 0 \\ 0 & 0 & 1 \end{bmatrix} \qquad NW = \begin{bmatrix} 1 & 0 & 0 \\ 0 & 1 & 0 \\ 0 & 0 & 1 \end{bmatrix}$$

$$\text{INV(NW)} = \begin{bmatrix} 1 & 0 & 0 \\ 0 & 1 & 0 \\ 0 & 0 & 1 \end{bmatrix}$$

$$\hat{a} = [\hat{a}_1, \hat{a}_2, a_3]$$

The coefficients for the $\hat{a}_x$ terms were selected from the **ITAE** criteria table for a third order characteristic equation. The values selected were $\hat{a}_1 = 1.75\omega_n$, $\hat{a}_2 = 2.15\omega_n^2$, $\hat{a}_3 = 1.0\omega_n^3$. [Ref. 8: pp. 129-130]. Equation (D.13) now equals

$$K' = \left[1.75\omega_n \;\; 2.15\omega_n^2 \;\; 1.00\omega_n^3\right]$$

Looking back at equation (D.21), let K = L.

A block diagram of the observer is shown in Figure 8 and in Figure 9.

APPENDIX E. GRAPHS OF ADDITIONAL SIMULATIONS

A. GRAPHS WITH NO ADDED MASS

1. Rigid Body with no load

The graphs for motor feedback with no damping and a load of 1.36 kg and $\omega_n = 3$ are shown in Figure 51, Figure 52, and Figure 53.

2. Flexible Body with no load

The graphs for flexible body with no damping and a load of 1.36 kg and $\omega_n = 4$ are shown in Figure 54, Figure 55, and Figure 56.

B. GRAPHS WITH AN ADDED MASS OF 1.36 KILOGRAMS

1. Rigid Body Model with Added Mass

For the examination of the Rigid Body model graphs with damping and added mass under going point to point control see Figure 57 and Figure 58 for $\omega_n = 1$ and Figure 59 and Figure 60 for $\omega_n = 3$.

2. Flexible Body Model with Added Mass

For an examination of the Flexible Body Model experiencing point to point control and added mass see Figure 61 and Figure 62 for $\omega_n = 2$ and Figure 63 and Figure 64 for $\omega_n = 4$.

C. GRAPHS WITH AN ADDED MASS OF 2.5 KILOGRAMS

1. Rigid Body Model with Added Mass

For the examination of the Rigid Body model graphs with damping and added mass undergoing point to point control see Figure 65 and Figure 66 for $\omega_n = 1$ and Figure 67 and Figure 68 for $\omega_n = 3$.

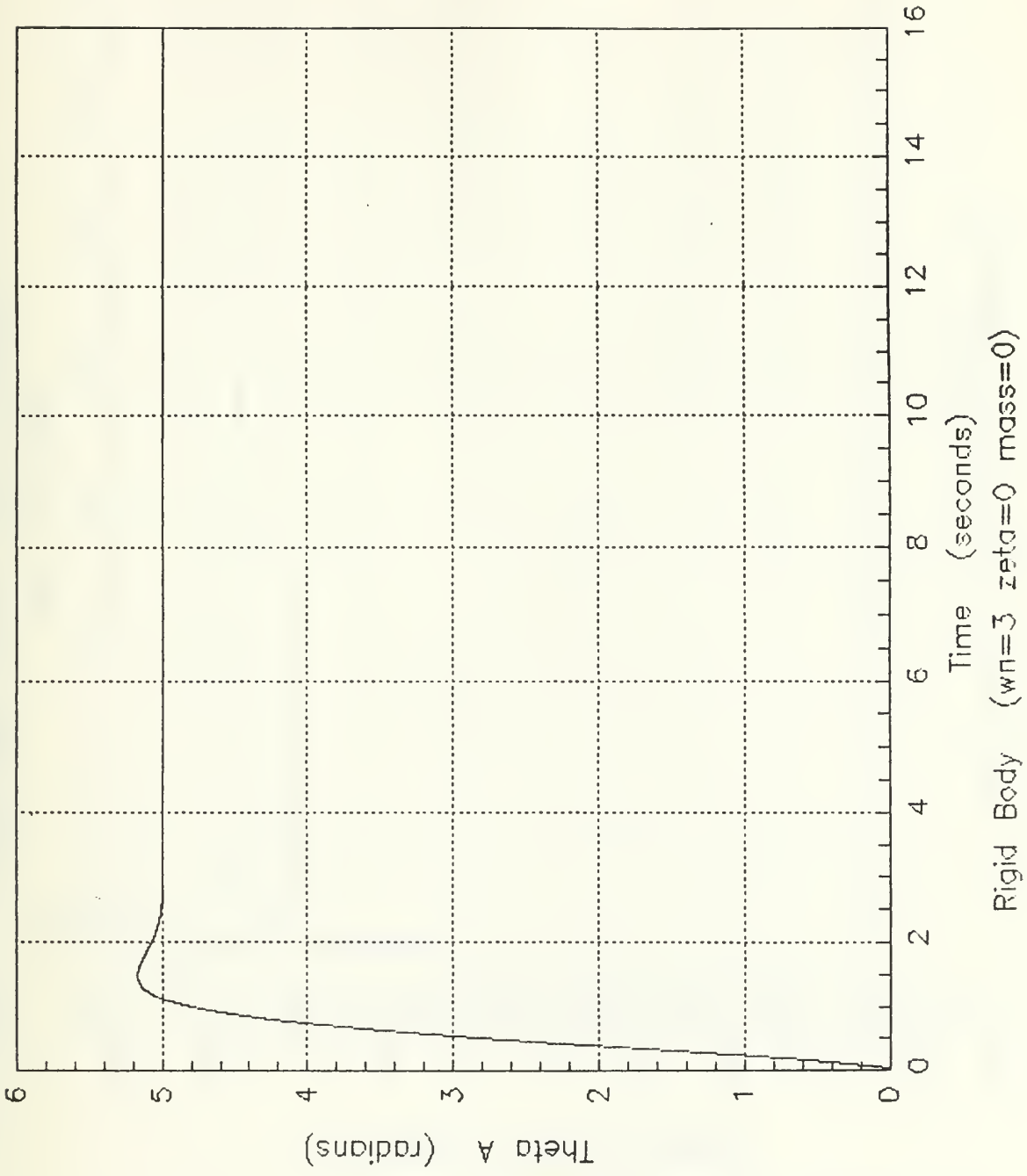

Figure 51. Rigid Body Model (motor feedback) (θ_a) ω_n = 3

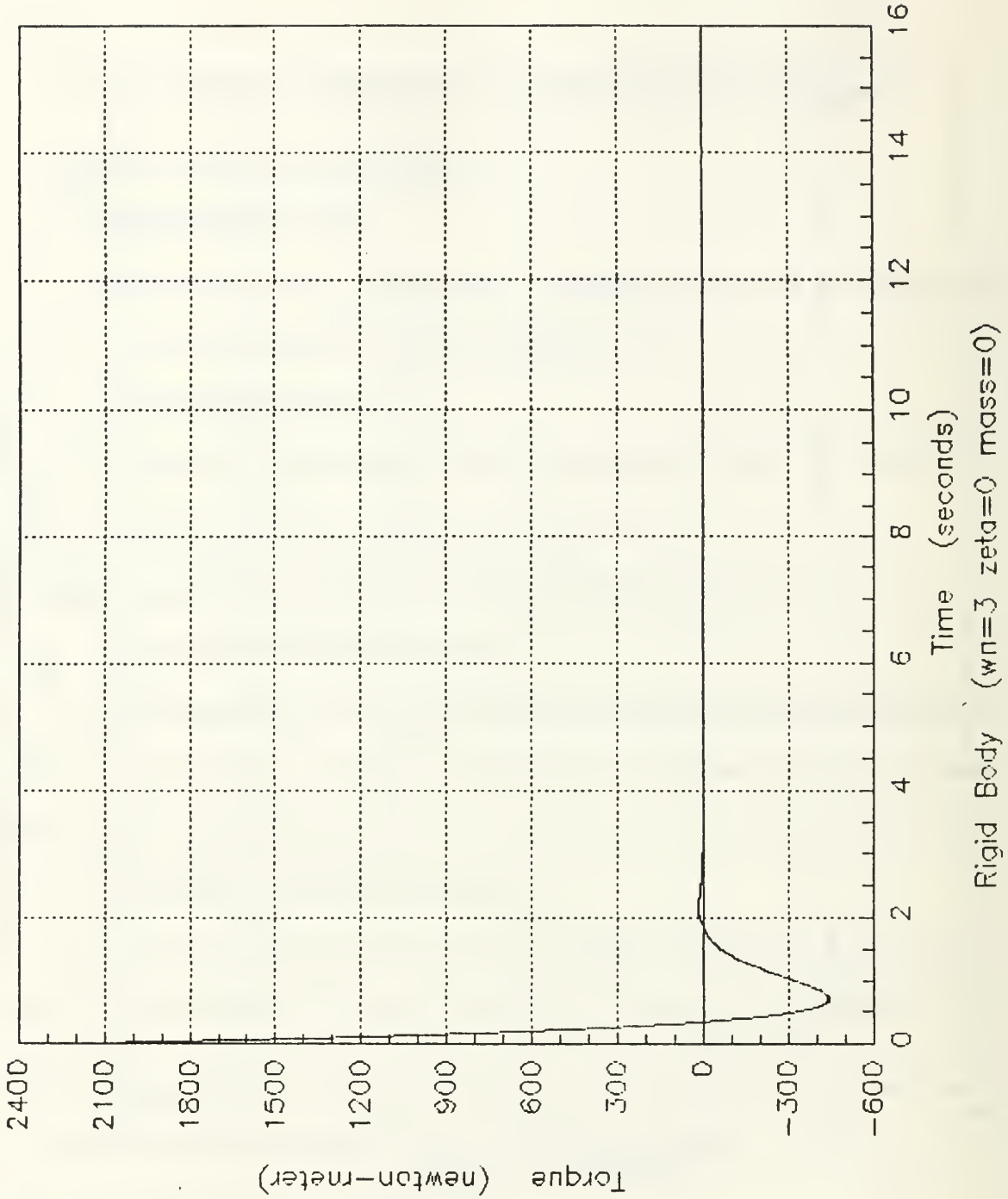

Figure 52. Rigid Body Model (motor feedback) (torque) ω_n = 3

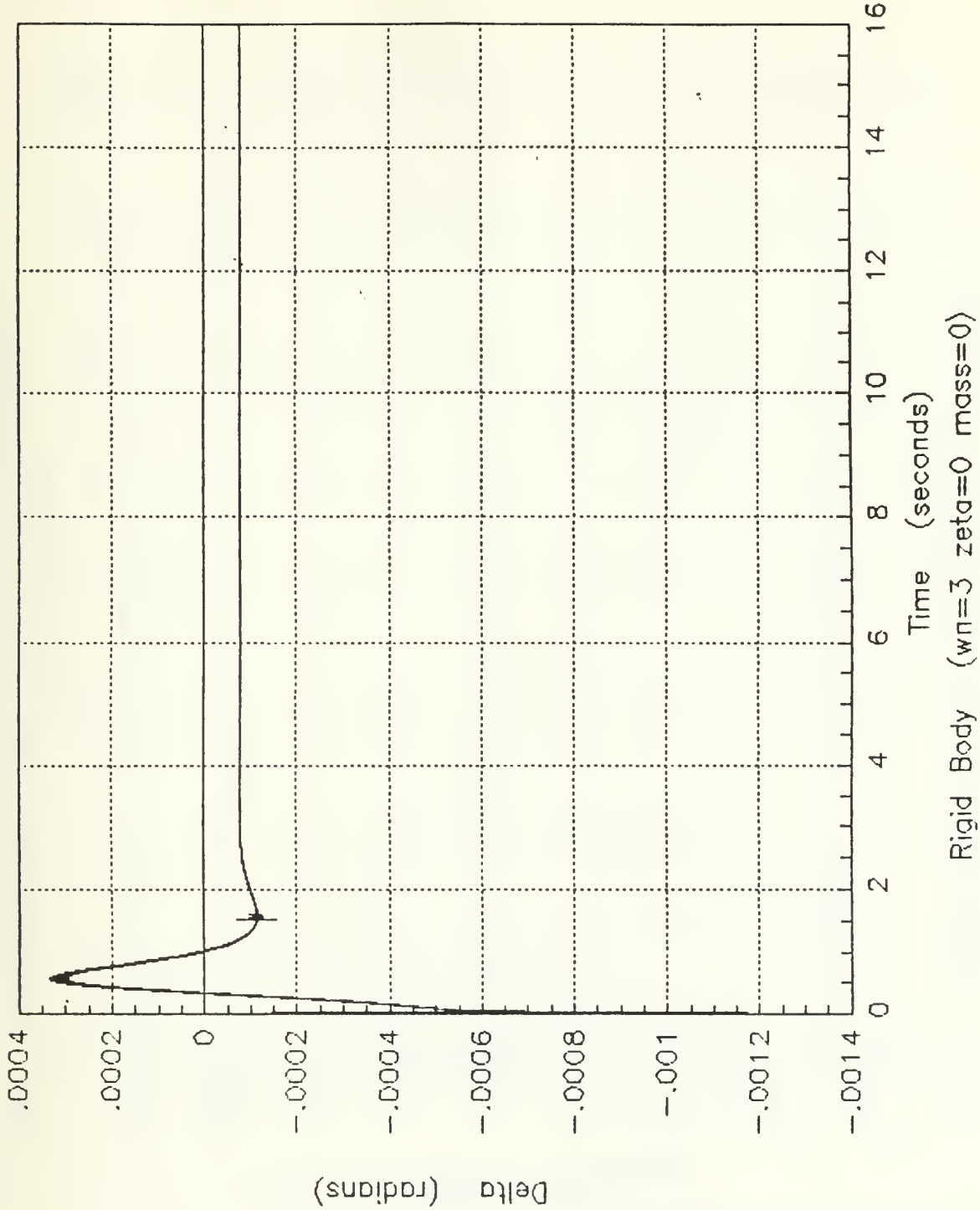

Figure 53. Rigid Body Model (motor feedback) (small motion) $\omega_n = 3$

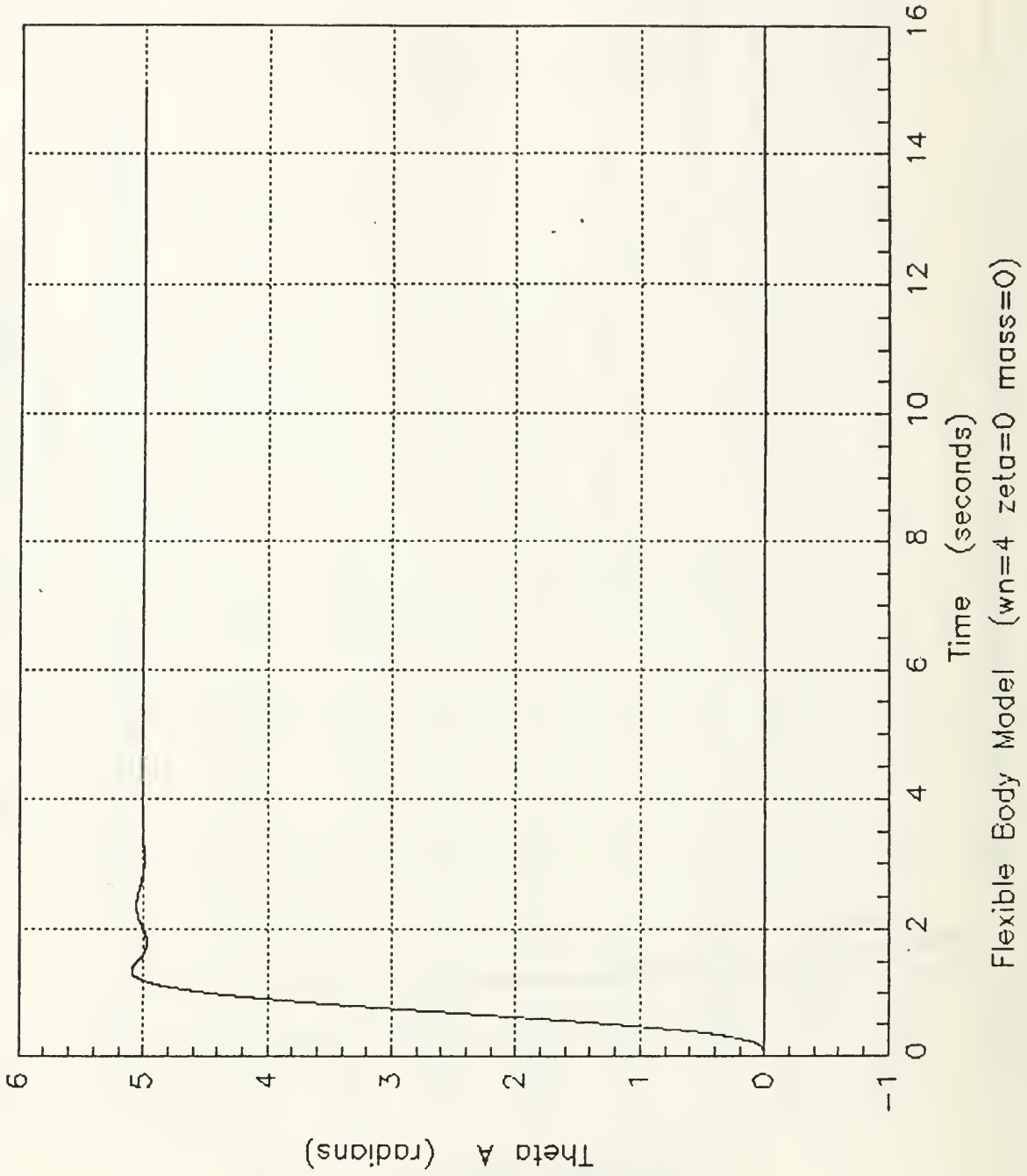

Figure 54. Flexible Body Model (θ_a) ω_n = 4

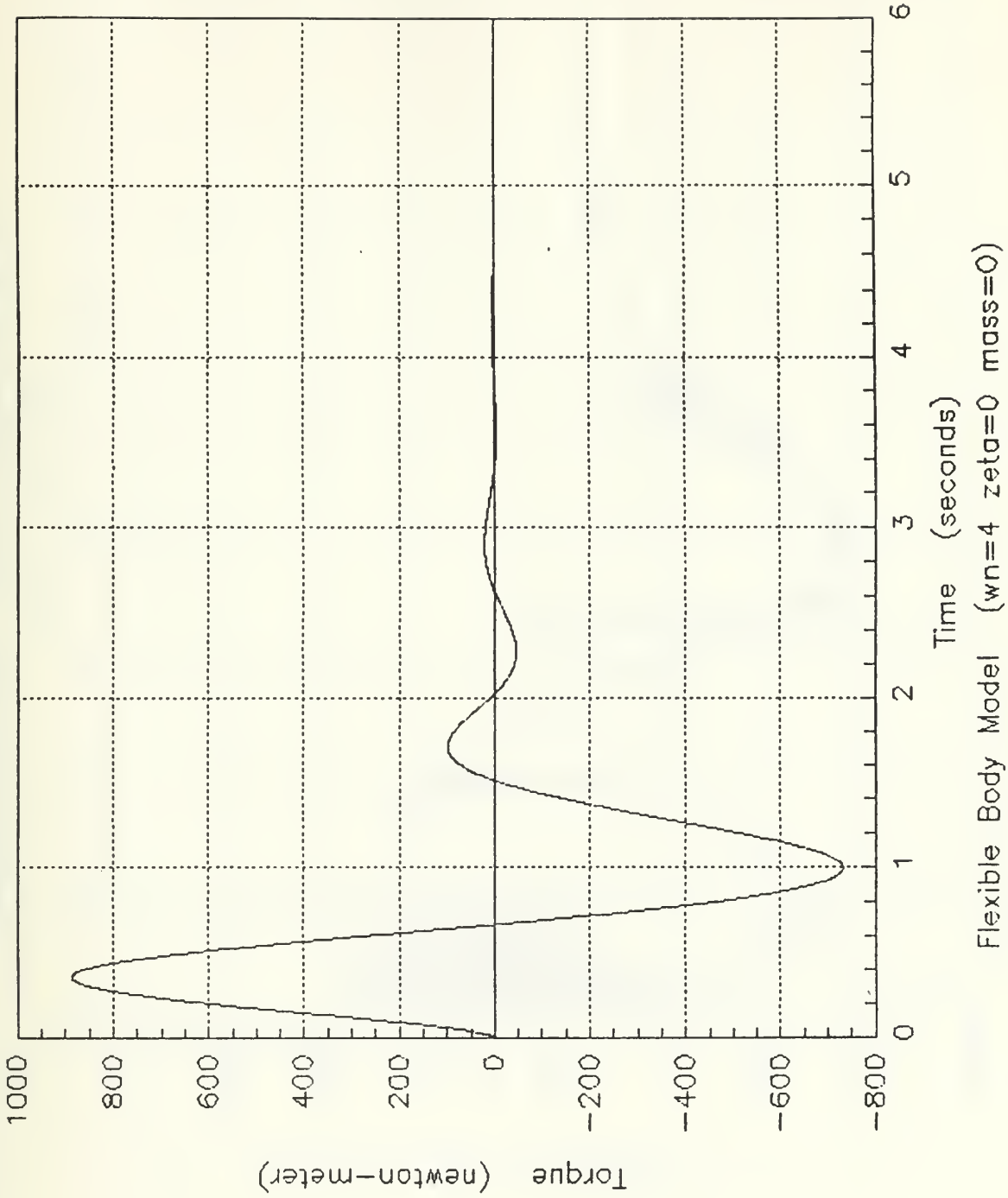

Figure 55. Flexible Body Model (torque) $\omega_n = 4$

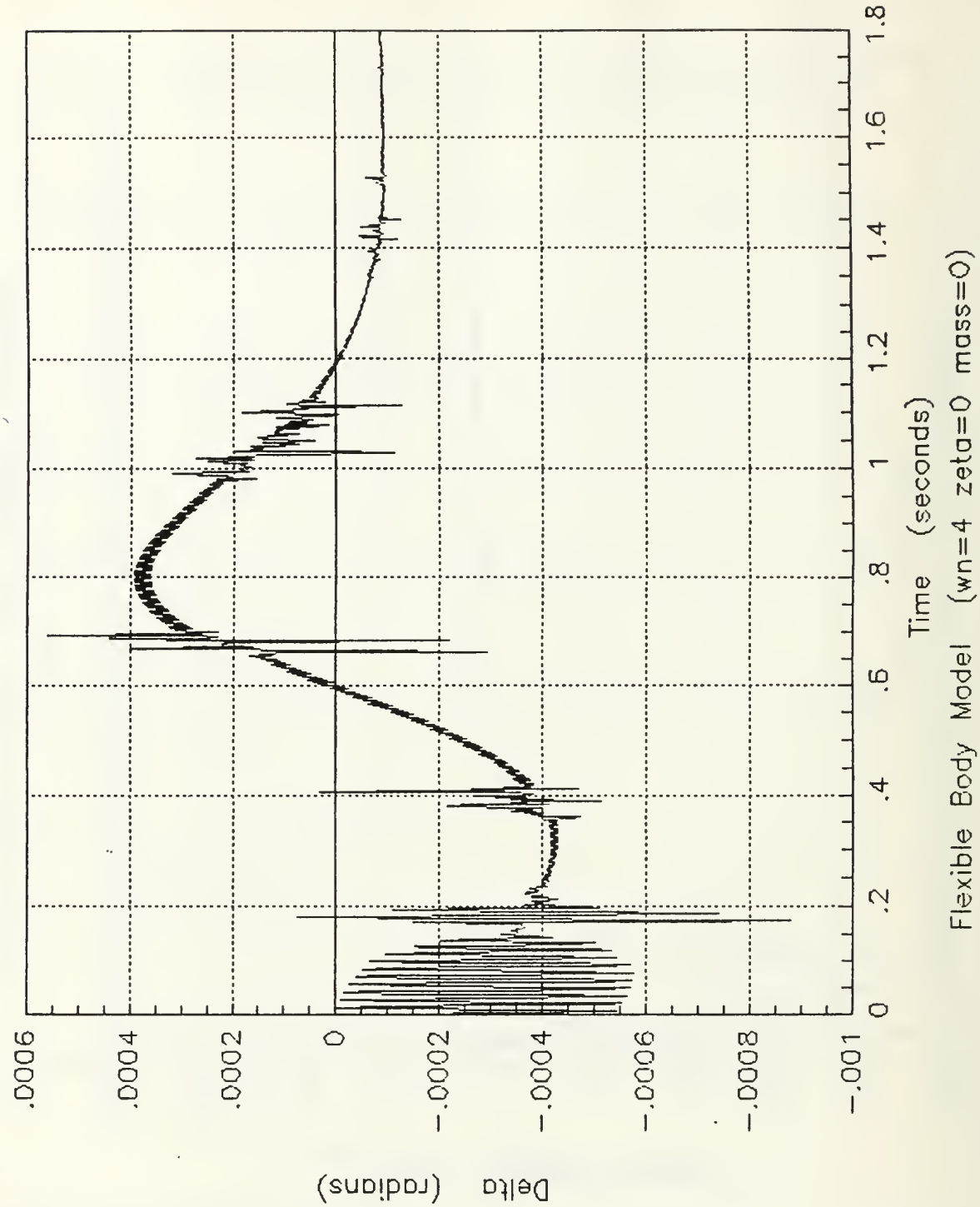

Figure 56. Flexible Body Model (small motion) ω_n = 4

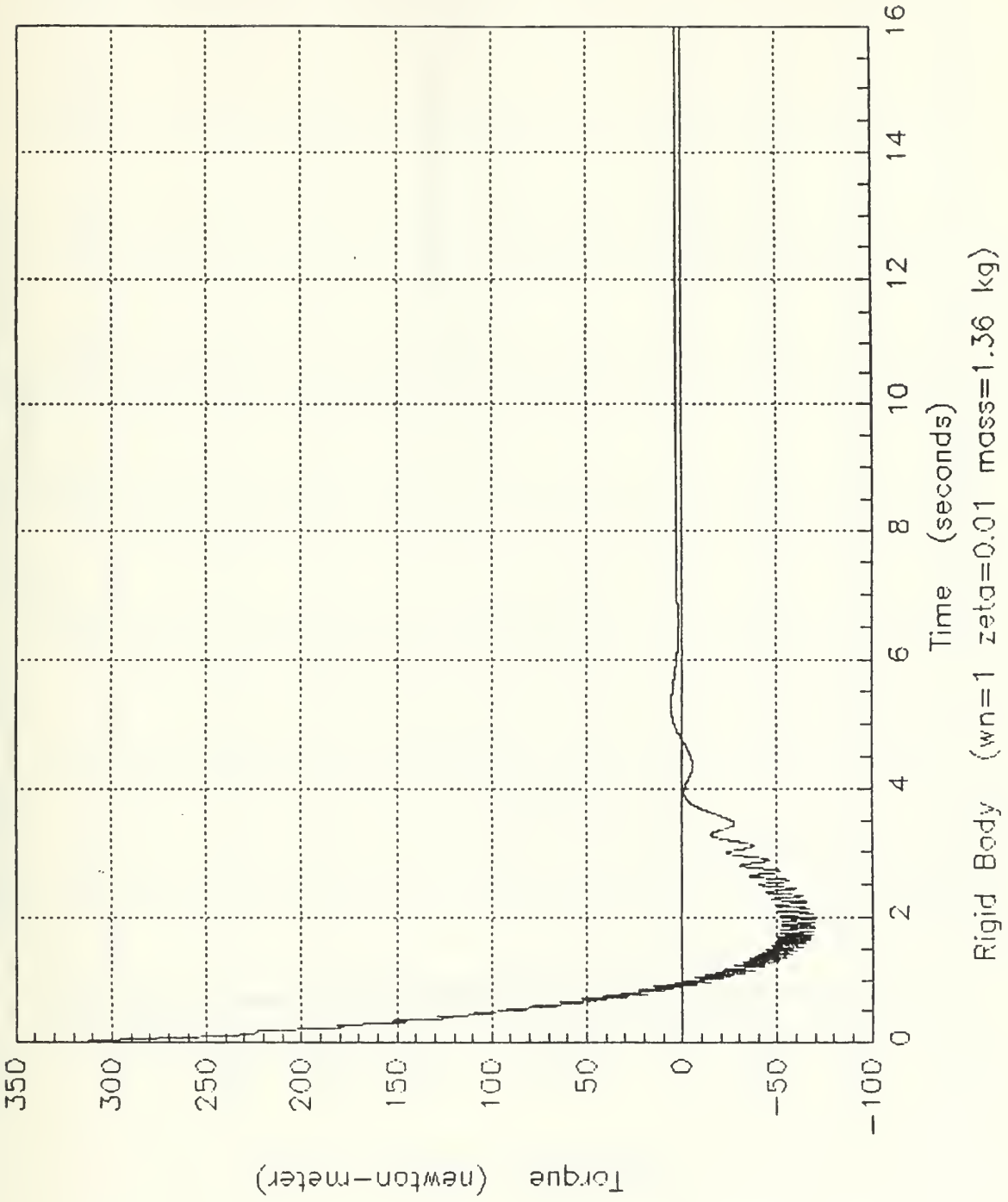

Figure 57. Rigid Body Model (torque) $\omega_n = 1$

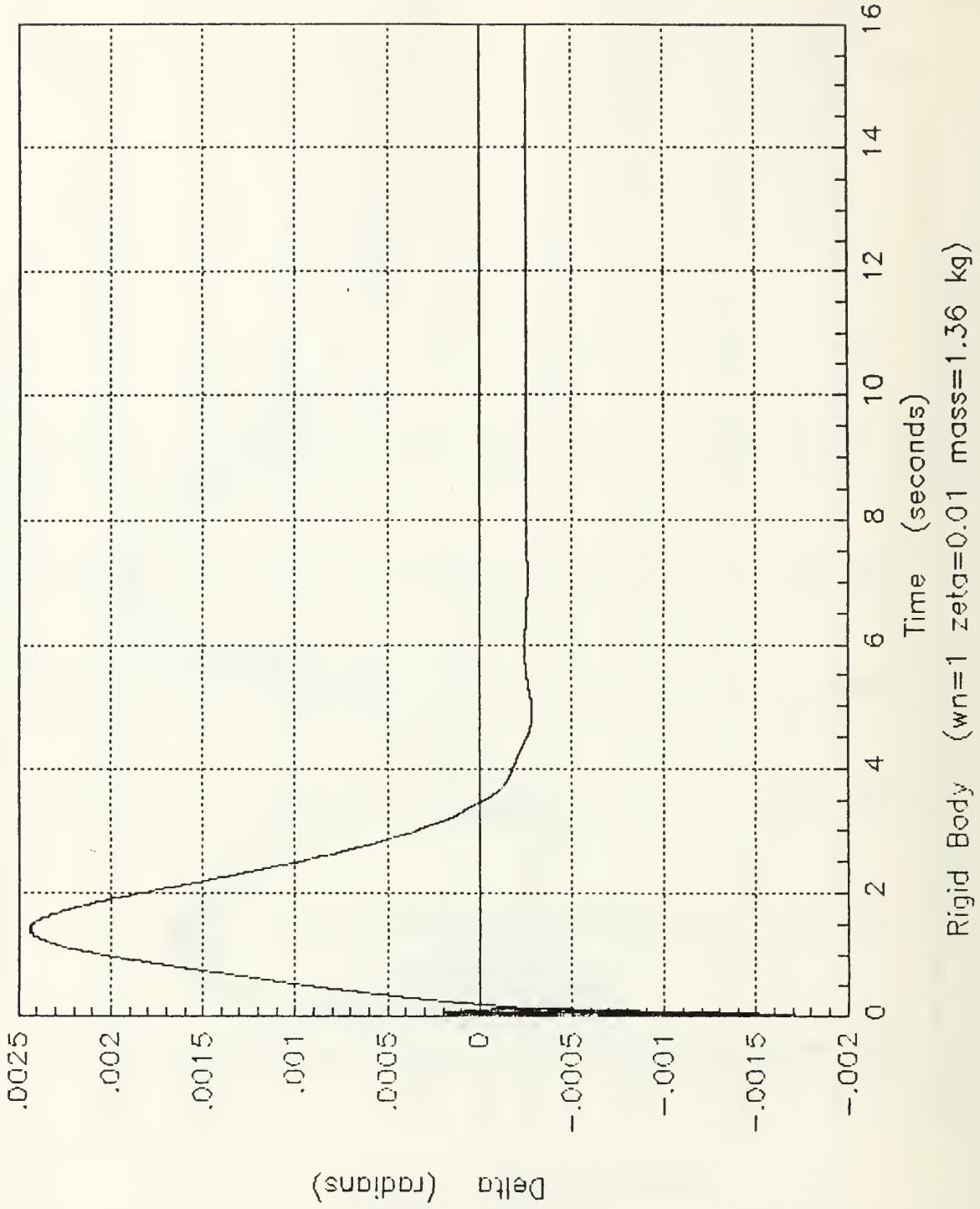

Figure 58. Rigid Body Model (small motion) $\omega_n = 1$

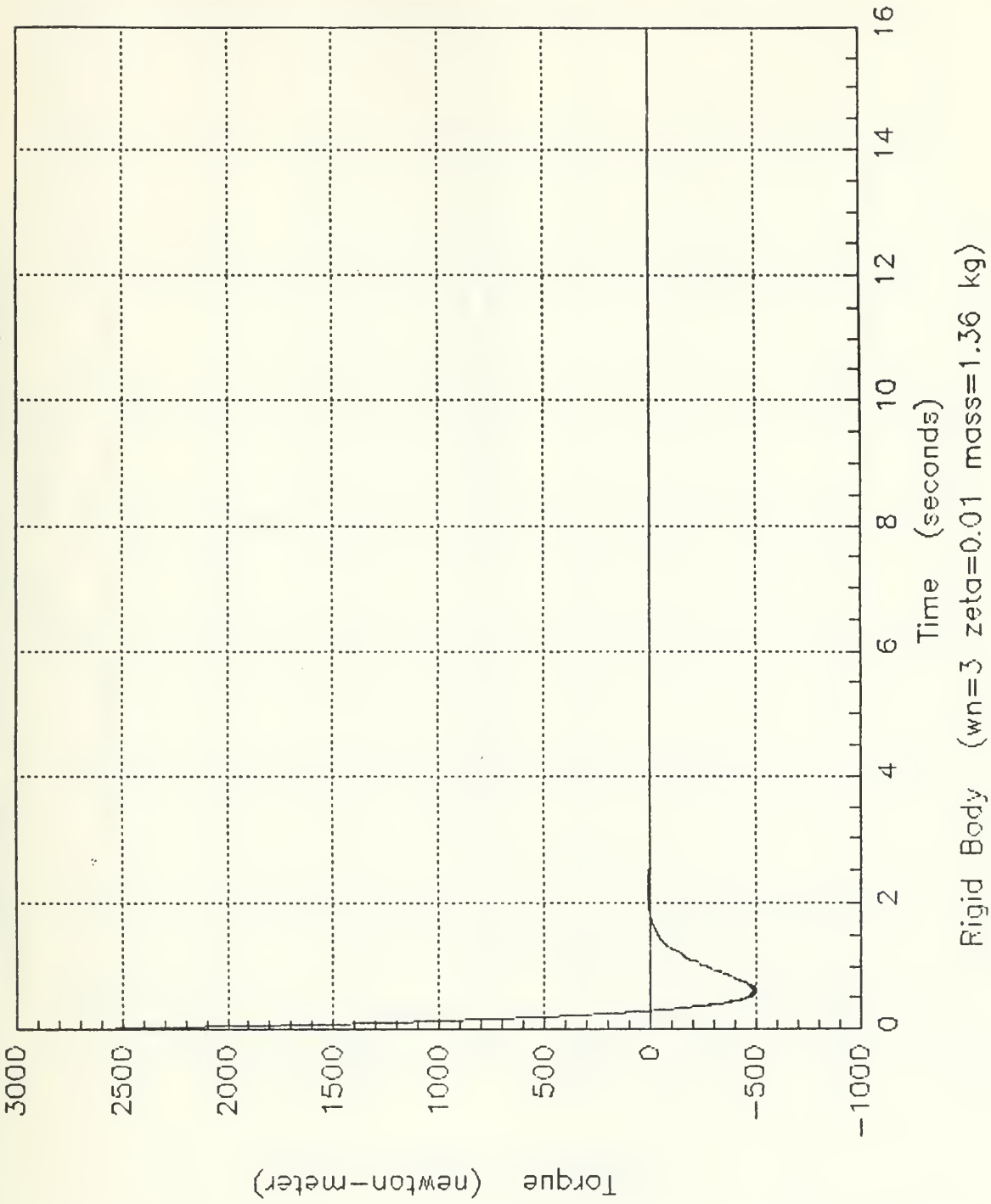

Figure 59. Rigid Body Model (torque) ω_n = 3

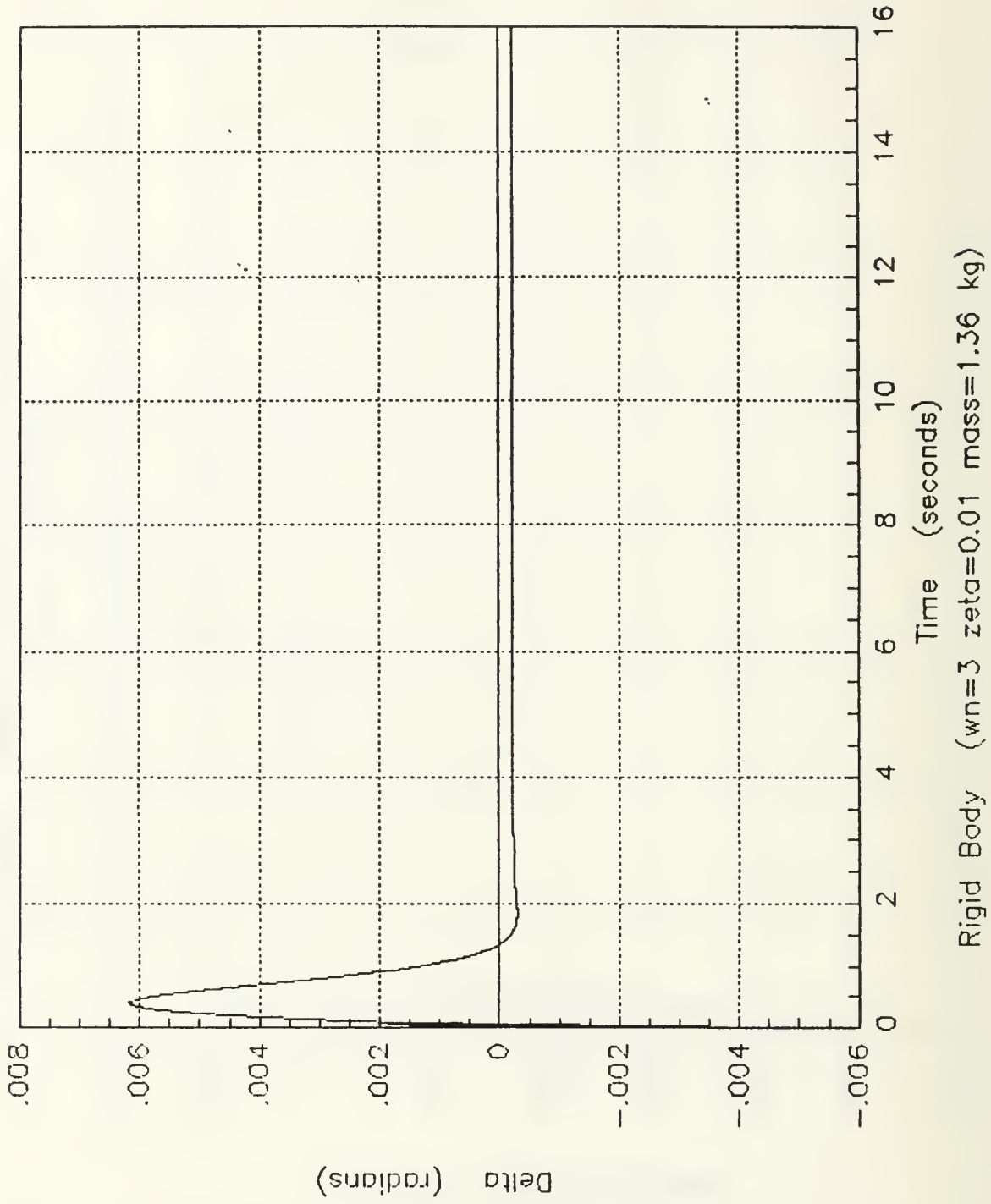

Figure 60. Rigid Body Model (small motion) $\omega_n = 3$

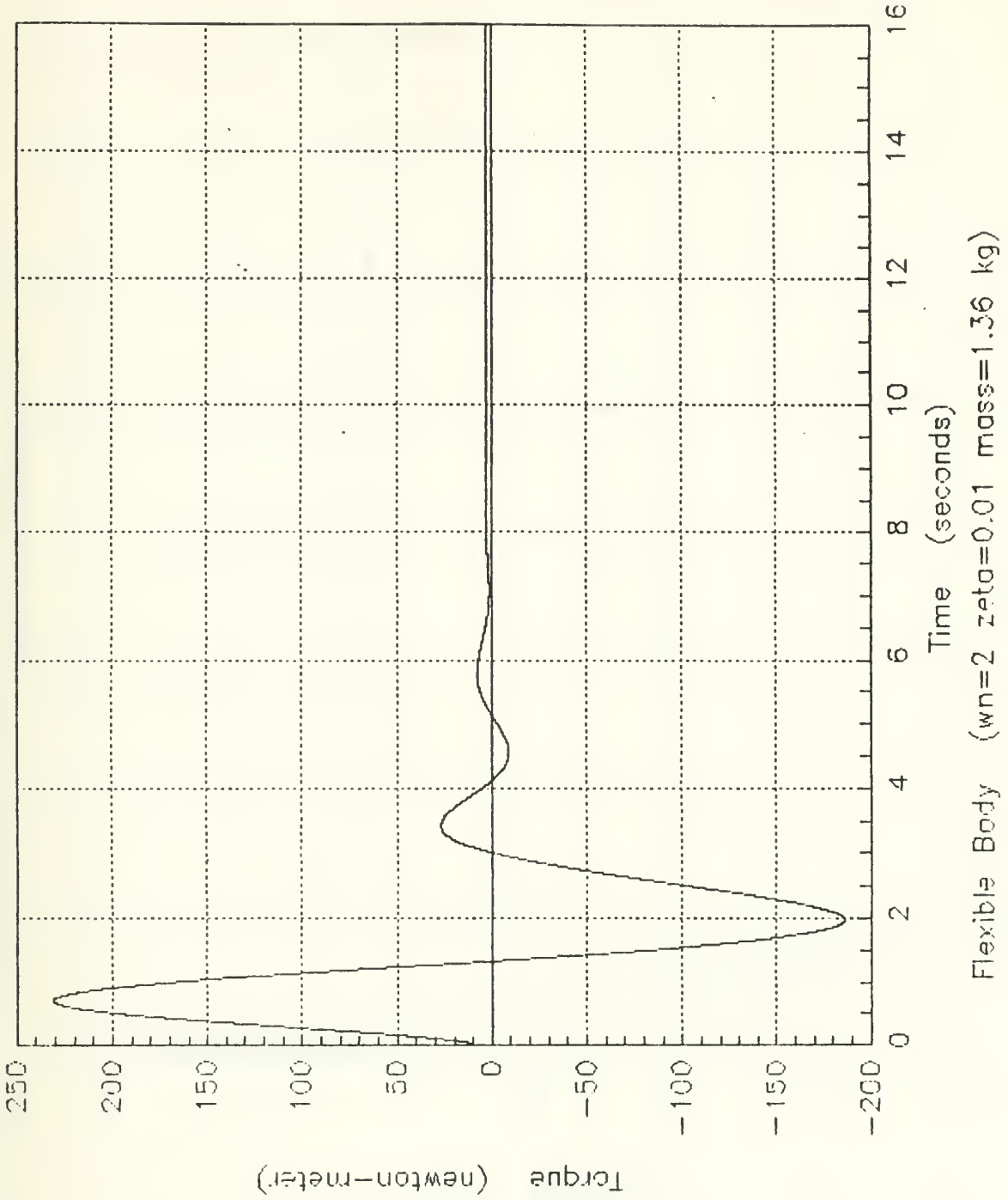

Figure 61. Flexible Body Model (torque) $\omega_n = 2$

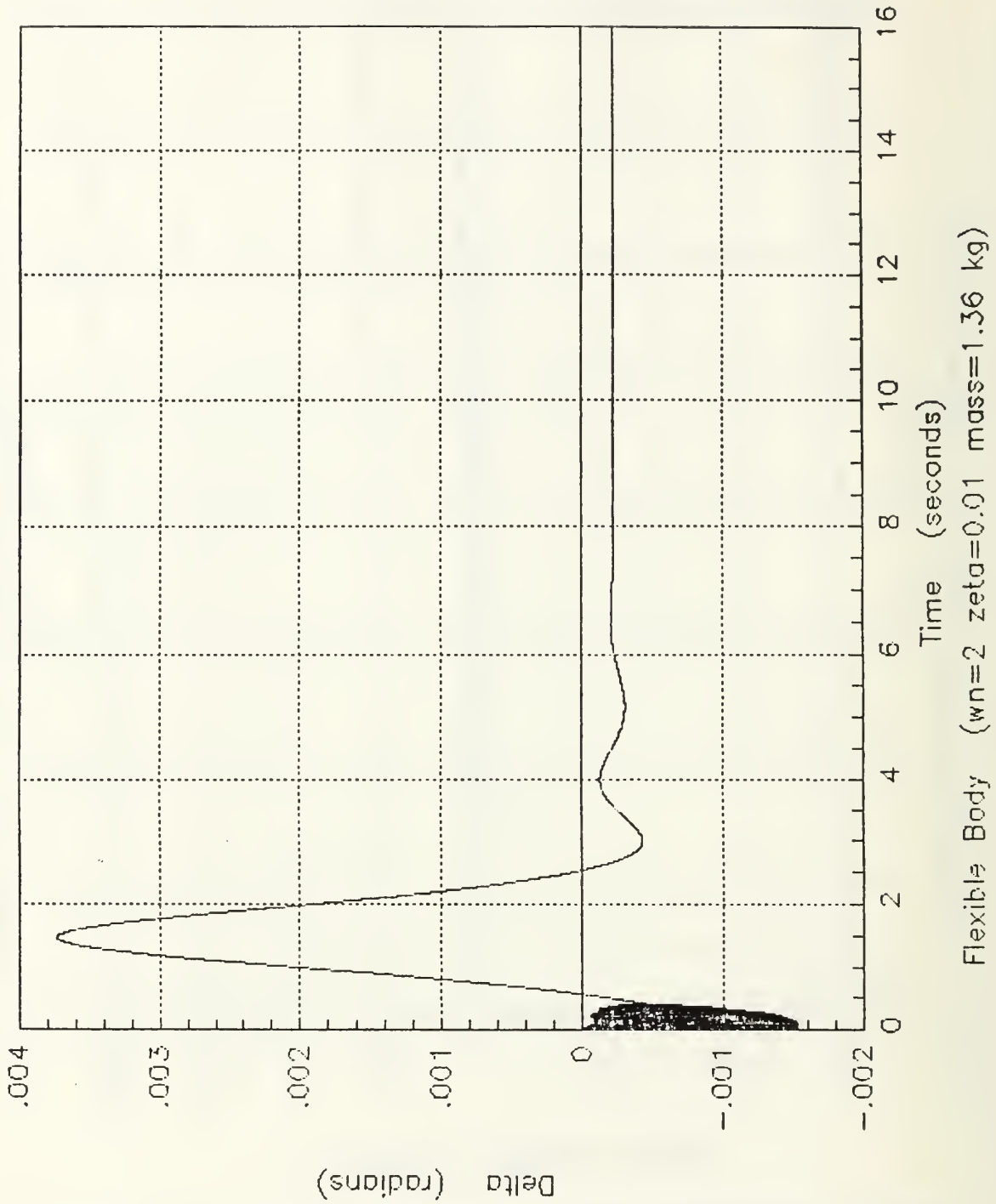

Figure 62. Flexible Body Model (small motion) $\omega_n = 2$

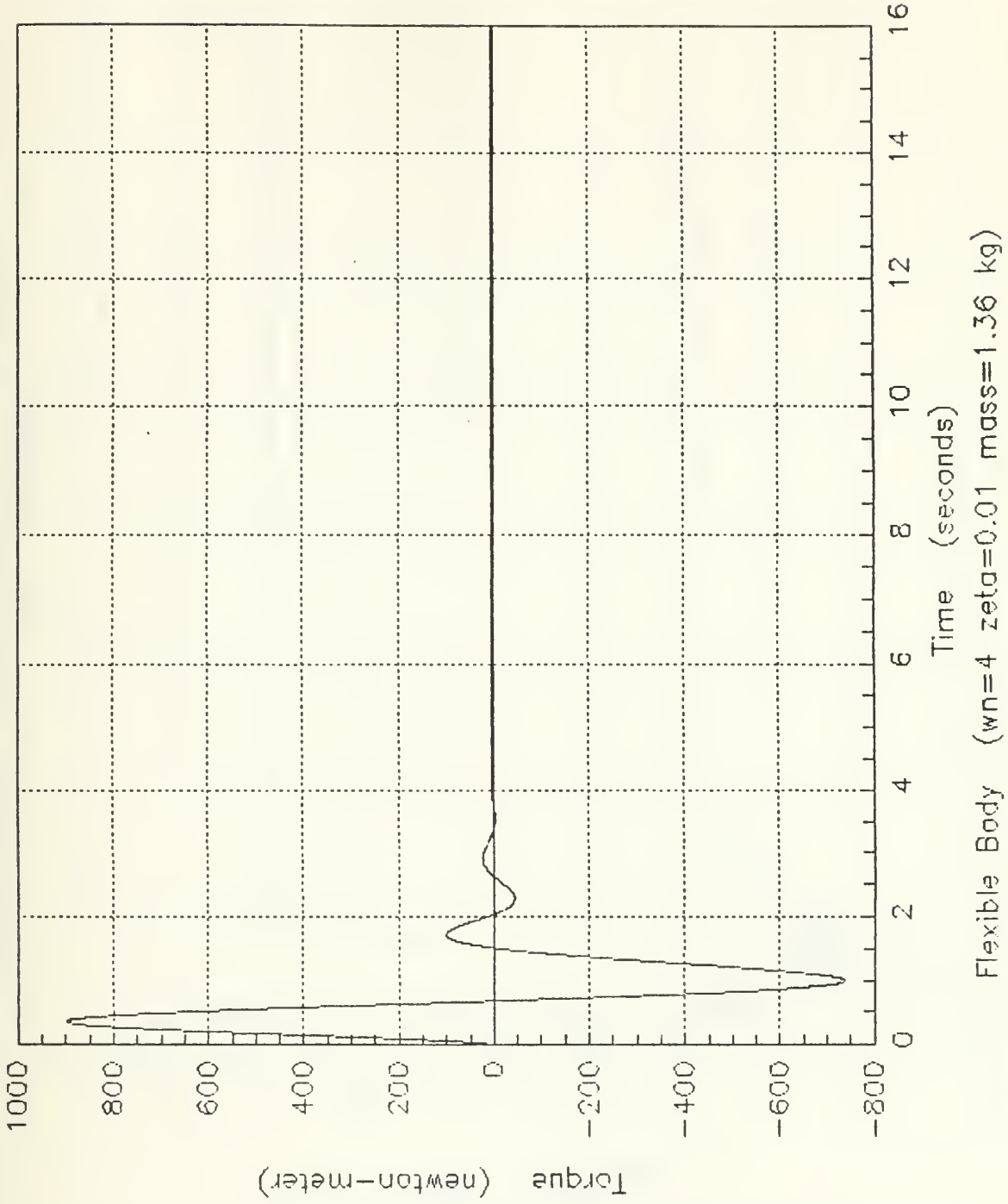

Figure 63. Flexible Body Model (torque) $\omega_n = 4$

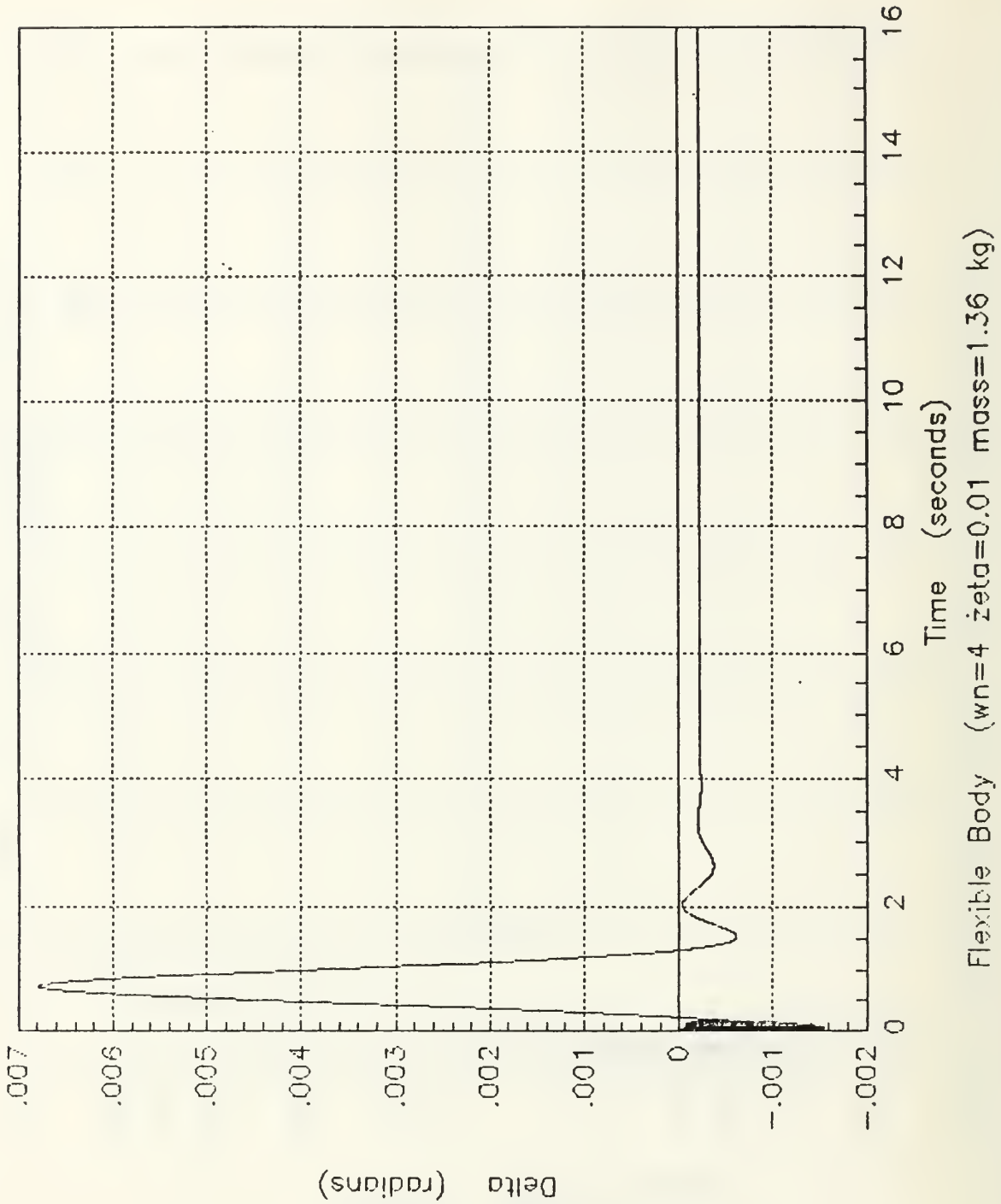

Figure 64. Flexible Body Model (small motion) $\omega_n = 4$

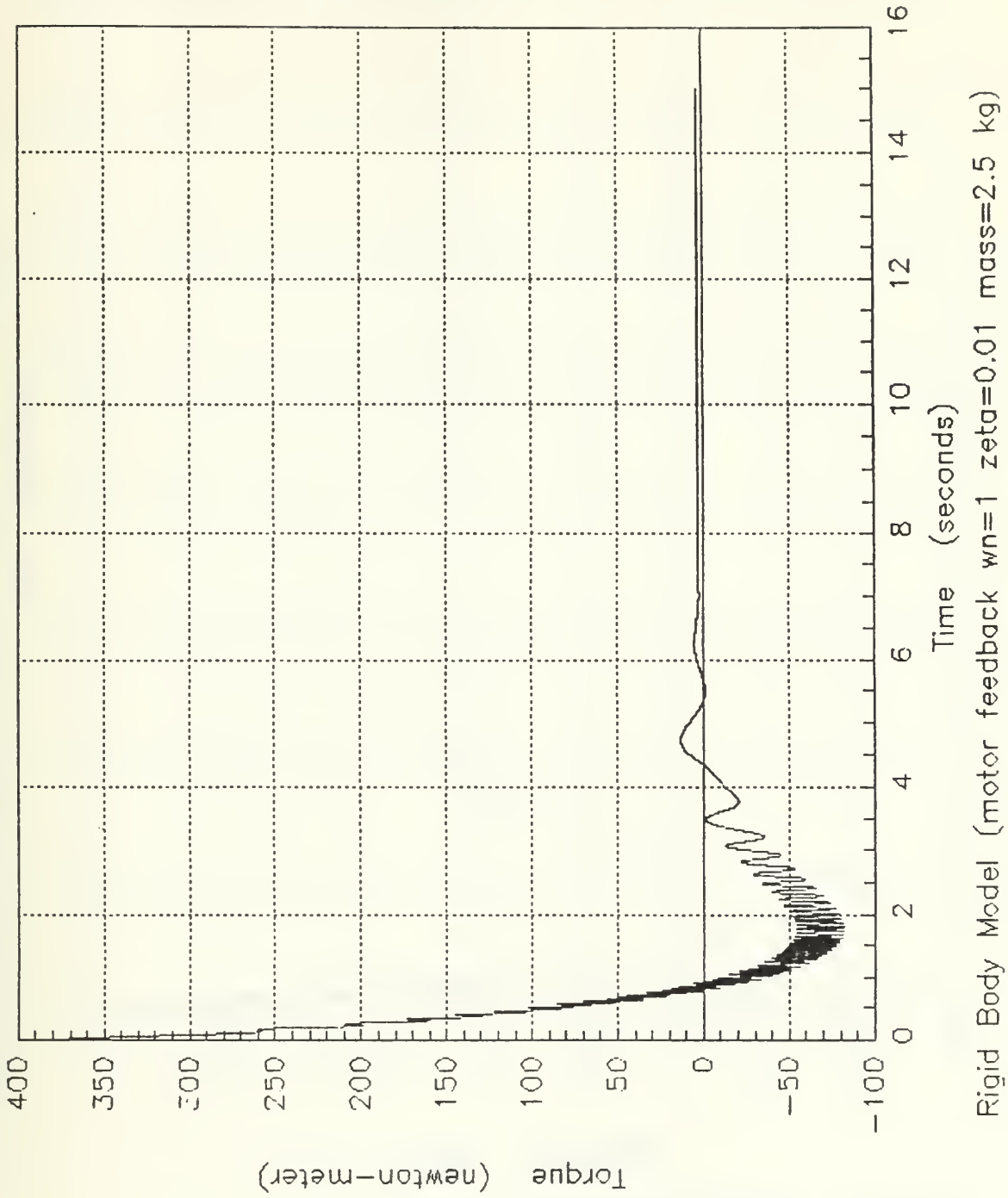

Figure 65. Rigid Body Model (torque) $\omega_n = 1$

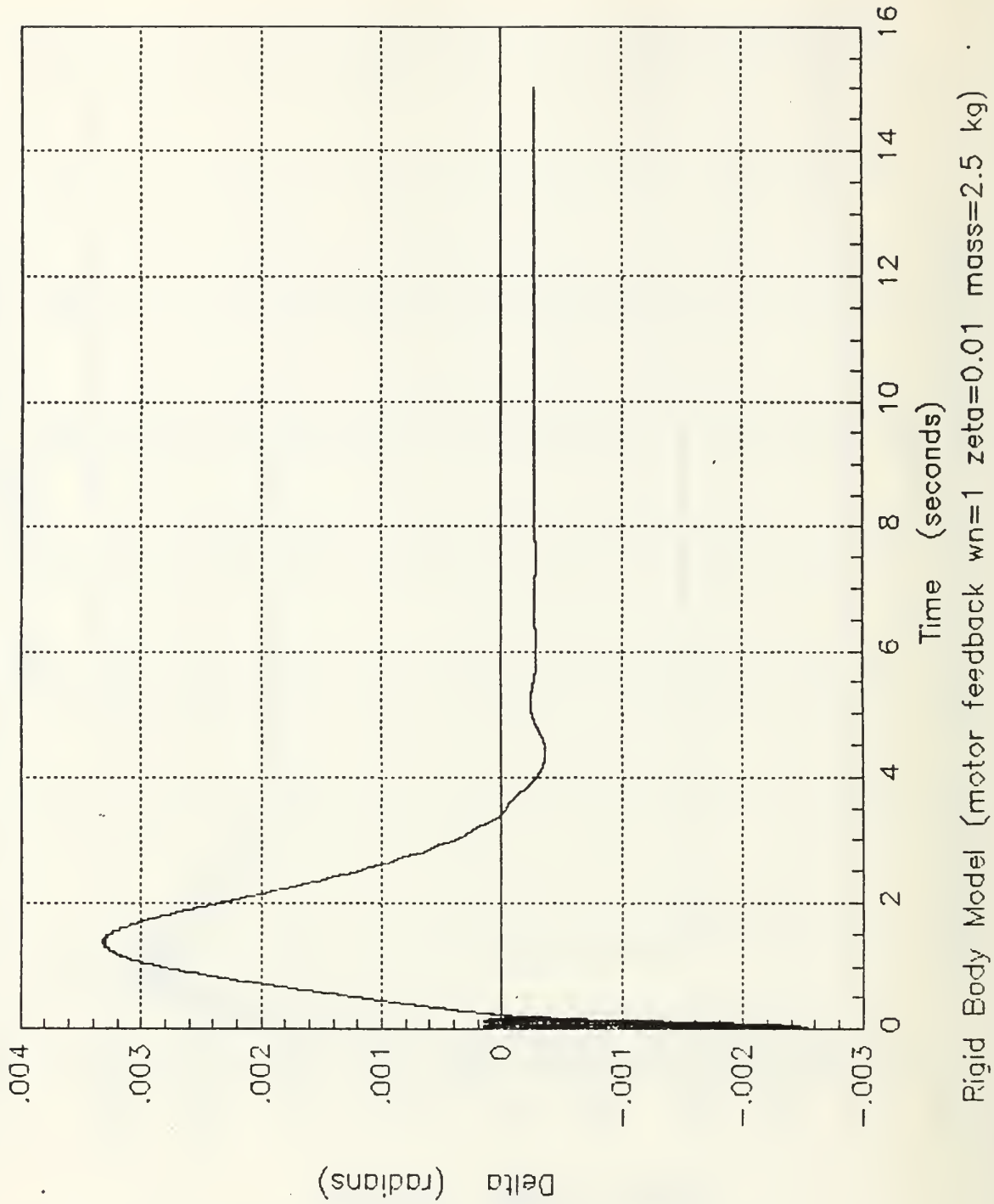

Figure 66. Rigid Body Model (small motion) $\omega_n = 1$

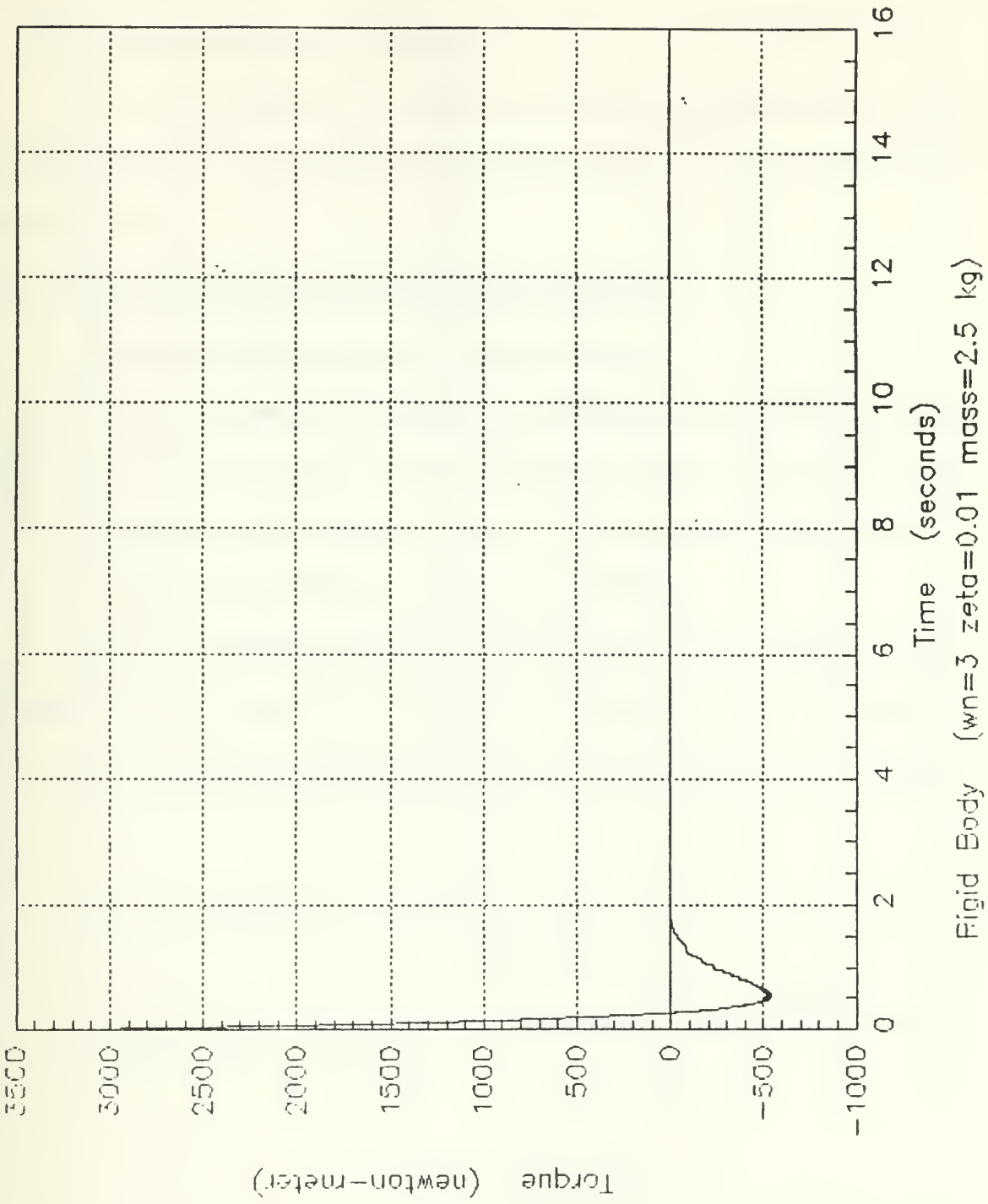

Figure 67. Rigid Body Model (torque) $\omega_n = 3$

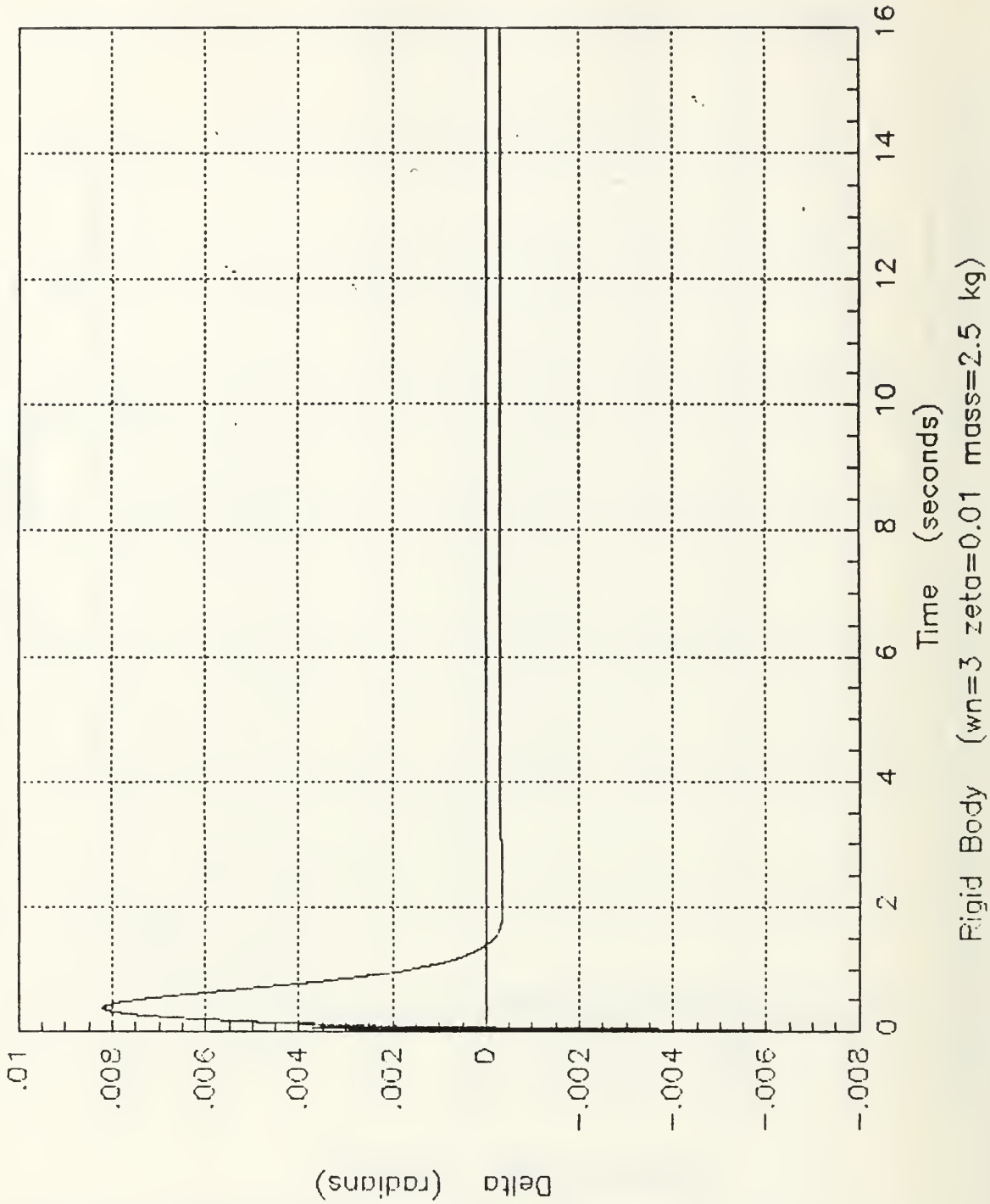

Figure 68. Rigid Body Model (small motion) $\omega_n = 3$

2. Flexible Body Model with Added Mass

For an examination of the Flexible Body Model experiencing point to point control and added mass see Figure 69 and Figure 70 for $\omega_n = 2$ and Figure 71 and Figure 72 for $\omega_n = 4$.

D. GRAPHS UNDERGOING TRAJECTORY TRACKING

1. Rigid Body Model Experiencing Trajectory Tracking

For the examination of the Rigid Body model graphs with and without damping and added mass, under going trajectory tracking see Figure 73 and Figure 74 for $\omega_n = 1$. See Figure 75 and Figure 76 for $\omega_n = 1$ with damping and added mass.

2. Flexible Body Model Experiencing Trajectory Tracking

For the examination of the Flexible Body model graphs with and without damping and added mass, under going trajectory tracking see Figure 77 and Figure 78 for $\omega_n = 2$. See Figure 79 and Figure 80 for $\omega_n = 2$ with damping and added mass.

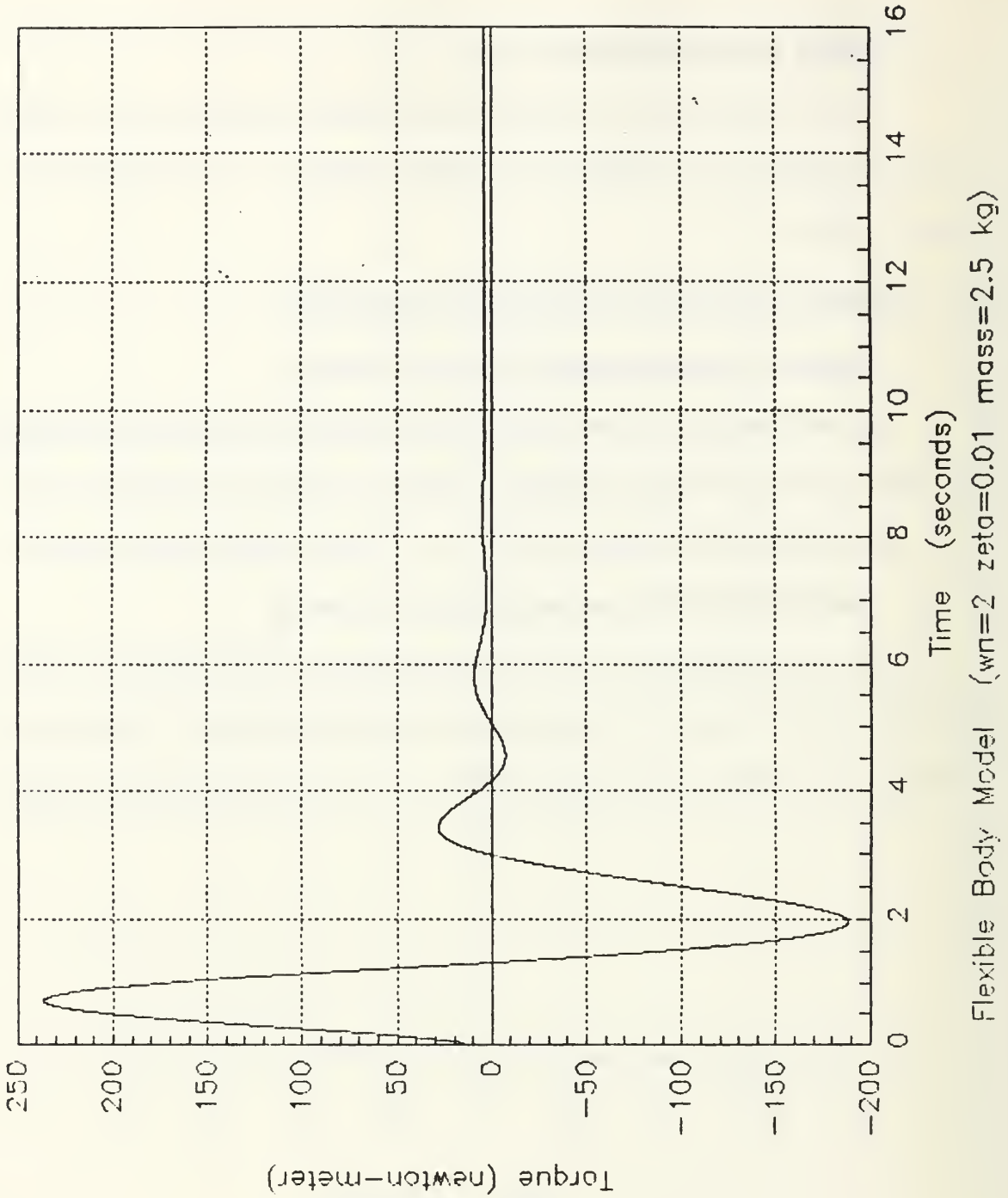

Figure 69. Flexible Body Model (torque) $\omega_n = 2$

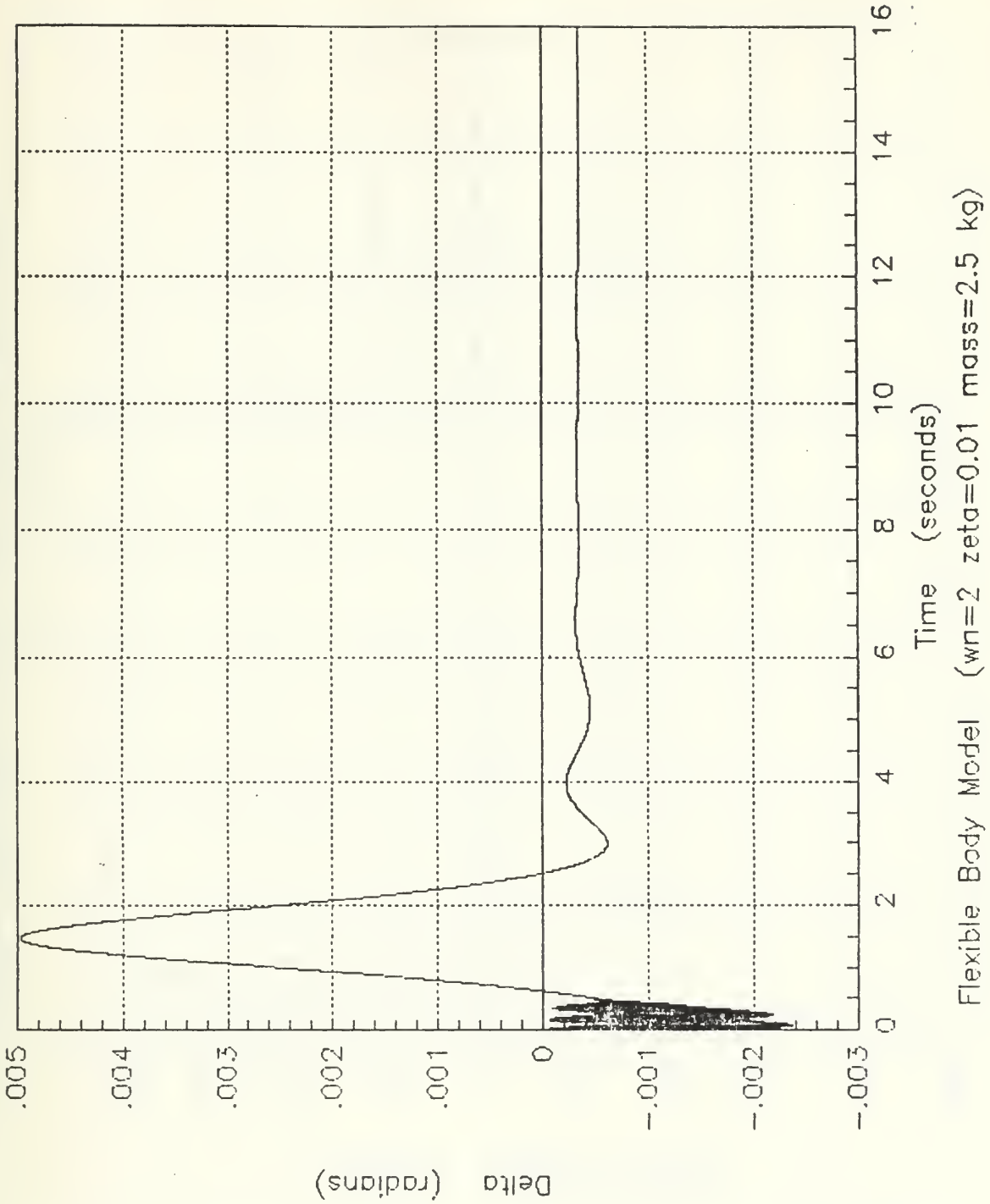

Figure 70. Flexible Body Model (small motion) $\omega_n = 2$

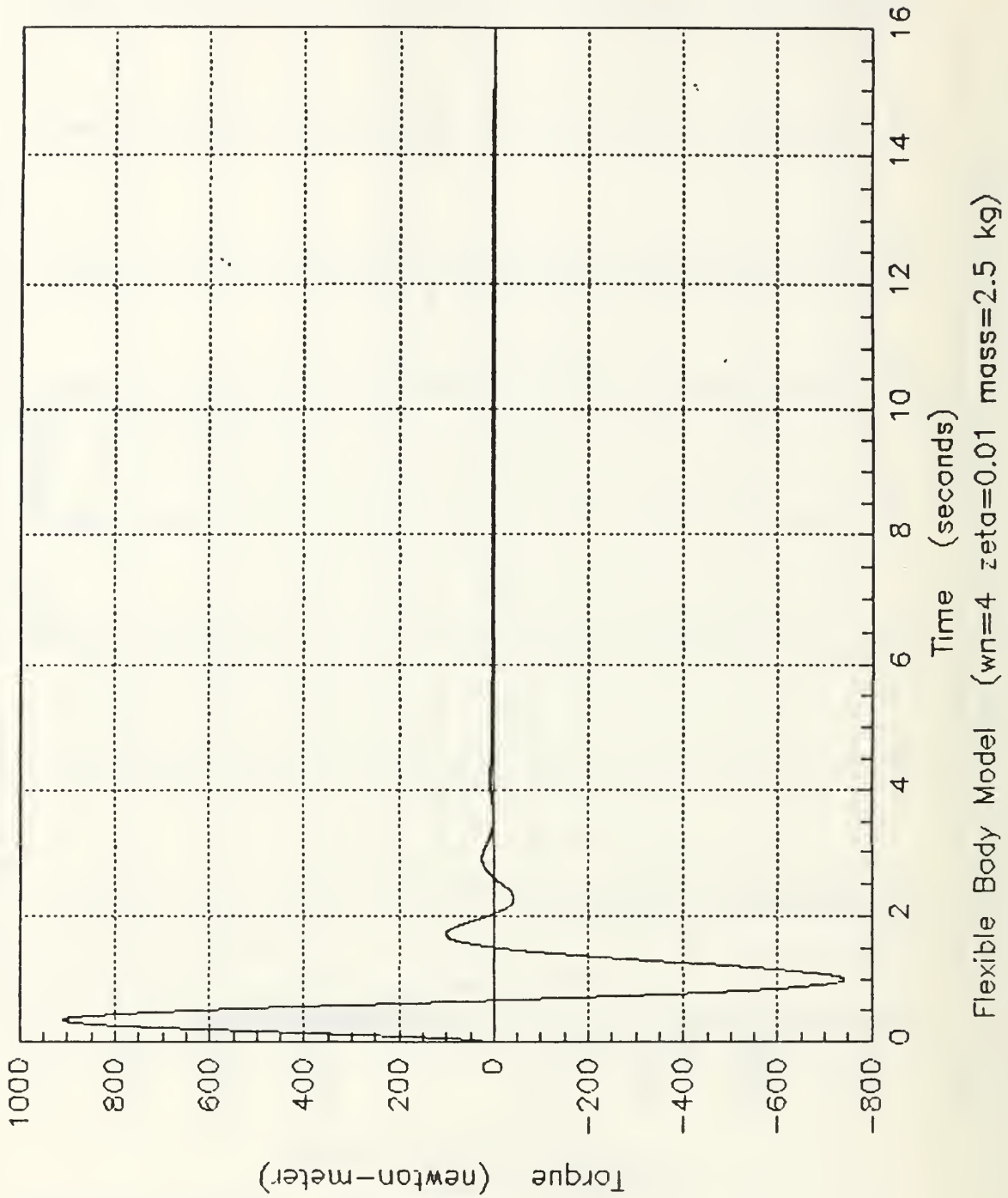

Figure 71. Flexible Body Model (torque) $\omega_n = 4$

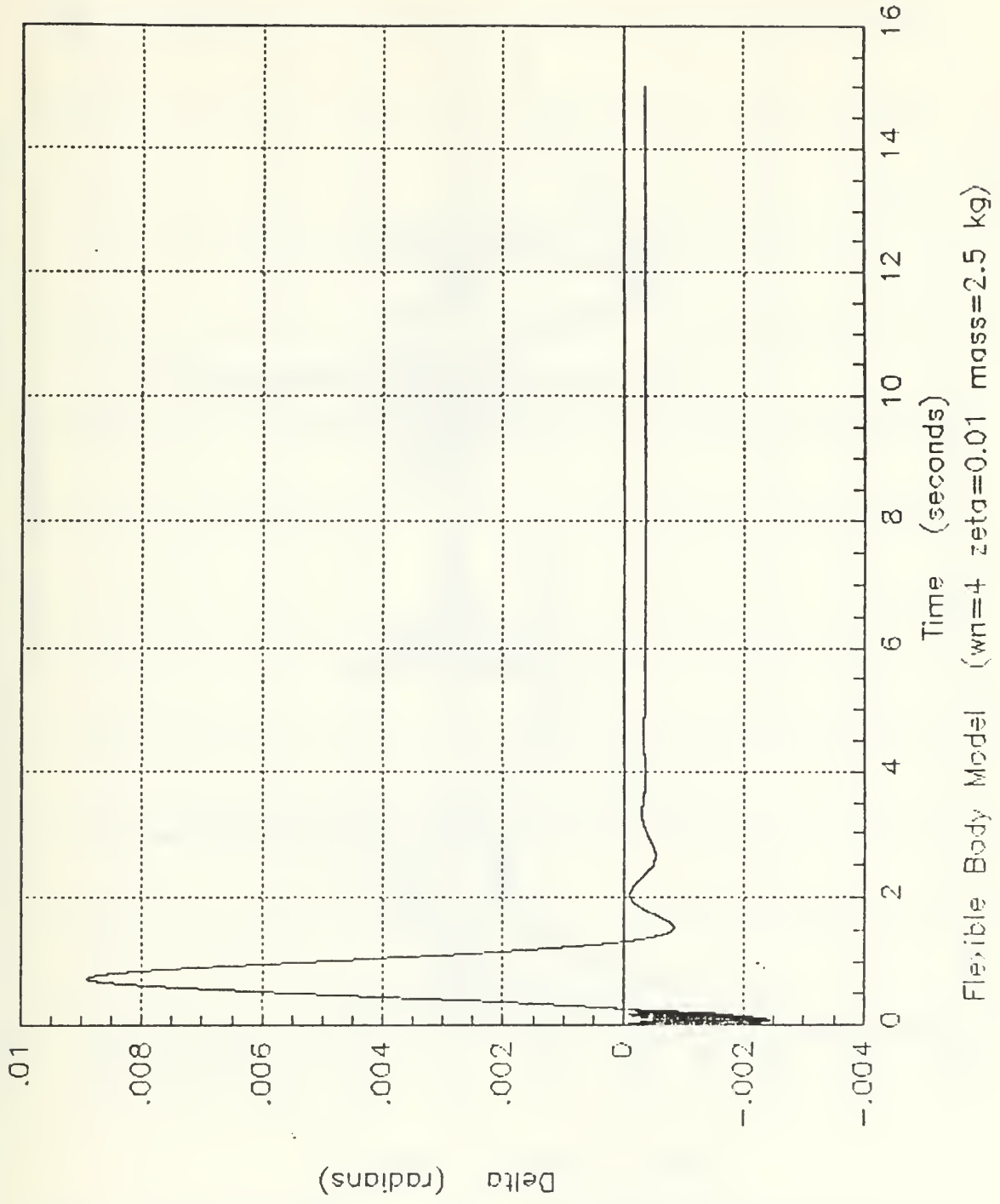

Figure 72. Flexible Body Model (small motion) $\omega_n = 4$

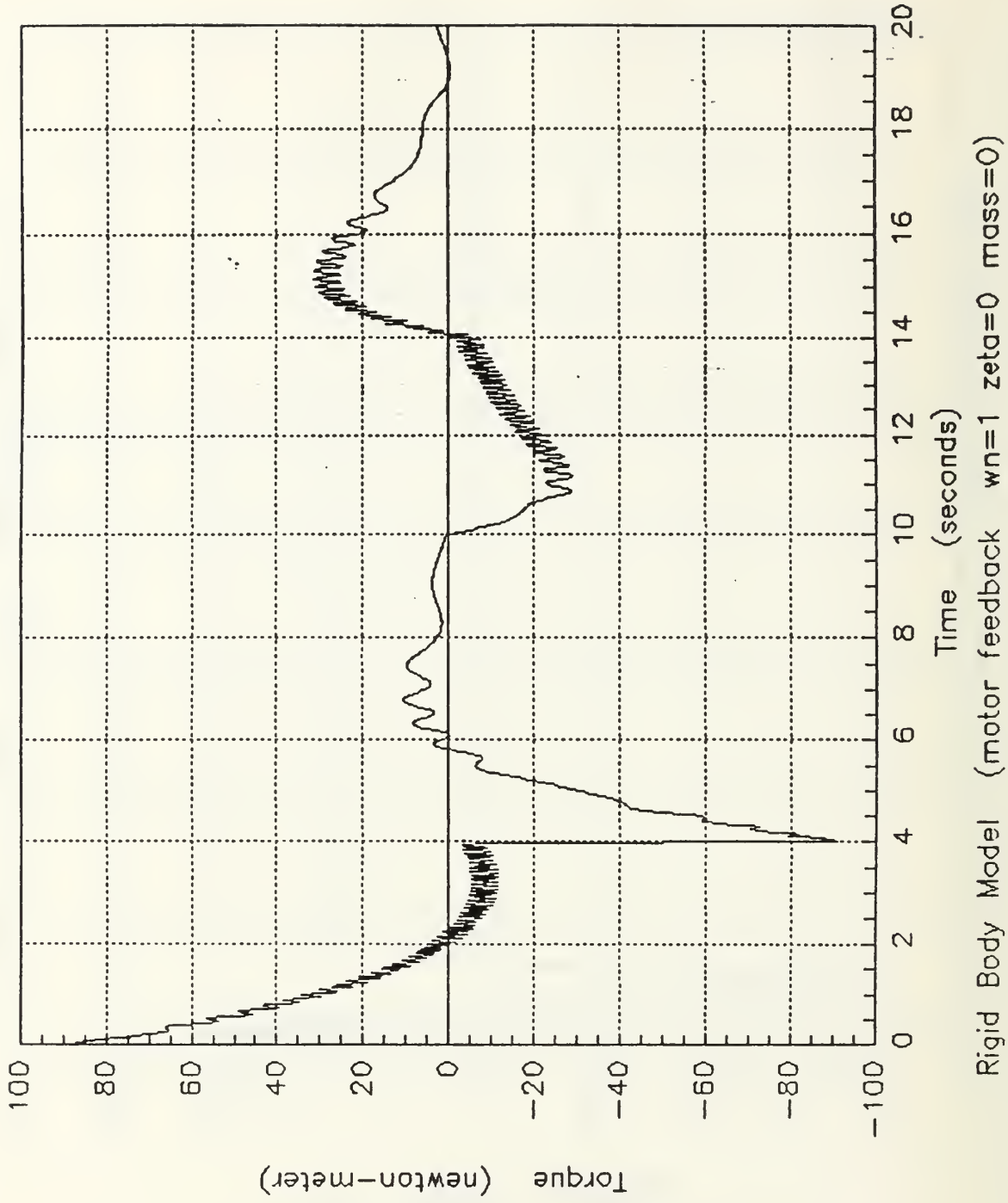

Figure 73. Rigid Body Model (torque) ω_n = 1 (ramp)

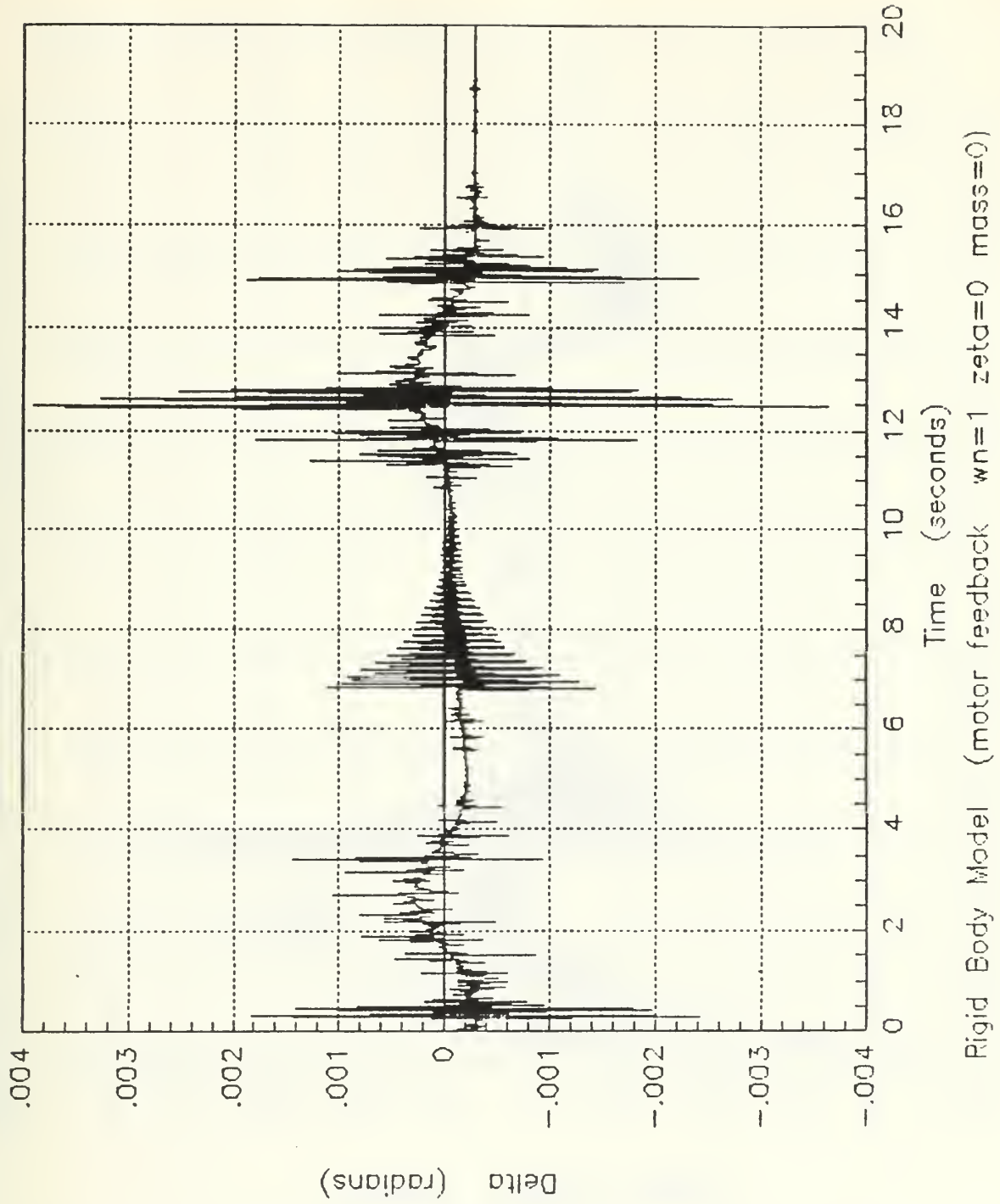

Figure 74. Rigid Body Model (small motion) $\omega_n = 1$ (ramp)

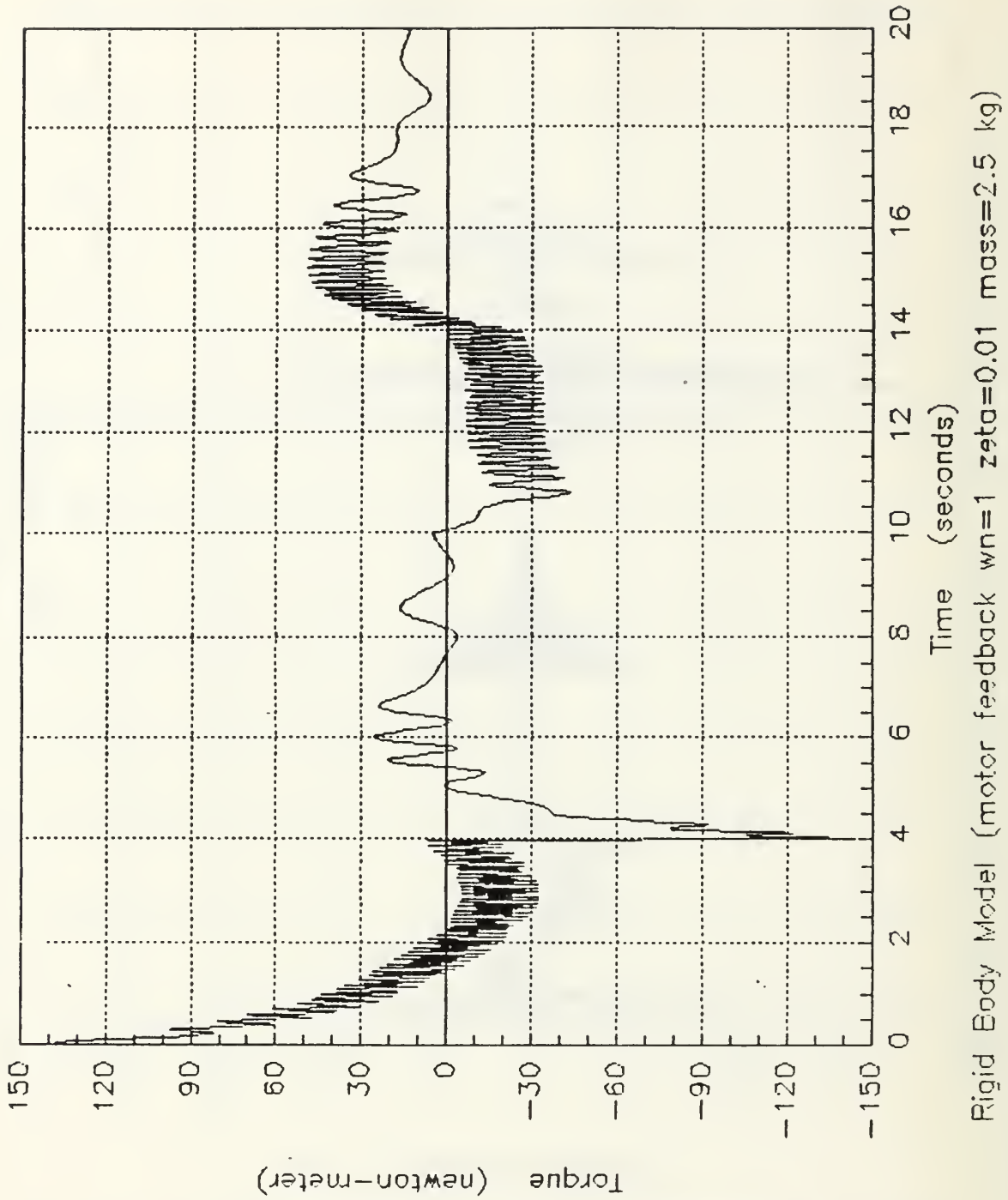

Figure 75. Rigid Body Model (torque) load ω_n = 1 (ramp)

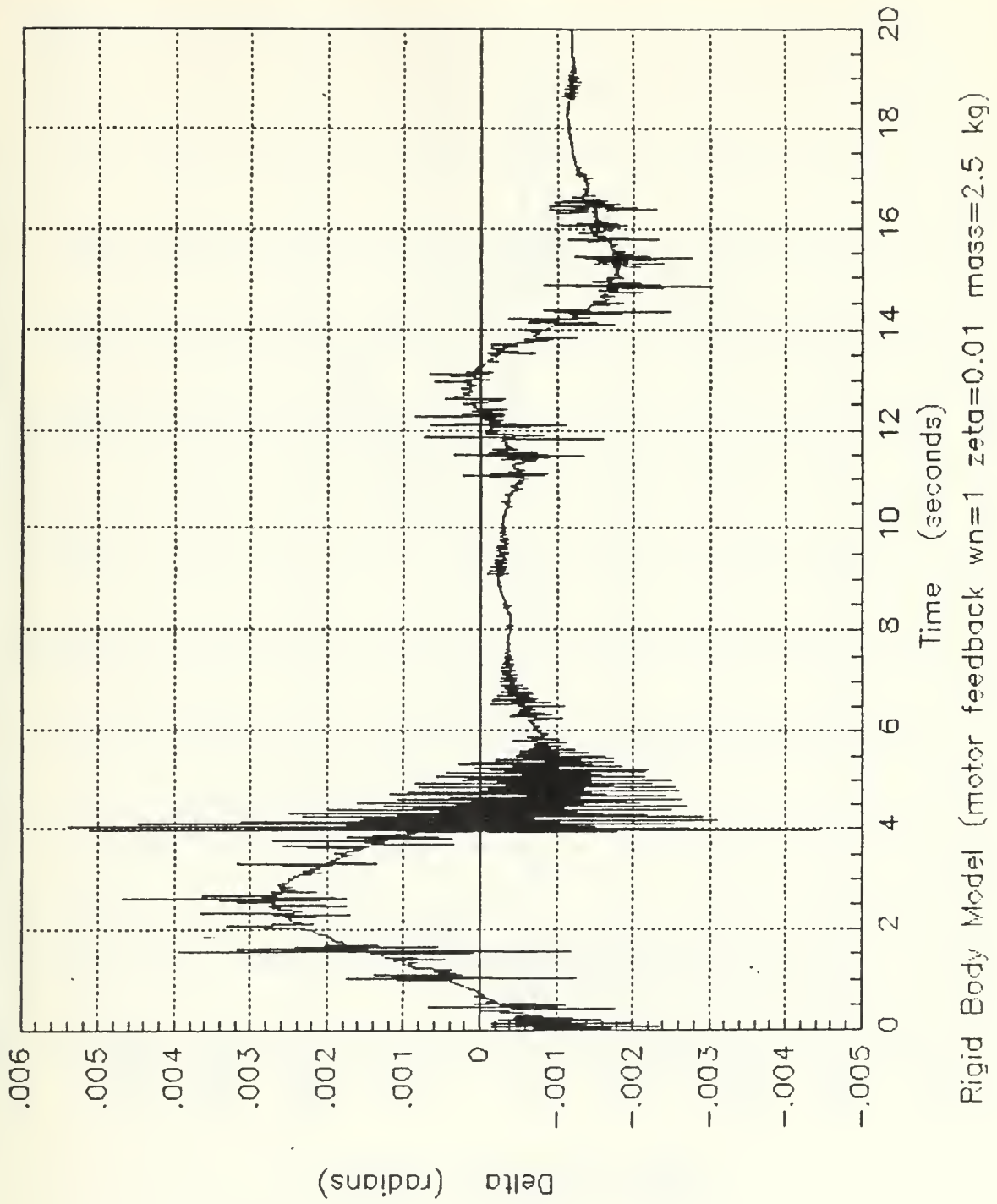

Figure 76. Rigid Body Model (small motion) load ω_n = 1 (ramp)

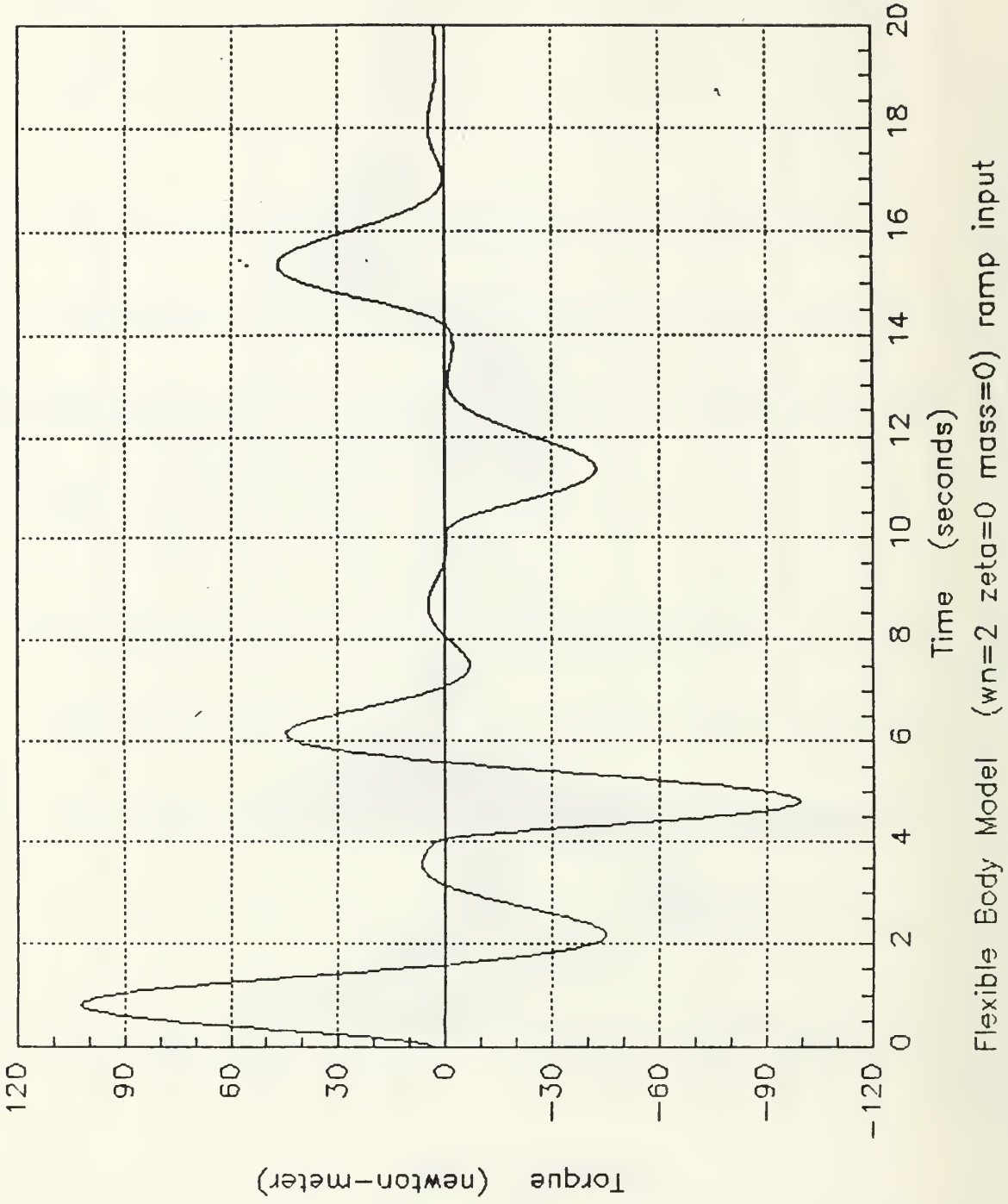

Figure 77. Flexible Body Model (torque) ω_n = 2 (ramp)

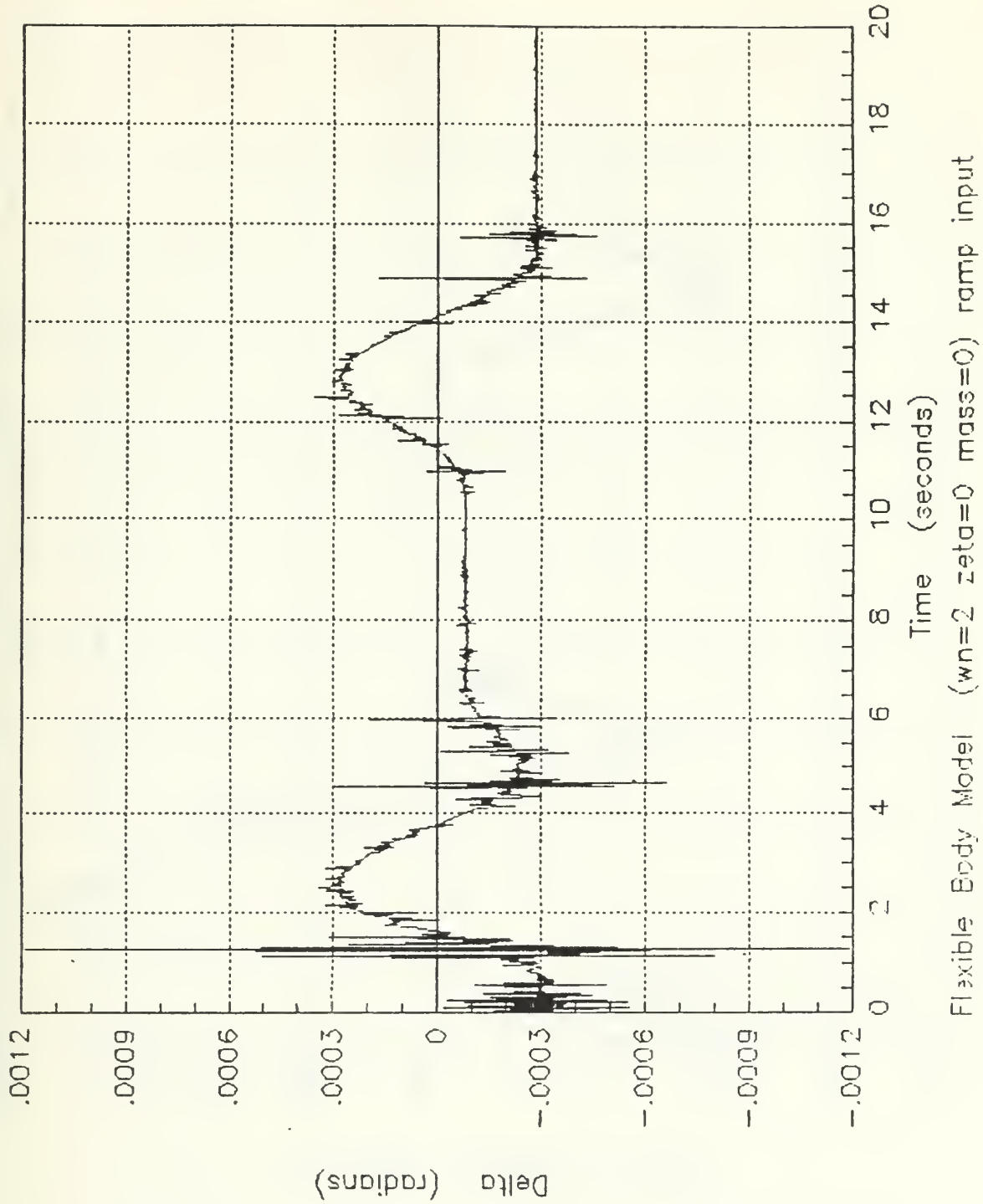

Figure 78. Flexible Body Model (small motion) ω_n = 2 (ramp)

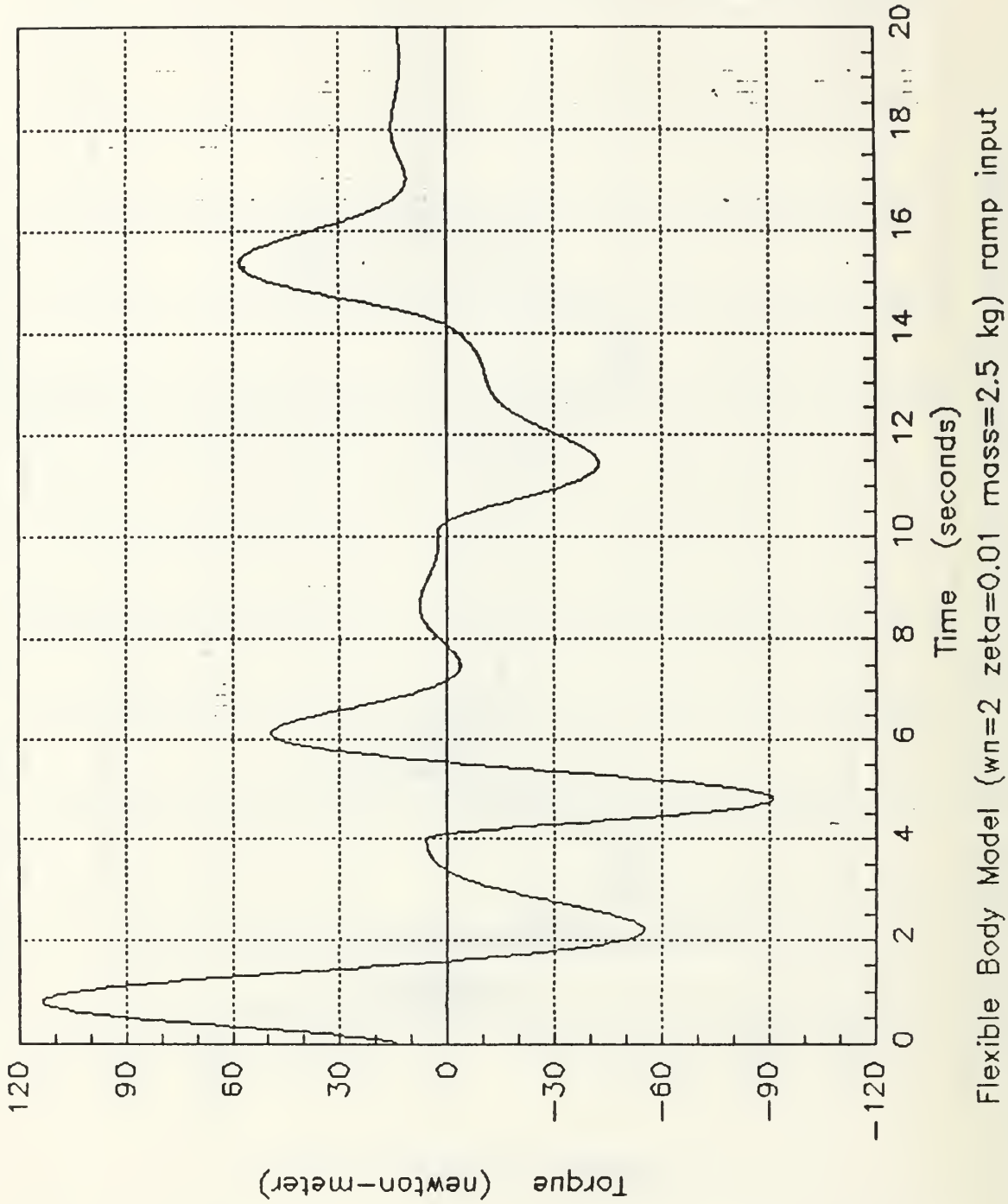

Figure 79. Flexible Body Model (torque) load ω_n = 2 (ramp)

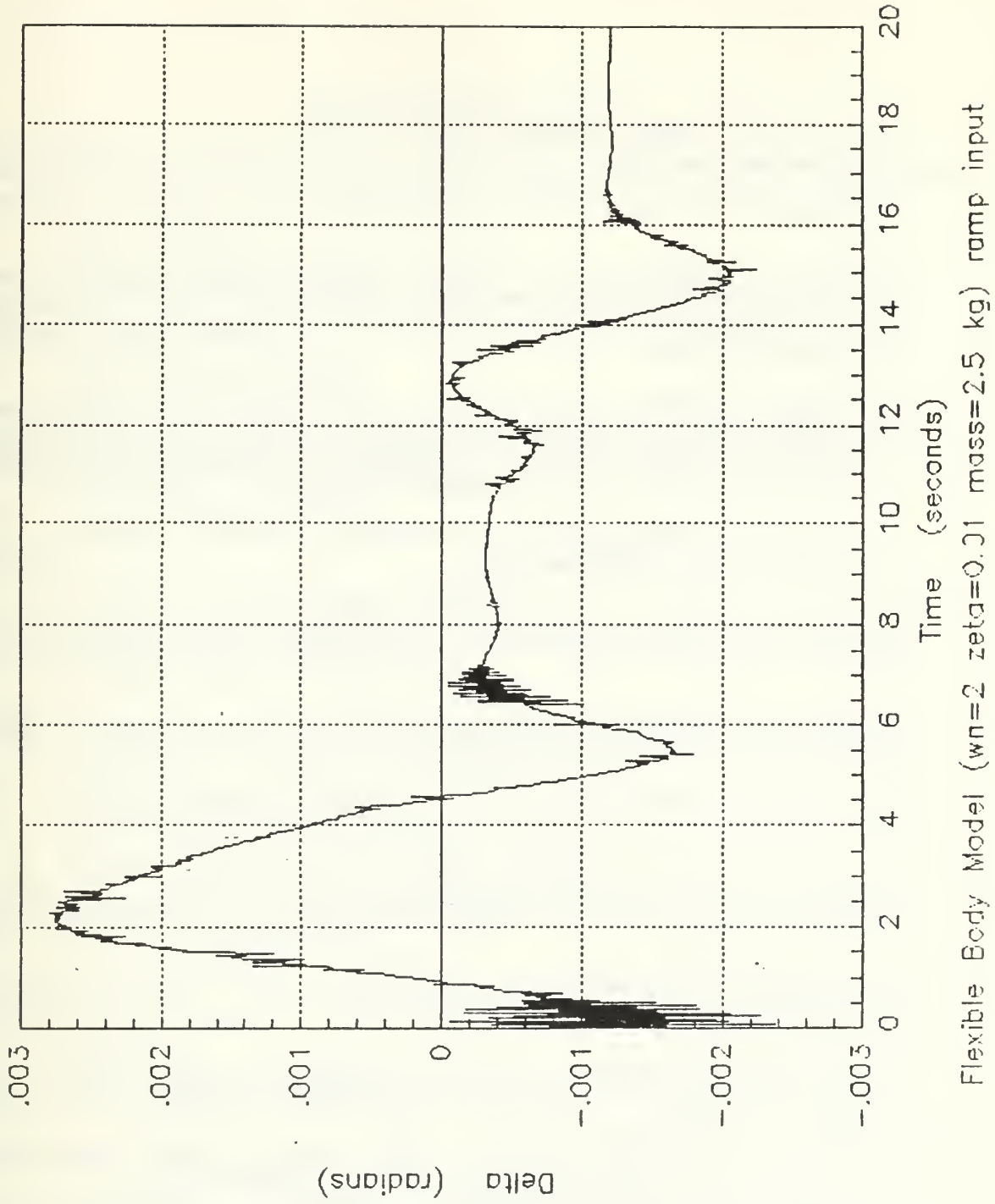

Figure 80. Flexible Body Model (small motion) load ω_n = 2 (ramp)

LIST OF REFERENCES

1. Babcock, S.M., and Forrest-Barlach, M.G., "Inverse Dynamics Position Control of a Compliant Manipulator," paper presented at the Proceeding of IEEE International Conference on Robotics, and Automation, San Francisco, California, April 1986.

2. Mario, R., and Spong, M.W., "Nonlinear Control Techniques for Flexible Joint Manipulators: A Single Link Case Study," paper presented at the Proceeding of IEEE International Conference on Robotics, and Automation, San Francisco, California, April 1986.

3. Good, M.C., and Sweet, L.M., "Re-definition of the Robot motion control Problem: Effects of Plant Dyanamics, Drive System Constraints, and User Requirements," paper presented at IFFF Proceeding of the third Conference on Decision and Control, Las Vegas, Nevada, December 1984.

4. Spong, M.W., "Modeling and Control of Elastic Joint Robots," ASME Journal, V. 109., pp. 310- 319, December 1987.

5. Book, W.J., Lynch, P.M., and Whitney, D.E., "Design and Control Configurations for Industrial and Space Manipulators," paper present at Proceedings for JACC, 1974.

6. Unimation, A Westinghouse Company, *Unimate Puma Mark II Robot, 500 Series Equipment Manual*, 398U1, August 1985.

7. Greenwood, D.T., *Principles of Dynamics*, 2d ed., Prentice-Hall, Inc., 1988.

8. Dorf, R.C., *Modern Control Systems*, Addison-Wesley Publishing Co., 1983.

9. Friedland, B., *Control System Design, An Introduction to State-Space Methods*, McGraw-Hill Book Co., 1986.

10. Integrated Systems Incorporated, **MATRIX**$_x$ User's Guide, *Engineering Analysis and Control Design*, version 6.0, pp. P-1-P-2, 1986.

11. Integrated Systems Incorporated, SYSTEM_BUILD User's Guide, *Engineering Analysis and Control Design*, version 6.0, pp. SB P-1-SB P-3, 1986.

12. Unimation, A Westinghouse Company, *Unimate Industrial Robot Programming Manual, Users Guide to VAL II Version 2.0*, 398U1, February 1986.

13. Gopinath, B., "On the Control of Linear Multiple Input-Output Systems," *The Bell System Technical Journal*, v. 50, no. 3, pp. 1063-1081, March 1971.

INITIAL DISTRIBUTION LIST

		No. Copies
1.	Defense Technical Information Center Cameron Station Alexandria, VA 22304-6145	2
2.	Library, Code 0142 Naval Postgraduate School Monterey, CA 93943-5002	2
3.	Department Chairman, Code 69Hy Department of Mechanical Engineering Naval Postgraduate School Monterey, California 93943-5000	1
4.	Professor Liang-Wey Chang, Code 69Ck Department of Mechanical Engineering Naval Postgraduate School Monterey, California 93943-5000	5
5.	Professor David Smith, Code 69Sm Department of Mechanical Engineering Naval Postgraduate School Monterey, California 93943-5000	1
6.	Naval Engineering Curricular Officer, Code 34 Department of Mechanical Engineering Naval Postgraduate School Monterey, California 93943-5000	1
7.	Dr. Shalom Fisher Code 8241 Naval Research Laboratory Washington, D. C. 20375-5000	1
8.	Professor Jeff B. Burl, Code 62Bl Department of Electrical and Computer Engineering Naval Postgraduate School Monterey, California 93943-5000	1
9.	Commander Naval Sea Systems Command Attn: LT Rellel Wyman Robotics Office Washington, D. C. 20362-5000	1

10. LCDR Robby L. Knight
106 Winder Road
Tabb, Virginia 23602

2

Thesis
K6221 Knight
c.1 Control system design
of the third flexible
joint of PUMA 560 Robot.